# Virtual Autonomous Operator Model For Construction Equipment Applications

BY

AHMED ADEL ELEZABY
BSc, Ain Shams University, Cairo, Egypt 2001
MSc, Ain Shams University, Cairo, Egypt 2006

THESIS

Submitted in partial fulfillment of the requirements
for the degree of Doctor of Philosophy in Mechanical Engineering
in the Graduate College of the
University of Illinois at Chicago, 2011

Chicago, Illinois

Defense Committee:

Sabri Cetinkunt, Chair and Advisor
Michael Scott
Saeed Manafzadeh
Elissa Budyn
Ernesto Indacochea

This work is dedicated to my Father, my Mother and my Brother.

## ACKNOWLEDGMENT

I would like to thank my academic advisor Professor Sabri Cetinkunt for giving me the opportunity to be a part of his research team and for funding this project until the end of my thesis. He provided me with valuable guidance and support. I am really grateful and I appreciate your trust and believing in me.

I would like to thank Dr. Mohamed Abdel Aziz and Dr.Salem Haggag from Ain Shams University in Cairo, Egypt who recommended me to join the Mechatronics Lab at University of Illinois at Chicago.

I would like thank the team at Caterpillar Inc. John Krone and JC LE Mentec for their help and contribution.

I would like to thank my final defense committee members. Their valuable suggestions improved the work in its final phase.

I am truly grateful for the support from my parents for their continuous love and support.

I would like to thank my colleagues at the Mechatronics lab Fabio Croce, Rami Nasrallah, Sirvani Sirisha Motomari, Vinay Gundi , Keshav Sud and Ralf Gomm.

AAE

## TABLE OF CONTENTS

## TABLE OF CONTENTS (Continued)

**CHAPTER** **PAGE**

## LIST OF FIGURES

## LIST OF FIGURES (Continued)

**FIGURE** **PAGE**

## LIST OF FIGURES (Continued)

## LIST OF FIGURES (Continued)

## SUMMARY

Designing a new construction equipment or modifying an old model for the world market requires investing a lot of time and money. After the design is done a few prototypes are built. These prototypes are tested by experienced operators through pre-defined tests. It is not unusual that many changes are made to the prototype design after this evaluation. The prototype is then modified and tested again. This iterative procedure continues until the prototype test results are satisfactory. This iterative test and evaluation procedure requires spending a lot of time and money in building prototypes and testing it. Virtual product development (VPD) tools aim to reduce these development costs by use of advanced computer aided engineering design tools and reduce the number of iterations and modifications done to the prototypes. Virtual product development has become an essential engineering process now in developing construction equipments to improve the machine quality, reliability and operability saving significant cost and time in building prototypes and testing them. The second problem is that the construction equipment operations quality, energy consumption and fuel efficiency depends to a great extent on the operator experience. Every operator does the operations depending on his level of experience and personal preference. Moving towards autonomous construction equipment operations will standardize operations and will take advantage of the maximum power, fuel and energy efficiency of the machine.

## SUMMARY (Continued)

The aim of this thesis is to build a virtual operator model that can control, test and evaluate a virtual construction equipment design before building the prototype, and autonomously control the construction equipment after being built so that virtual product development tools form a complete set, including the operator, hence reduce the iterative tests and modifications process thereby reducing the product development costs.

The thesis propose an operator model for construction machines in order to test digital mockups of the machines before building the prototypes of the machines thus help decrease the design cost and time significantly. A novel operator model based on neural networks that can modify itself to test different sizes and models of the machine without requiring any modification from the user were developed. The virtual operator model is considered a further step towards a complete autonomous operation.

# CHAPTER 1

# INTRODUCTION

## 1.1 Motivation

Designing a new construction equipment or modifying an old model for the world market requires investing a lot of time and money. After the design is done a few prototypes are built. These prototype are tested by experienced operators through pre-defined tests. It is not unusual that many changes are made to the prototype design after this evaluation. The prototype is then modified and tested again. This iterative procedure continues until the prototype test results are satisfactory. This iterative test and evaluation procedure requires spending a lot of time and money in building prototypes and testing it. Virtual product development (VPD) tools aim to reduce these development costs by use of advanced computer aided engineering design tools and reduce the number of iterstions and modifications done to the prototypes. Virtual product development has become essential now in developing construction equipments to improve the machine quality, reliability and operability saving significant cost and time in building prototypes and testing them.

Construction equipment operations quality, energy consumption and fuel efficiency depends to a great extent on the operator experience. Every operator does the operations depending on his level of experience and personal preference. Moving towards autonomous construction


Figure 1. Examples of Construction Equipments.

equipment operations will standardize operations and will take advantage of the maximum power, fuel and energy efficiency of the machine.

## 1.2 Literature Review

The literature review section is divided into five categories. The first category is the operator and machine modeling. The second category is about virtual product development. The third category reviews some research in modeling driver behavior. The fourth category is for virtual proving ground. The fifth and the last category is for path tracking.

### 1.2.1 Operator and Machine Modeling

We introduced the idea of our version of the virtual operator modeling in [1] and [41]. The initial results of a virtual operator model were presented. The operator model was able to test digital mock ups of wheel loaders. An operator model which is able to give human commands to a virtual wheel loader model based on events received by human operator has been presented. Compared to an human operator performance, the virtual operator model generated commands are within 10% of a measured human-operated truck loading cycle in terms of distance traveled and cycle time. This model were considered a first step towards developing a full cognitive operator model. This type of model is to be used in performance assessment of the wheel loader before building the prototype. Closed loop command tracking algorithms at the lower level of control algorithm hierarchy was PID type. It was not able to modify itself for controlling different models of the machine. In [2] Filla presents the initial results to a simulation model of a human operator. The operator model developed by Filla follows generic rules that describe the work cycle. The advantage of this over a predefined path is to make the model independent

from the machine technical parameters. The machine parameters can be changed without affecting the simulation validation. The model developed by Filla can be used to estimate the performance of the machine. Figure (2) shows a simplified power transfer scheme of a wheel loader loading gravel used by Filla. In figure (3) Filla presented the relationship between the operator model and working task description. Working task was defined by Filla as the summary of all descriptions of how the simulated machine will be operated in its environment. The operator model describes how the machines will be controlled to accomplish the working task.

A more complicated operator model needs less description of the working cycle than a simple operator model [3]. This way the description of the working cycle will be much simpler. The simple operator model can be compensated by detailed description of the working cycle. This means that a more complicated operator model will require less information of the machine [3].

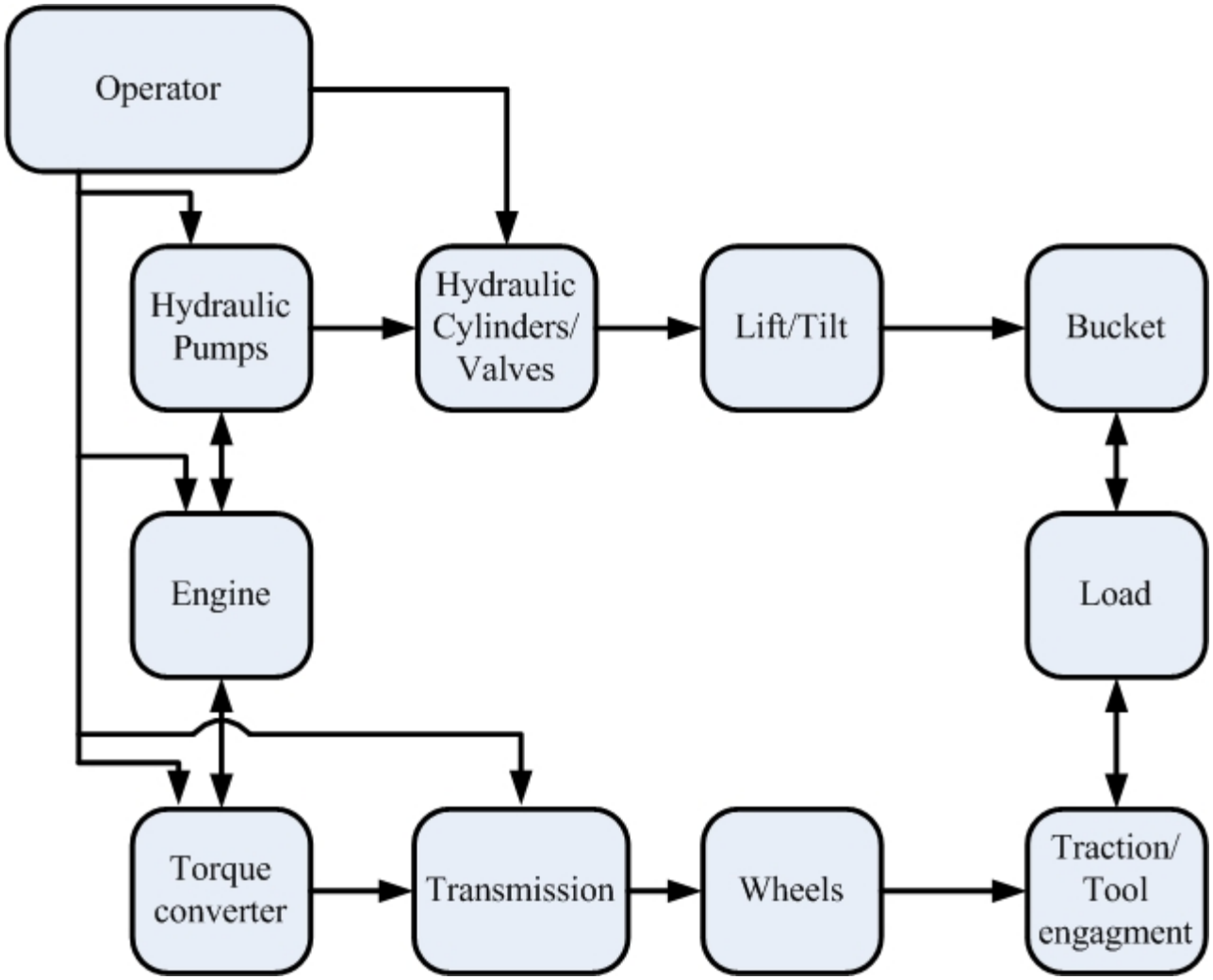


Figure 2. Simplified machine control scheme of a wheel loader loading cycle[2].

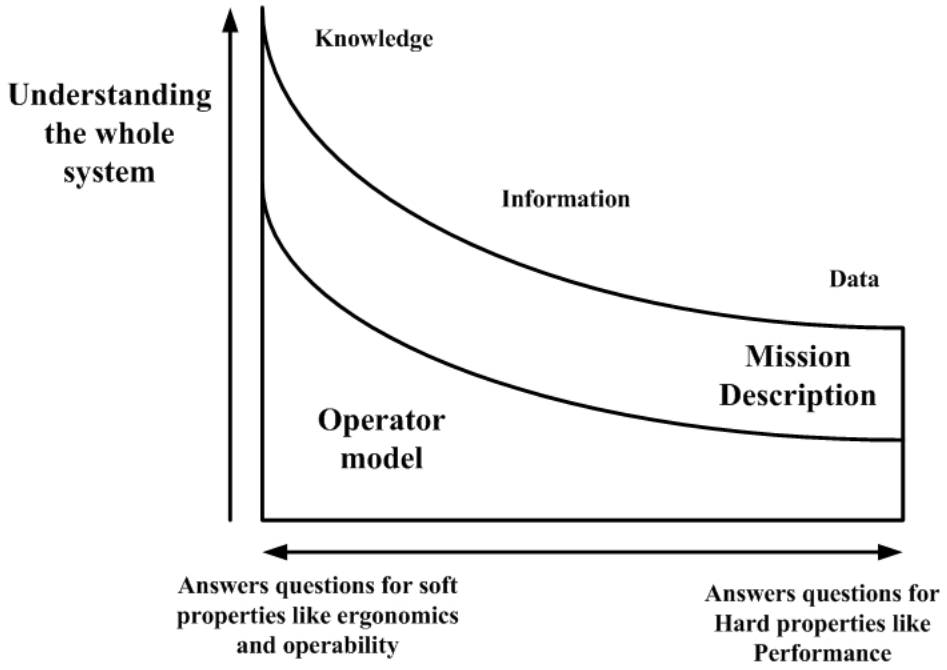


Figure 3. Relationship between the complexity of the operator model and the description of the loading cycle [3].

In the paper [3] a bucket filling was modeled with a simple strategy (Fig 4). We are going to use the same strategy in the operator model. Filla explained in [3] that the most efficient way to fill a bucket is to move the bucket forward and up through a graved pile with a velocity vector of a bearing angle equals to the pile slope angle. The bucket filling process will start with a bucket parallel to the ground. The cutting edge of the bucket should remain at an angle of attack relative to the bucket velocity. The bucket bottom angle of clearance will be relative to the ground pile. It was showed in [3] that this is more efficient than just driving the bucket

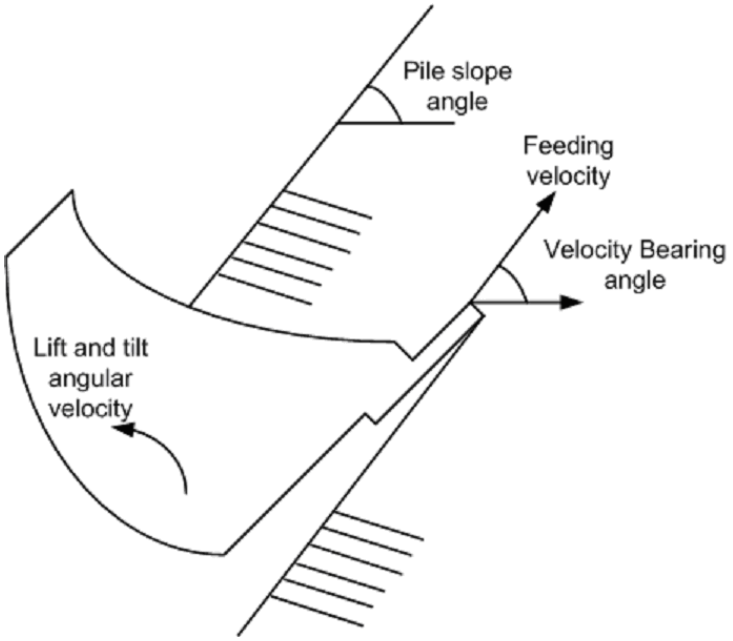


Figure 4. Bucket filling strategy explained by Filla in [3].

towards the bucket and tilting it backward until it was filled.

In [4] Filla simulated the loading cycle shown in figure 5 using the operator model presented in [3]. Short loading cycle is divided into different phases, and some examples are given for especially interesting situations that occur in some phases. Phase 1, in the cycle defined by Filla starts when the cutting edge of the bucket contacts the pile. The operator then shifts to the lowest gear to gain torque. Then the operator starts to lift the load increases the load on the front axle and improves traction. The operator then uses the throttle, lift and tilt controllers to fill the bucket. Phase 2, in Fillas cycle, starts when the bucket is fully tilted back. The operator

lifts the bucket and puts the machine in reverse and increases the machine speed. After leaving the pile the operator starts steering in the machine in a V-pattern. The operator continues lifting the load till the machine arrives to the truck which the beginning of the phase 5. Phase 3 of the cycle is called retardation. When the operator estimates the remaining distance to the truck and sees if it is sufficient for lifting the bucket high enough for unloading the bucket in the truck. The operator prefers moving a longer distance than stopping longer time by the truck to lift the bucket to an appropriate height that can unload the bucket without hitting the edge of the truck. Most of operators prefer engine braking than using the service brakes. Phase 4 is called reversing [3]. The operators put the machine in forward while backing which increases fuel consumption. Because the torque converter is forced to rotate forward while rotating backward until an enough torque is built up to move the loader forward. Phase 5 is the motion towards the load receiver, which is simply going towards the truck to unload the bucket. It starts when the loader starts moving forward and the operator starts steering the loader in a classic V-pattern for short cycles. It ends when the loader arrives to the truck in an angle that allows him to unload the bucket. If phase 3 was done correctly according to the operator estimation, the loader arrives the truck with a sufficient height that can allow the operator to unload the bucket without hitting the truck. Typically experienced operators can quickly change the height of the bucket to reach an appropriate height. Phase 6 is the bucket-emptying phase. It is the phase where the operator attempts to unload the bucket to the truck. The operator drives the loader slowly forward towards the truck slowly while at the

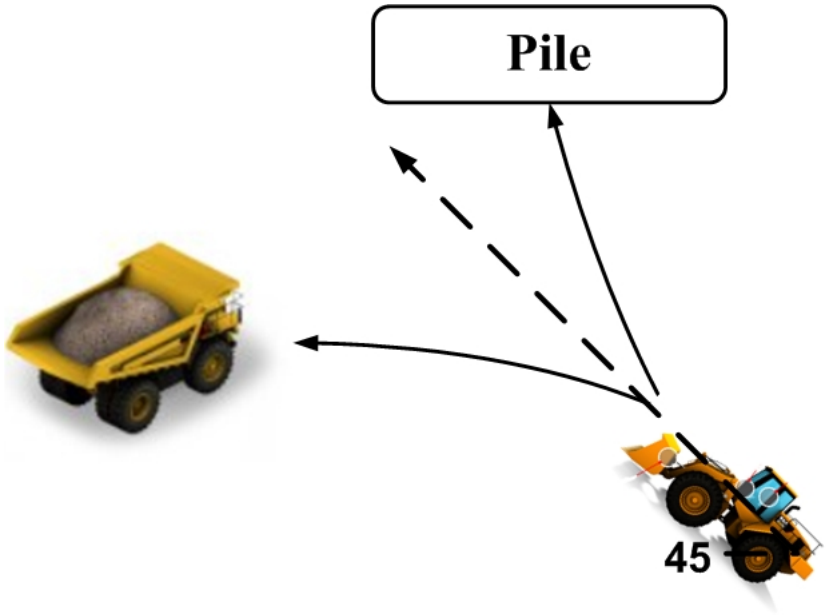


Figure 5. Short loading cycle [3].

same time lifting the bucket. The operator tries to place the load so the truck would be evenly loaded without spillage.

In this thesis a virtual operater model is devolped based on event-driven approach, the model is adaptable to basic variations in workplace layout and machine capability. With this, a human element can be introduced into dynamic simulation of complete machine operation, giving more relevant answers with respect to total machine performance, fuel efficiency, and possibly even operability in complete loading cycles.

In [5] optimal bucket filling stratiges for autonomous vehicle operations were discussed.

In [6], Singh provides a study for the automation progress in earthmoving systems. The Author divided the cycle of earthmoving operations into three divisions. First is sensing where the machine defines its own state and the environment. The second division is planning where the machine plans the actions depending on the sensing and the description of the goal. The third division is execution where the machine executes the goal and does the pre-defined job.

In [7], Marshall presents an example of autonomous control of excavator using load-haul-dump (LHD) underground mining machine. This example was very useful for understanding the control schemes in excavation.

In [8], the Author gives an example of control schemes of automating loading of load-haul-dump (LHD) underground mining machine. The loader was modeled as a robot manipulator, with scooping forces and complete kinematic model. A trajectory of motion during scooping is determined depending on study of the forces and a simple control scheme. The goal was to find the minimum energy consuming trajectory for the edge of the bucket.

In [9], Shi et al. uses fuzzy behavior programs to control excavation process and he presents the experimental results of his model. The excavation goal is achieved by dividing the process into tasks. The tasks are specified by finite state machines that define the situation and determine which task to be executed. He also defined behavior finite state machines. The method of determining the behavior is based on fuzzy logic rules which depend on human experiences. The

results indicate that the proposed control scheme is more efficient than previous control schemes.

In [10], Ericsson and Slattengren present a model simulating forces on the wheel loader and shovels. The forces between the bucket and the material to be moved were described and the basic formulation were defined. They also defined the internal forces in the pile. The formulations can easily adapted to different types of materials. The parameters they used in the formulations are internal cohesion, density, The angle of friction of the material to be moved and finally the adhesion between the tool and the material to be moved. They used ADAMS software to implement their methodology and formulations. This analysis were used for the analysis of Volvo wheel loaders. The method have been verified with measuring the cylinder pressures while operation.

### 1.2.2 Virtual Product Development (VPD) in Construction Machinery

The following are four groups of issues considered in the design construction equipments [3], which are: First group contains size and shape requirements, the second group contains loads, torques, forces, speed and power requirements, the third group contains fuel consumption and emissions and the last group contains the parameters that define machine precision, bandwidth and repaetability. Simulation driven design requires [3] specifying the goals of the simulation, which are, reduce cost and duration of the product development. Design of construction equipment using simulation depends on using results analysis to build optimized machines [3]. The goals of the simulation had to be defined. The goals of the simulation and virtual product

development (VPD) should allow us to build machines with a robust design, better performance, higher efficiencies and better operability. In [3] Filla presents a vision of design process of the virtual product development (VPD)the focus is on analysis and optimization of overall performance and related aspects (Fig.6).

### 1.2.3 Operator Behavior Modeling

In [12] Vogel presents the overview of driver behavior in various traffic conditions. In [13] The author presents a new cellular automaton (CA) traffic model. The model incorporates the vehicle limitations like maximum acceleration and decelerations to define an accident free movement. The model also takes into consideration mechanical restrictions of the vehicles and human over reaction. Also a model for synchronized flow and the time- headway distribution of free flow is presented. The results recommend using platoon formation if vehicles to achieve free flow of vehicles.

In [14], Bengtson used the experimental results of seven different drivers participated in variety of different traffic situations. The results of the experiments were analyzed and used in determination and estimation of the driver models. The driver models were used to define an experimental platform for adaptive cruise control and driver modeling. He also described the human driver using dynamic models.

In [15], Macadam studied the role of the human driver as a primary controller of the vehicle. Basic control tasks like path-following, obstacle avoidance, and headway control are basic

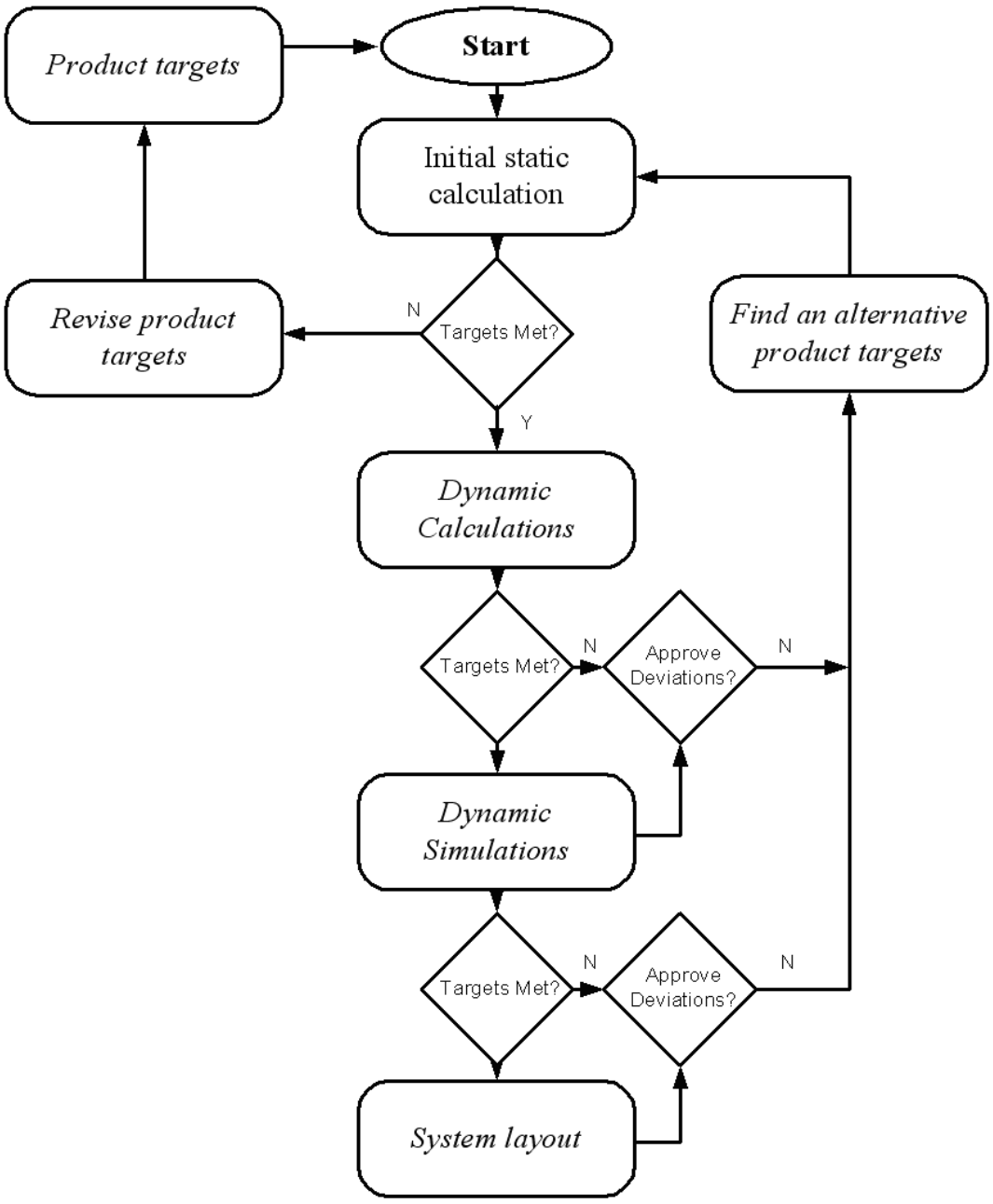


Figure 6. VPD design process [3].

control actions performed by the human. Also the physical limitations of the human driver are defined. The results were used to estimate the performance of the combined driver-vehicle control tasks.

### 1.2.4 Virtual Proving Ground

In [16], Grant presented the evaluation process of the Iowa Driving Simulator as a virtual proving ground for construction equipment simulation. The evaluation process is multi-phased. In Phase I an "open-loop" mode evaluation phase is done for the Iowa Driving Simulator as a virtual proving ground for construction equipment simulation. During this phase they assess it is ability to simulate a common wheel loader operation. They also assess the ability to test human operators while doing these maneuvers. A typical wheel loader truck loading cycle includes many directional shifts. To increase the productivity of the typical wheel loader truck loading cycle, these directional shifts must be executed at full engine throttle. Working at full engine throttle cause the acceleration and jerk level to the machine to be high enough to cause operator discomfort and can also cause material spillage. The paper presented control strategy for the transmission that can minimize directional shift times and material loss. The new strategy can also optimize the operator comfort during these transmission shifts. To optimize the operator comfort, a study of factors and the aspects of the motion produced by shifts were conducted. The Iowa Driving Simulator motion system was also used to train operators on different directional shifts strategies. The result was used to optimize the operator comfort levels. The operator feedback about the relative comfort of the strategies are gathered and

analyzed. The results gathered from the Iowa simulator was able to confirm the machine shift criteria invented by the manufacturer. In Phase II, a complete virtual proving ground that simulates the wheel loader operation was created on the Iowa Driving Simulator. A method for quantitive evaluation was developed too. The virtual proving ground included a visual model of a mine pit developed for Caterpillar, Inc. by engineers at its National Center for Supercomputing Applications Center. A 3D real time dynamic model of wheel loaders were developed. These models are able to simulate different sizes of wheel loaders to a great extent. These models were interfaced with Iowa Driving simulator and the mine pit visual model. They used the combination of these models to simulate frequent changes in the wheel loader designs and to prove it virtually before building prototypes. A comparison between test results using Iowa Driving Simulator virtual proving ground environment and the actual test results in the actual proving ground is also presented. A comparison of the off-line model's predictions of machine response to swept-sinewave steering input was also shown.

### 1.2.5 Path Tracking

Hellstrm and Ringdahl present traditional path tracking algorithms [17]. They used the vehicle position information to calculate the steering commands. The steering commands are responsible for making the vehicle follow a pre-defined path as close as possible. They also presented in this paper a new path tracking algorithm that uses recorded steering commands. By using this algorithm they were able to overcome the problem of corner cutting. Their algorithm depends on behavioral paradiagram used commonly in robots. The behavioral paradiagram is divided into three separate and different behaviors. Each behavior is responsible for a different

aspect of tracking the required or the desired path. They implemented the algorithm on both a simulator for forest machines and a small-scale robot. They compared the results of their new algorithm to the traditional ones and the new algorithm showed a significant improvement in efficiency and performance.

### 1.2.6 Machine Modelling and Autonmous Control

In [22], the Author presented another example of control algorithms for a high volume construction machine. He studied the control of electro-hydraulic open centered non-pressure compensated valve system. The analysis of the study was used to evaluate the gains of implementing digital velocity servo control. The control strategy objectives was to meet the operator perceived response, smoothness requirements and to create a system that can execute the commands of an autonomous controller. The paper also presents the implementation of closed loop digital velocity control. The control was used in the racking motion of the wheel loader. The controller used PID (proportional-integral-differential) and a dynamic valve transform algorithm. The control scheme was modeled and tested in a simulation environment.

In [23], excavation operation involving different types of materials and under ground operations were discussed

In [26], the Author presented a good example of computerized intelligent excavator. The Author presented the results of implementing of an integrated, real-time, artificial intelligence based control system to achieve autonomous excavation. The control scheme is based on a new motion control strategy for excavator bucket motion through the ground. The control scheme was developed by gathering extensive test data while a big number of experienced operators

were operating the excavator.

In [27]-[40], many examples of autonomous control of various vehicles like commercial vehicles, agriculture vehicles, mining, construction, and material handling vehicles were disscused. There are also examples for different control scheme for different mobile machines like including tractors, combines, load-haul-dump vehicles, trucks, paving machines, fork trucks, and many more. The objectives for all of these examples are to reduce operational costs, improve productivity and increase safety.

## 1.3 Objectives

The objectives of this thesis is to bdevelop a virtual operator model that can

1. control, test and evaluate a virtual construction equipment before building the prototype.
2. autonomously control the construction equipment after being built.

so that virtual product development tools form a complete set, including the operator, hence reduce the iterative tests and modifications process thereby reducing the product development costs.

## 1.4 Thesis Outline

### Chapter 2

This chapter presents an overview of the construction machine which the virtual operator will control, evaluate and test. Also explain the normal operations, the tests and tasks that this machine and designed prototypes perform for evaluation.The steps followed to complete this

thesis is presented. An analysis of the human operator recorded test results and a brief explaining for the virtual machine model used in this thesis.

**Chapter 3**

In this chapter, the deveolped operator model is explianed.

**Chapter 4**

In chapter four, the results are presented.

**Chapter 5**

This chapter draws the conclusion and an outlook for future proposed work is stated.

# CHAPTER 2

# PROJECT DESCRIPTION

This chapter presents a background, the steps followed to develop the operator model, an analysis for the operator model behavior and the machine model.

## 2.1 Background

Before explaining the proposed idea and the work done, we believe it is beneficial to present an overview of the construction machine which the virtual operator will control, evaluate and test. Also explain the normal operations, the tests and tasks that this machine and designed prototypes perform for evaluation.

The machine used in this research is a wheel loader. It has various models with three main sizes small, medium and large depending on the load carrying capacity. The main function of the wheel loaders is loading. The operator controls are tilt and lift of the bucket, throttle, gear, steer and brakes.

### 2.1.1 The Truck Loading Cycle

A typical truck loading cycle can be described by the following events as shown in Figure (7). The loader starts with empty bucket on the floor. The loader then goes to the pile and digs. After digging is done the loader backs from the pile then moves towards the truck while lifting the bucket. The loader then dumps the load in the truck. The loader then backs from

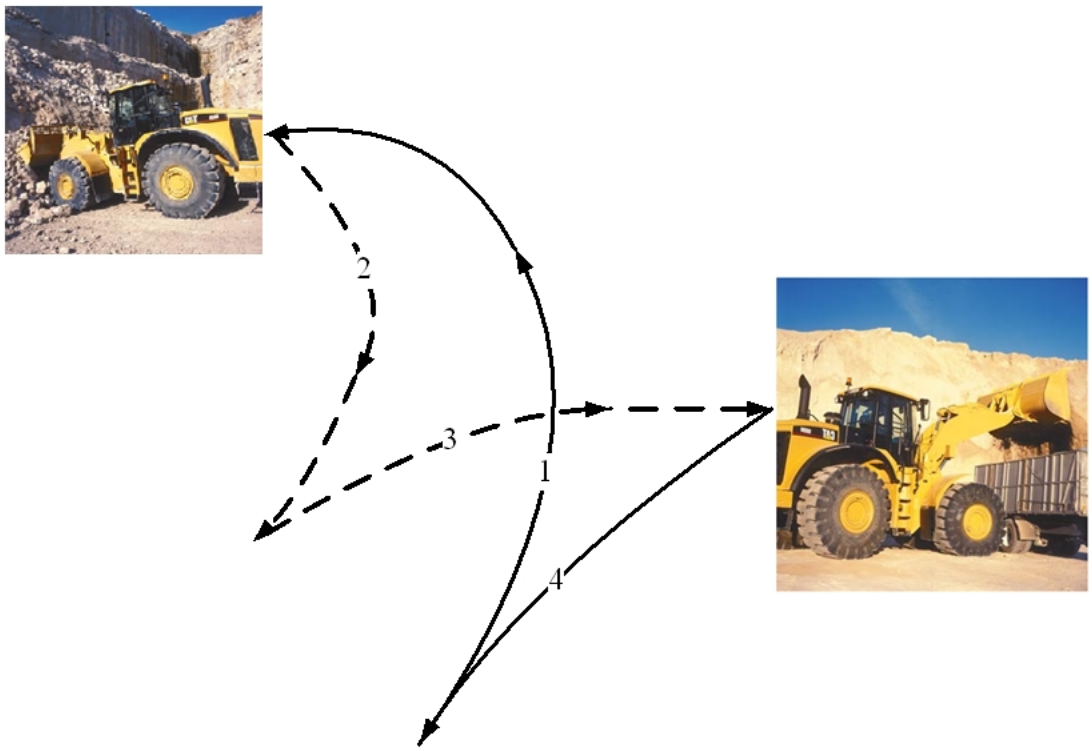


Figure 7. Truck loading cycle.

the truck while racking back and lowering the bucket. These events are repeated until the truck is filled with payload.

### 2.1.2 The Evaluation Tests

Five evaluation tests are used to determine the performance and the controllability of the wheel loaders and they are explained briefly in this section

a) Test 1: raise to a point (Figure 8). The objective is to quantify the ability to quickly

Figure 8. Test 1: raise to a point.

and accurately raise a load to a given height. The machine setup is full throttle, neutral transmission, parking brake ON, racked bucket, at rest slightly above ground line and the response measurements are:

1. time from start to end point (sec).

2. position error relative to target point (mm).

b) Test 2: lower to a point (Figure 9). The objective is to define the ability to quickly and accurately lower a load to a given height above ground line. The machine setup: full throttle, neutral, parking brake ON, racked bucket, at rest near full height. The response measurements are:

1. Time from start to end point (sec).

Figure 9. Test 2: lower to a point.

2. Position error relative to target point (mm).

c) Test 3: curl bucket at a given height (Figure 10). The objective is to define the ability to curl the bucket cutting edge at a given target height. The machine setup: full throttle, neutral, parking brake ON, racked bucket, lift slightly above level arms, at rest aligned with target height. The response measurements are:

1. Time from start to full dump (sec).

2. Time for return, full dump to full rack (sec).

3. Sum position error equals to sum absolute value [variation error about target arc] (mm).

d) Test 4: vertical line test (Figure 11). The objective is to define the ability to quickly and accurately control the bucket cutting edge to a vertical straight line. The machine setup:

Figure 10. Test 3: curl bucket at a given height.

full throttle, neutral, parking brake ON, level bucket, at rest slightly above ground-line. The response measurements are:

1. Time = start to upper end point (sec).
2. Sum position error up = sum absolute value [variation error about string line] (mm).
3. Time = upper end point to ground-line stop (sec).
4. Sum position error down = sum absolute value.

d) Test 5: follow a string test (Figure 12). The objective is to define the ability to control the bucket cutting edge to follow a taught string line as accurately and quickly as possible while traveling rough terrain. The machine setup: 1st gear, forward, carry position, full rack-back, align cutting edge with string both start and end. The response measurements are:

Figure 11. Test 4: vertical line test.

1. Time = start to full dump (sec).

2. Sum position error = sum absolute value [variation error about string line] (mm).

## 2.2 The Steps Followed to Develop the Virtual Operator Model

- Analyze the previous recorded data of wheel loaders testing.
- Determine the main sub tasks done by the wheel loaders operator.
- Experimental testing of the wheel loaders.
- Analyze the operator behavior through different tasks while testing.
- Develop the virtual operator model.
- Testing the virtual operator model results against experimental results.

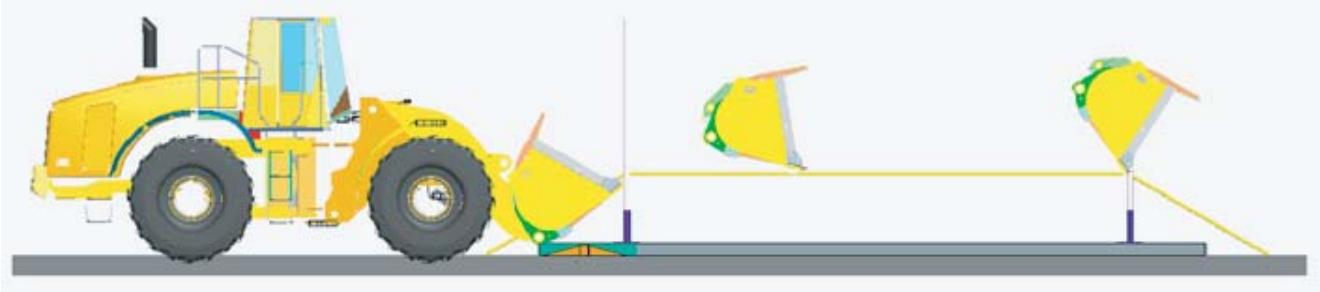

Figure 12. Test 5: follow a string test.

## 2.3 Analysis of Operator Performance

The operator behavior in the recorded data of testing and normal operations was analyzed with a software package, which is specialized in interpreting human behavior (Fig. 13). The purpose of this analysis is to determine the operator decisions while operating the machine. It was found from the analysis that wheel loader operations can be divided into nine tasks, which are the following:

- Lift to a point.
- Lower to a point.
- Dump the load.
- Rack the bucket.
- Backing from the truck.
- Approaching the site.

- Filling the bucket.
- Backing from the site.
- Going to the truck.

All the wheel loader operations use these tasks to accomplish the selected mission either in series or parallel. The aim now is to model these tasks then design a higher-level control algorithm to control these tasks either in parallel or series to accomplish the tasks defined in the background section. The model should modify itself to control various models and sizes of the machine without required change in the model by the user.

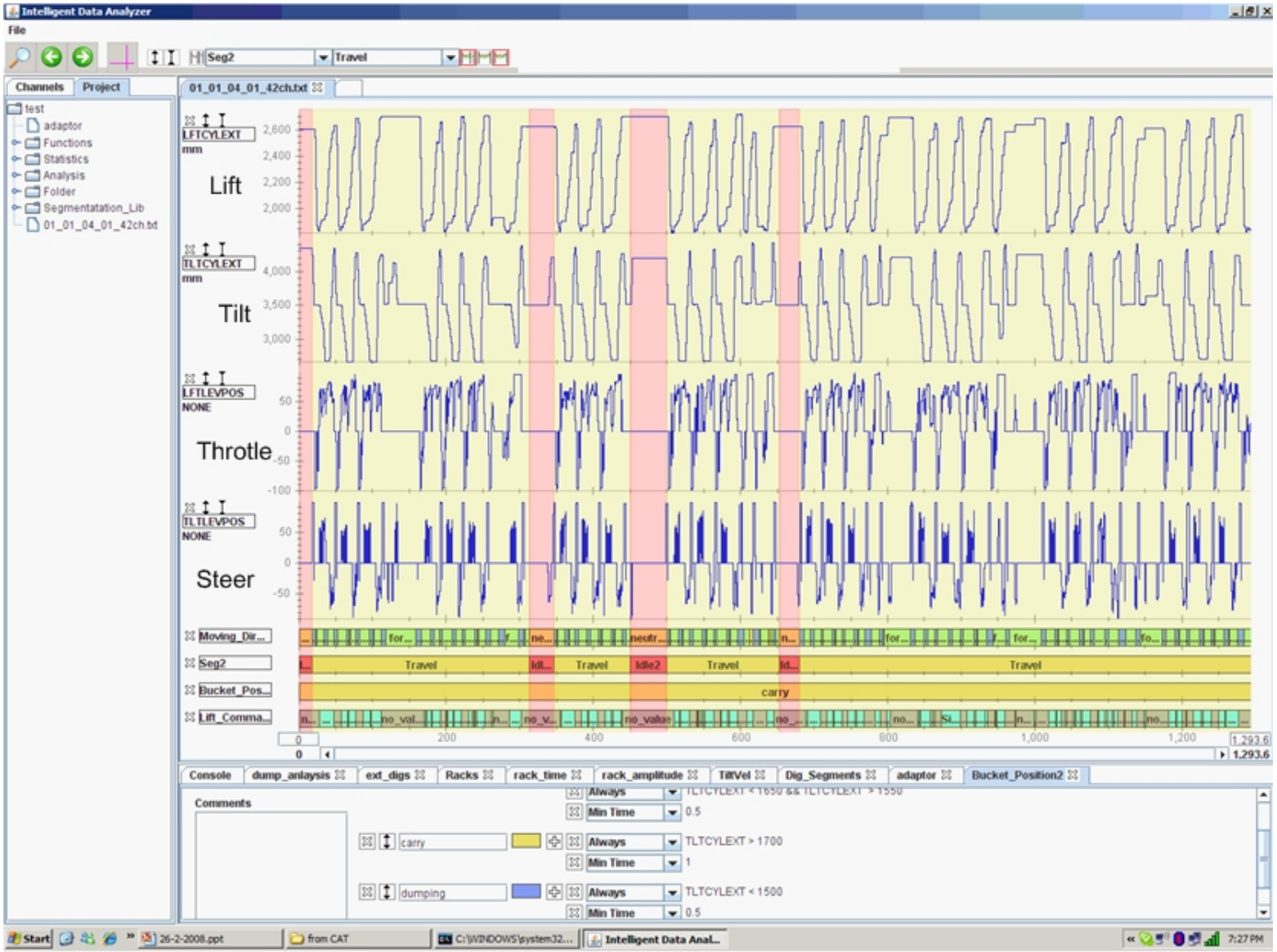


Figure 13. The software package used to analyze the human behavior.

## 2.4 The Machine Model

The wheel loader model illustrated Figure (14) is a three dimensional body with tires model that simulates a medium size articulated type wheel loader mainly used for digging gravel, mud and rocks with different grain sizes. The wheel loader has an articulated type steering, which enables the vehicle to turn by articulating the front and rear frames about the hitch point. The wheel loader can be divided into four subsystems: 1) power train, 2) brakes, 3) steering, and 4) hydraulic implements. The power train consists of a power source, which is typically a diesel engine. Power transmitted to a mechanical transmission via a torque converter, which connects to differential drives and finally tires.

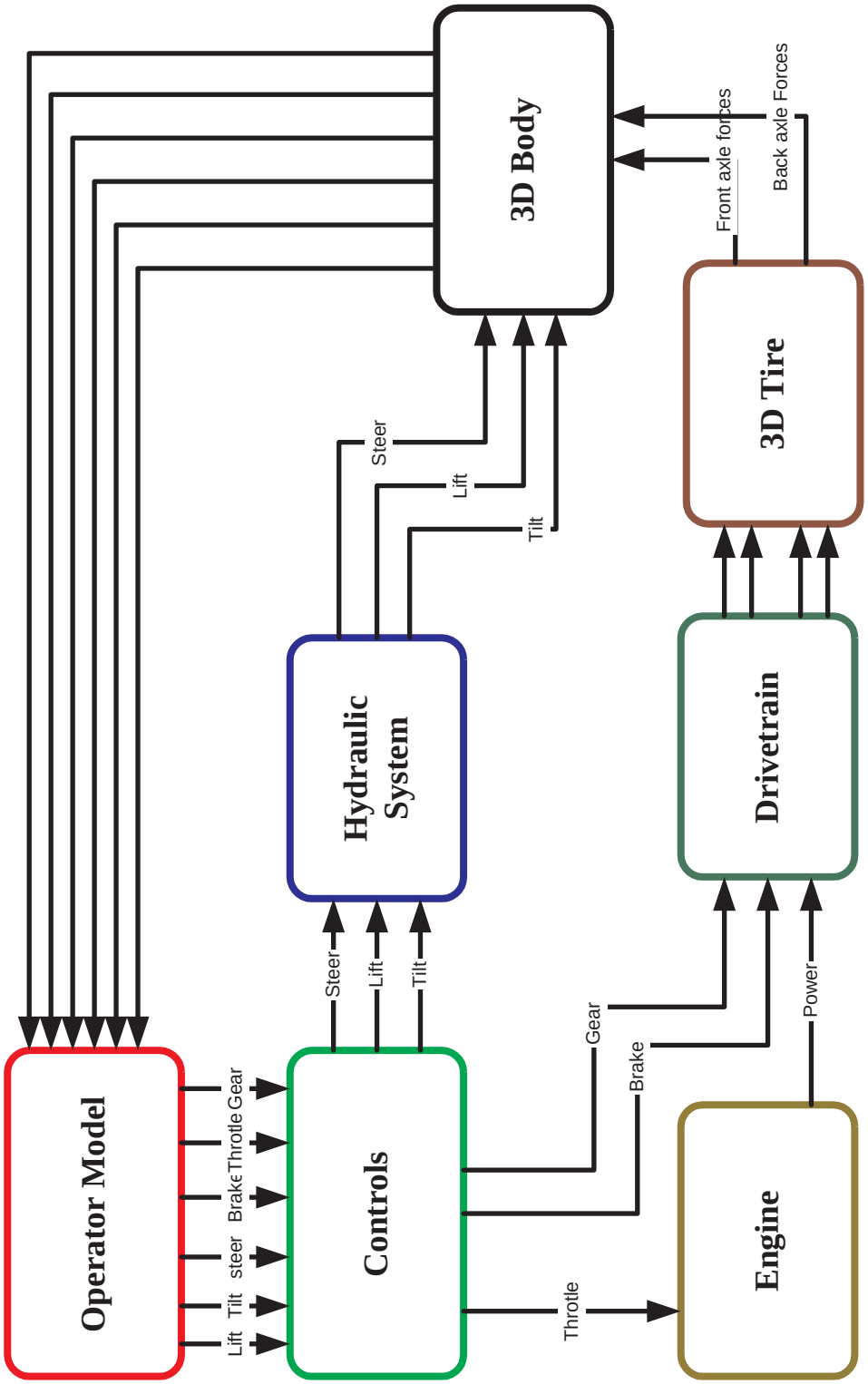


Figure 14. The machine model schematic.

### 2.4.1 Virtual Machine Model in Dynasty

In this section we explain the machine model created in Dynasty environment.

The top level of the wheel loader model as done in Dynasty software is shown in figure (15). The SIMINTF1 block is the interface with operator model (implemented in Simulink/Matlab environment). The current figure shows six signals input to the operator model. The six signals are position of the multi points in the wheel loader read from the linkage block. The operator model outputs sic signals to the super control block. the six signals are throttle, brake, gear, steer, lift and tilt. The throtle and the brake signal are from 0 to 100%. The steer, lift and tilt signal are from -100% to 100%. The super control block gives throttle signal to the super power block, two signals (brake and gear) to the super powertrain block and three signals (steer, lift and tilt) to the super hyd_sys block, which represents the hydraulic system. The drive train block gives four signals to the tires block, which represent the torque for the four wheels of the vehicle. The super linkage block receives two signals from the tires block, which are the front and the rear axles forces on the body. The super linkage block also receives three signals from the hydraulic system, which represent the steer, lift and tilt hydraulic cylinders forces on the body. The top level contains the fluid block and the ground block. All the information about the fluid used in the hydraulic system is defined in the fluid block. The ground properties are defined in the ground block.

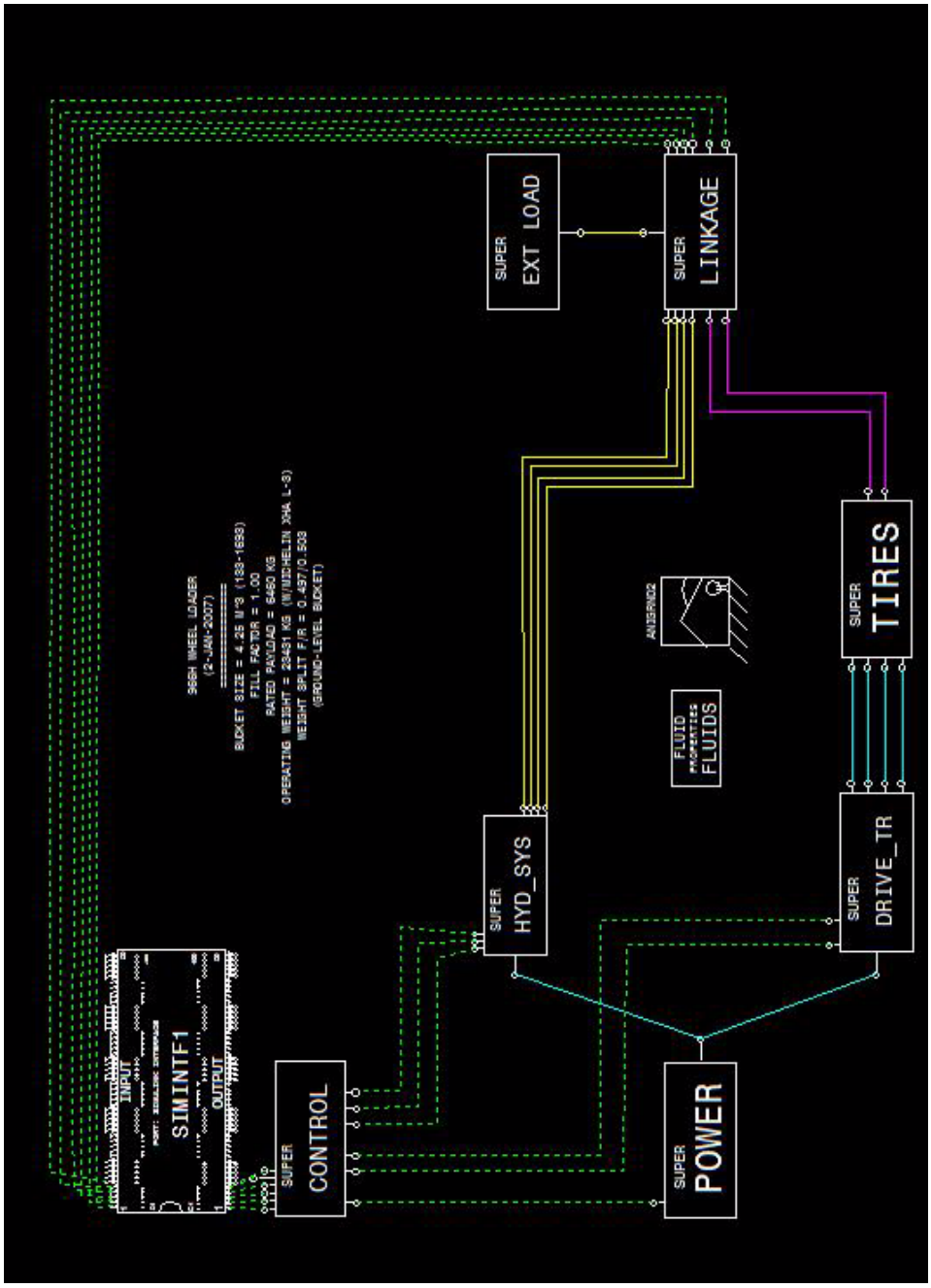


Figure 15. The Dynasty model top level.

The super control block is shown in figure 16. The super control block represents the cabin in the wheel loader. It receives the signals from operator model in percentage and converts them to scaled commands, depending on the input/output relation between the percentage and the outputs of each actuator. Using interpolation methods, the super control block converts the throttle signal to throttle opening angle, the brake signal to brake spool movement, steer signal to steer wheel angle, lift and tilt signals to lift and tilt lever movement.

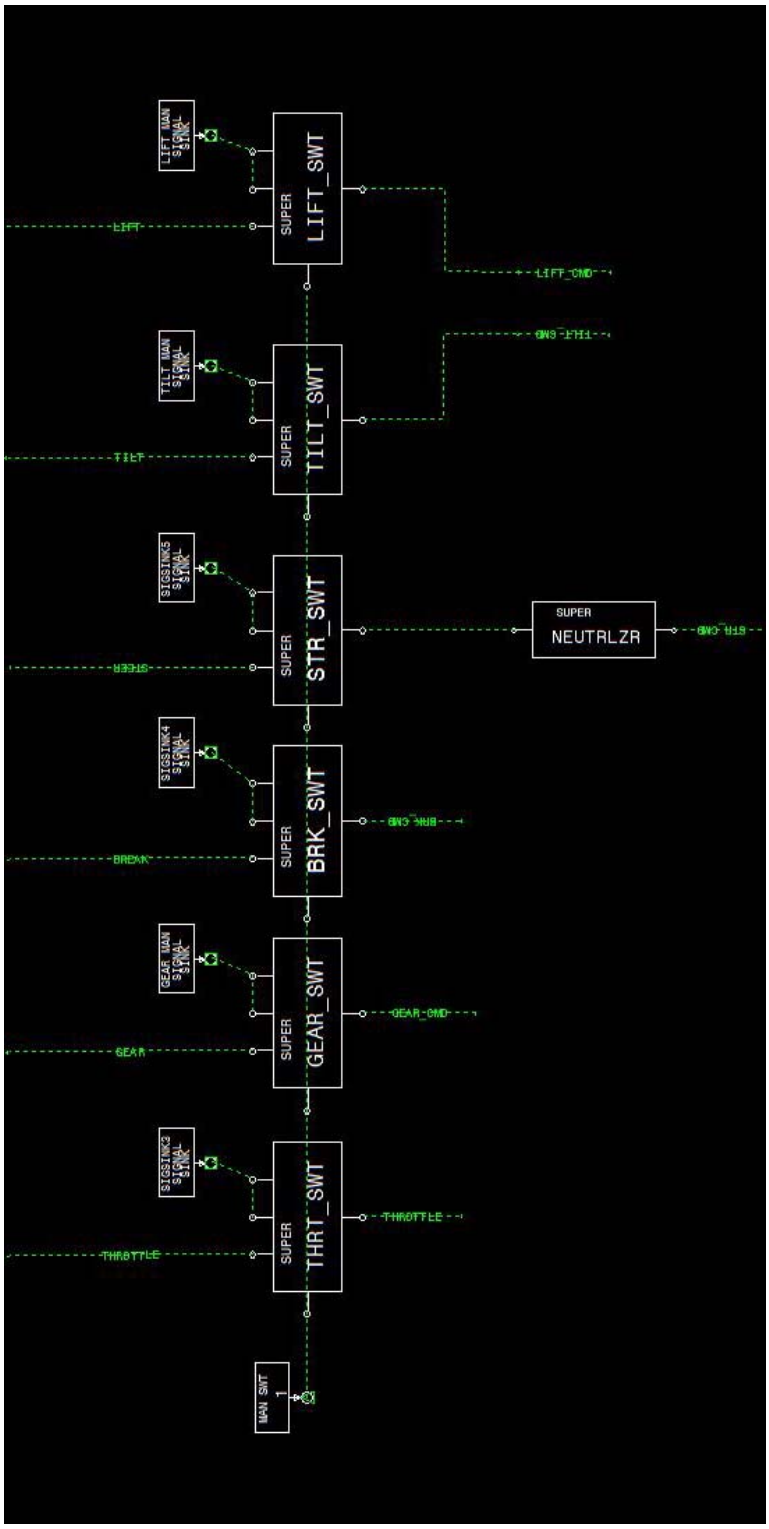


Figure 16. The super control block.

The super block for power flow is shown in figure 17. The super power block represents the engine in the model. It receives the throttle opening command from the super control block. The command is received by the engine model. The engine model used is the CAT C11 engine. More information about the CAT C11 engine is presented in the appendix. Depending on the throttle opening the angular velocity of the engine flywheel is determined. Using the angular velocity/Torque relation defined in MAAC3 load/torque block, the output torque is calculated. The super power block outputs the torque and angular velocity to the hydraulic system and the drive train models.The engine lug curve is modeled as follows.

$$1. \quad u_{fuel}(s) = G_{eng}(s)\ u_{cmd}(s) \tag{2.1}$$

$$2. \quad T_{eng}(t) = f_1(u_{fuel}(t), w_{eng}(t)) \tag{2.2}$$

where $u_{fuel}$ is the rate of fuel injected to the engine, $G_{eng}$ is a delay, $u_{cmd}$ is the throttle command, $T_{eng}$ is the engine torque and $w_{eng}$ is the engine speed.

The super drive_tr block is shown in figure 18. It represents the power train in the model. It receives the engine torque and angular velocity from the super power block and receives the gear and brake commands from the super control block. The engine torque and the gear command signals go to the super XSMN block (the gear box will be explained later). The XSMN block outputs the torque and angular velocity to the differential gear box at each wheel. The brake signal goes to interpolation curve that converts the brake command signal to brake pressure. The brake pressure signal goes to the brake pads on each wheel. The super drive_tr

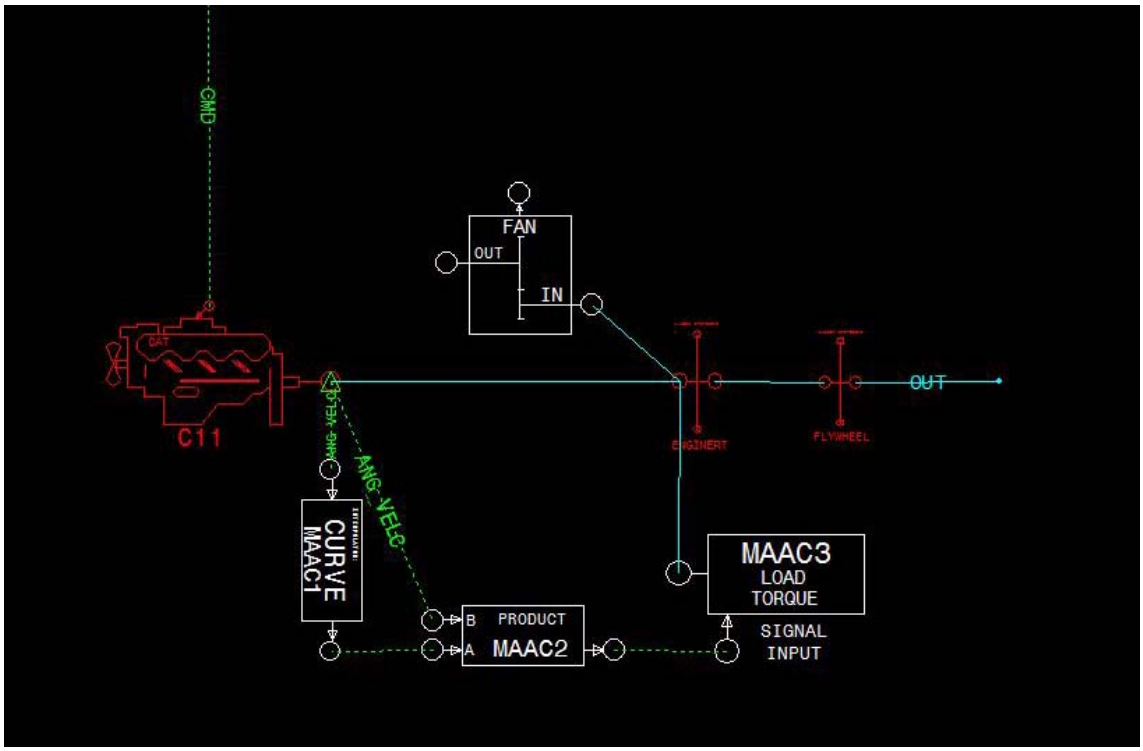


Figure 17. The super power block.

block delivers the torques and angular velocity on each wheel. The super XSMN block is shown in figure 19. The engine torque/angular velocity information is received by different sets of planetary gears. The gear command signal is received by the control unit block, which selects which set of planetary gears to be chosen depending on the load. The torque converter is modeled as follows.

$$T_{imp}(N_w, w_{imp}) = T_p(N_w) \cdot (\frac{w_{imp}}{w_{rated}})^2 \tag{2.3}$$

$$T_{turb}(N_w, w_{imp}) = N_T(N_w) \cdot T_{imp} \tag{2.4}$$

where $T_{imp}$ is the impeler torque, $N_w$ is the speed ratio, $w_{imp}$ is the impeler speed, $T_p$ is the primary torque, $T_{turb}$ is the turbine torques, $N_T$ is the torque ratio and $w_{rated}$ is the maximum rated speed.

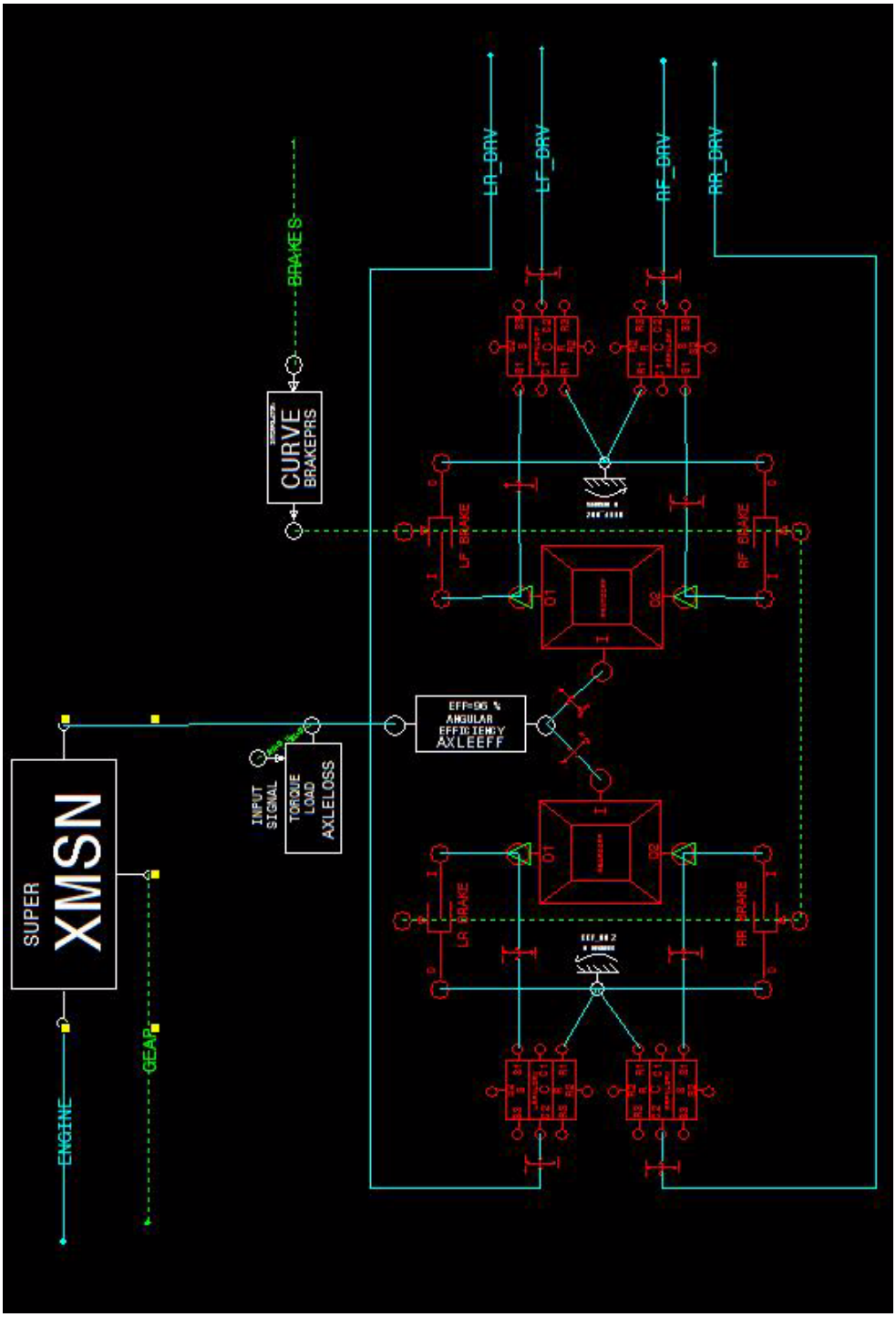


Figure 18. The super drive_tr block.

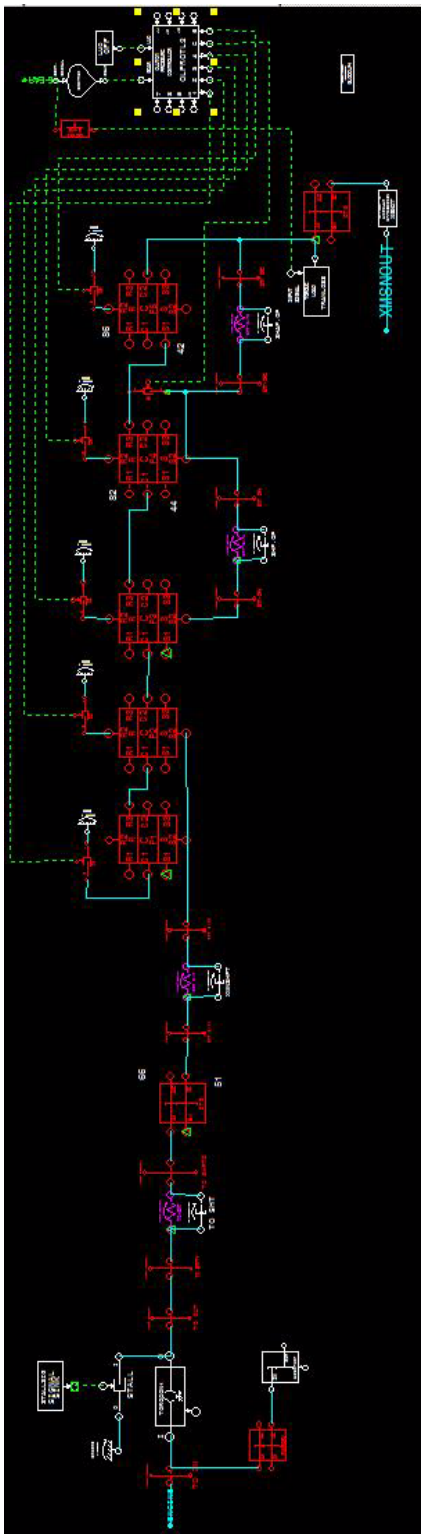

Figure 19. The super XSMN block.

The super tires block is shown in figure 20. It receives the torque and velocity for each wheel from the super drive_tr block and fed it to 3D tires model (details shown in figure 21). The 3D tires model calculates the forces and velocities in all directions. The forces of each axle is calculated and fed to the linkage block.

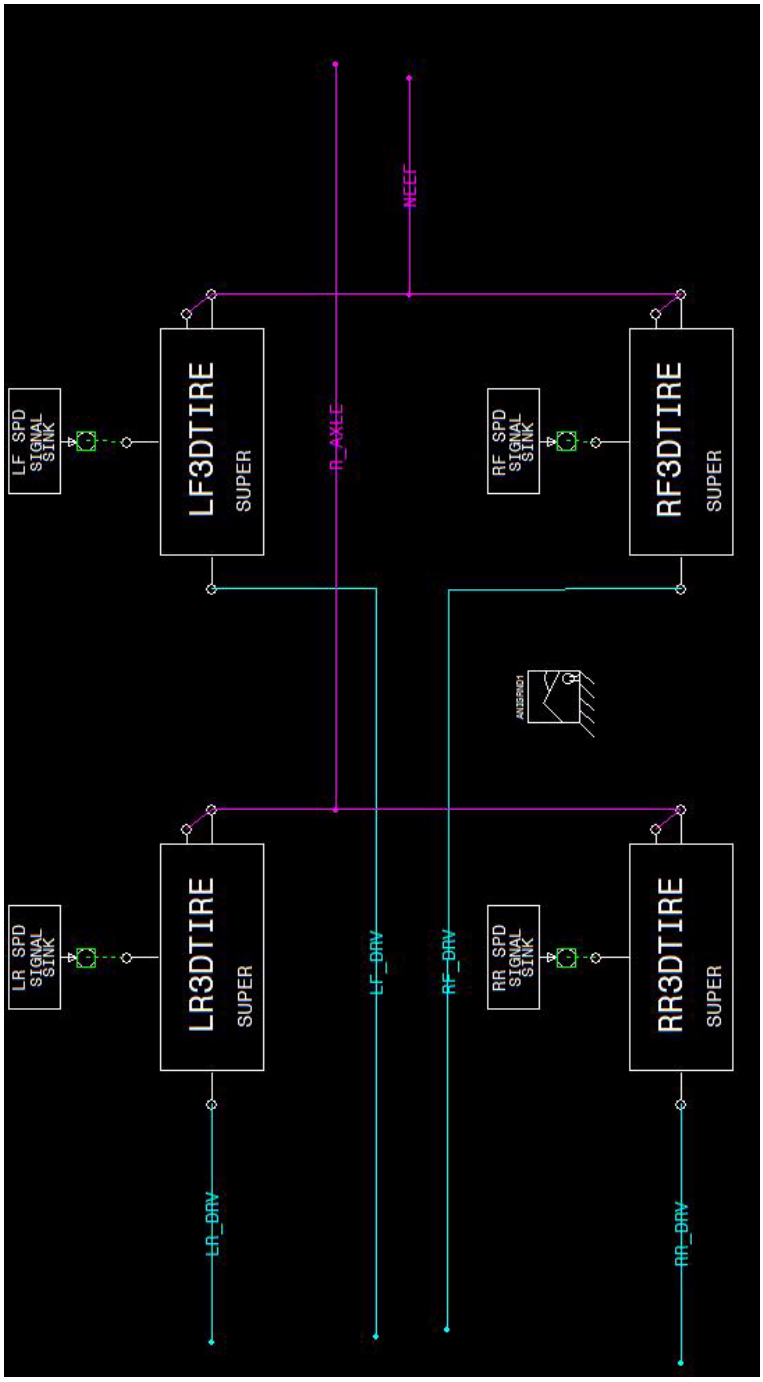


Figure 20. The super tires block.

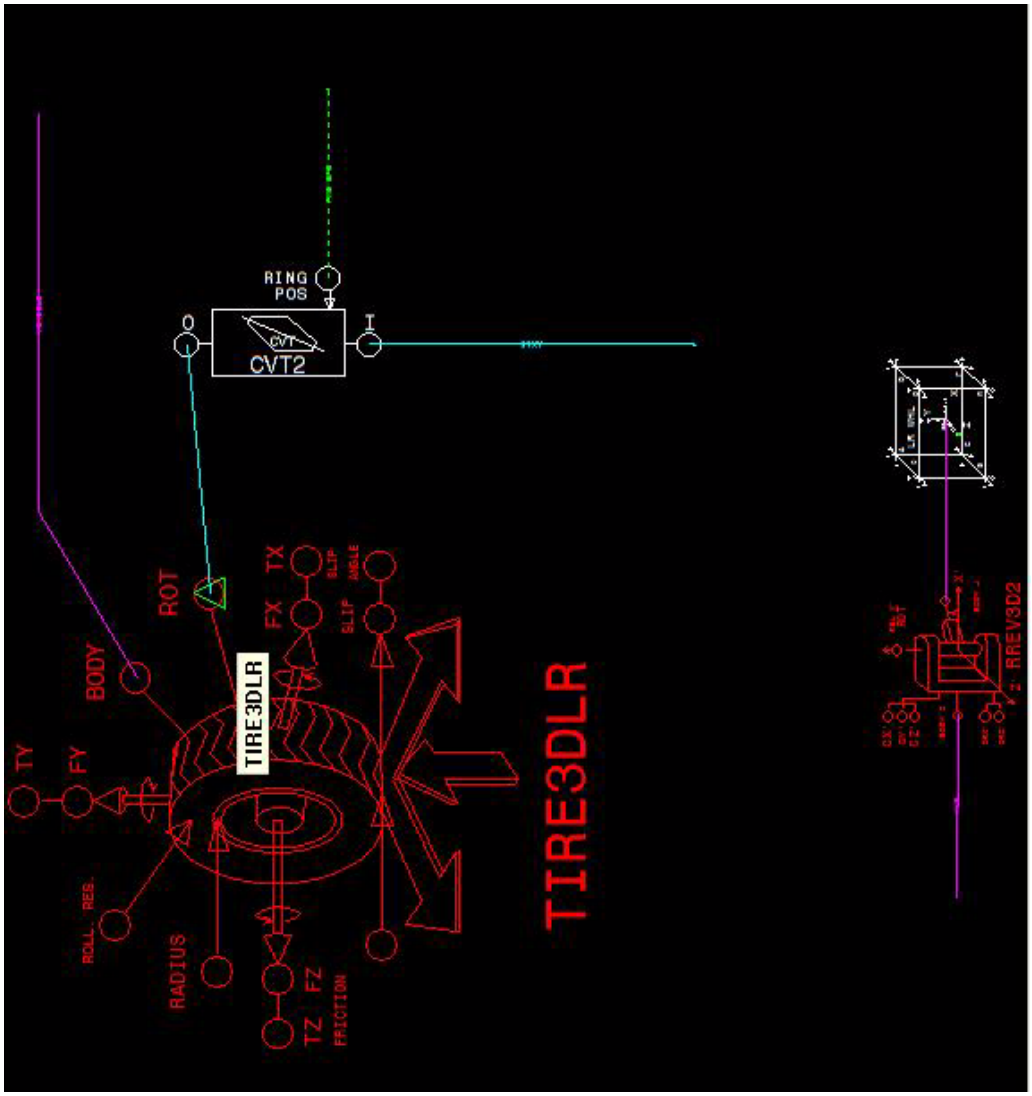


Figure 21. Three dimensional dunamic model of the tire.

The super HYD_SYS is shown in figure 22. It represents the hydraulic circuit of the wheel loader. It receives the torque/angular velocity from the super power block (CAT C11 engine) and the steer, lift and tilt commands from the super control block. The inputs are used in two different routes, one for steering circuit and the other one for the tilt/lift circuit. The engine torque/angular velocity and the steer command signals goes to the super FII STR block which determines the linear displacement of each steering hydraulic cylinder. The steering hydraulic cylinders models calculate the forces by each cylinder. For the tilt/lift circuit, the engine torque/angular velocity is received by the pump block which models the pump used and calculates the fluid pressure and flow rate. The fluid pressure/flow rate information is fed to the super M3PC which models the hydraulic valves used for tilt and lift. The super M3PC (details shown in figure 23) depending on the tilt and lift lever displacement received from the super control block. The M3PC block determines the fluid flow and pressure to the tilt cylinder and the two lift cylinders. The cylinder models calculate the displacement and the forces from each cylinder. The super HYD_SYS block delivers the steering, tilt and lift cylinder forces, displacement and velocities to the linkage block. The equation used in hyraulic circuit eguations are the following (see [5]).

$$\sum Q_{in} - \sum Q_{out} = 0 \tag{2.5}$$

$$\sum i_{in} - \sum i_{out} = 0 \tag{2.6}$$

$$\sum \Delta P_i = 0 \tag{2.7}$$

$$\sum \Delta V_i = 0 \tag{2.8}$$

$$Q(t) = C_d \cdot A(t) \cdot \sqrt{p_1(t) - p_2(t)} \tag{2.9}$$

$$\frac{dp(t)}{dt} = \frac{\beta}{V(t)} \cdot (Q_{in}(t) - Q_{out}(t)) \tag{2.10}$$

$$Q_p(t) = \eta_v \cdot D_p(t) \cdot w_{shaft}(t) \tag{2.11}$$

$$T_{shaft}(t) = D_p(t) \cdot p_p(t)/\eta_m \tag{2.12}$$

$$\eta_m = \frac{P_{out}}{P_{in}} = \frac{p_p(t)D_p(t)w_{shaft}(t)}{T_{shaft}(t)w_{shaft}(t)} = \frac{p_p(t)D_p(t)}{T_{shaft}(t)} \tag{2.13}$$

$$\eta_v = \frac{V_{out}}{V_{in}} = \frac{Q_{out} \cdot \Delta t}{D_p(t)w_{shaft}(t)\Delta t} = \frac{Q_{out}}{D_p(t)w_{shaft}(t)} \tag{2.14}$$

$$Q_m(t) = \frac{D_p(t) \cdot w_{out}(t)}{\eta_v} \tag{2.15}$$

$$T_m(t) = \eta_m \cdot D_m(t) \cdot p(t) \tag{2.16}$$

$$Q_c(t) = A_c \cdot \frac{dx(t)}{dt} \tag{2.17}$$

$$F_c(t) = A_{he} \cdot p_h e(t) - A_{re} \cdot p_{re} \tag{2.18}$$

$$Q_{leak}(t) = f(\Delta p(t)) \approx K_{leak} \cdot \Delta p(t) \tag{2.19}$$

$$\Delta p = f(l, d, \theta, RF) \tag{2.20}$$

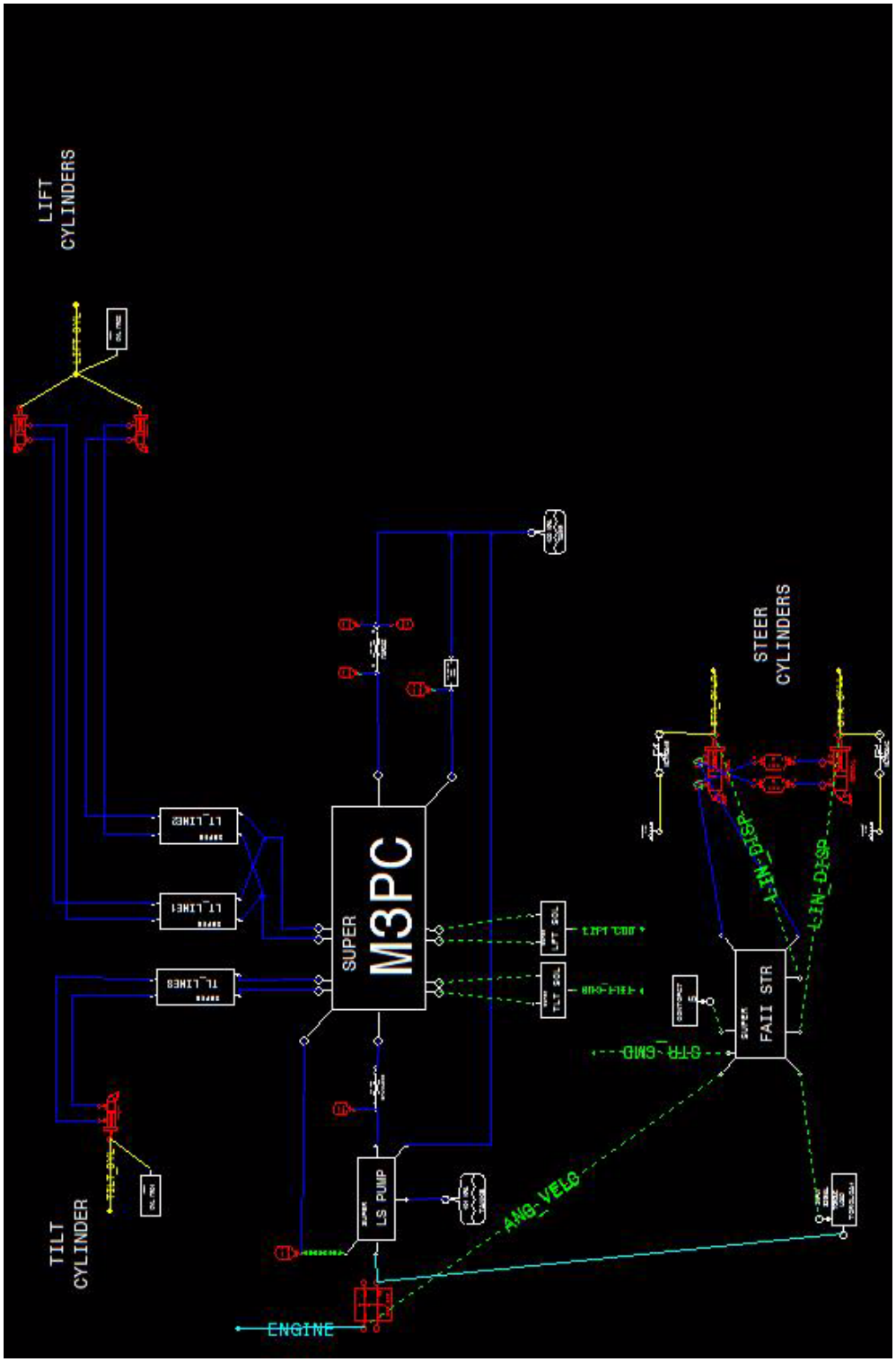


Figure 22. The super HYD_SYS block.

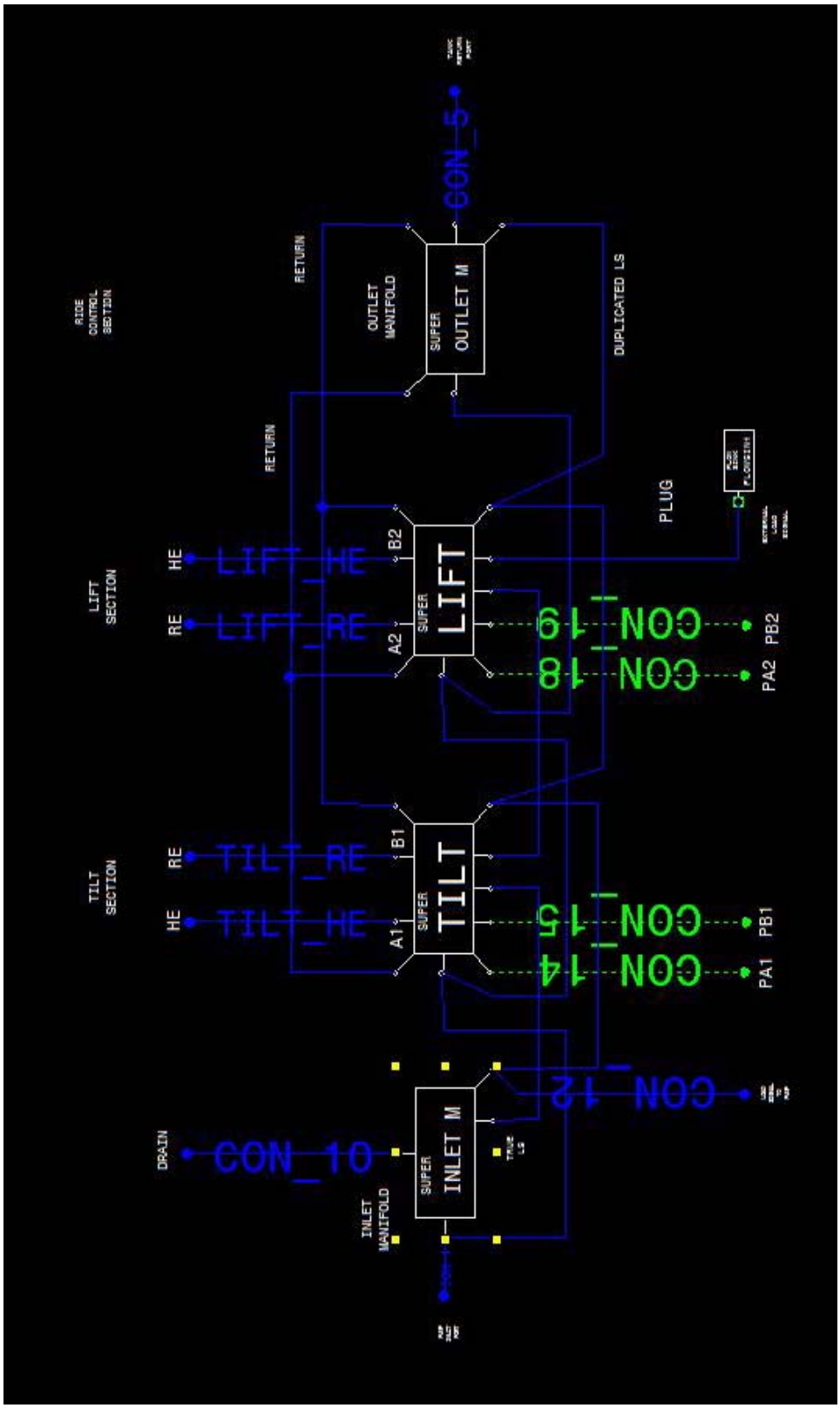


Figure 23. The super M3PC block.

The super linkage block is shown in figure 24. It represents the 3D articulated body of the wheel loader. It receives seven signals. The displacement and forces from the five hydraulic cylinders from the super HYD_SYS block and the two axles forces from the super tires block. The super linkage model consists of three blocks. The first block represents the engine end frame (EEF). The second block represents the non-engine end frame (NEEF). The third block models the Z bar details of the Super Z BAR block is shown in figure 20. The displacement and the force of the steering cylinder are received by the hinge between the EEF and the NEEF to determine the steering angle of the body. The EEF receive the forces from the rear axle. The NEEF receive forces from the front axle. The velocity, displacement, direction and position of the NEEF are fed as an input to the operator model. The super Z BAR model (shown in figure 25). It receives the displacement and forces from the tilt and lift cylinders. It feeds back the position and the velocity of the bucket back to operator model. The equation used in modeling are:

$$1. \quad m \cdot \ddot{\vec{x}}_G(t) = \vec{F}_{net}(t) \tag{2.21}$$

$$2. \quad \frac{d}{dt}(\vec{H}_G(t)) = \vec{T}_{G,net}(t) \tag{2.22}$$

$$3. \quad \vec{g}(x_i(t)) = 0 \qquad \text{connnection constraints} \tag{2.23}$$

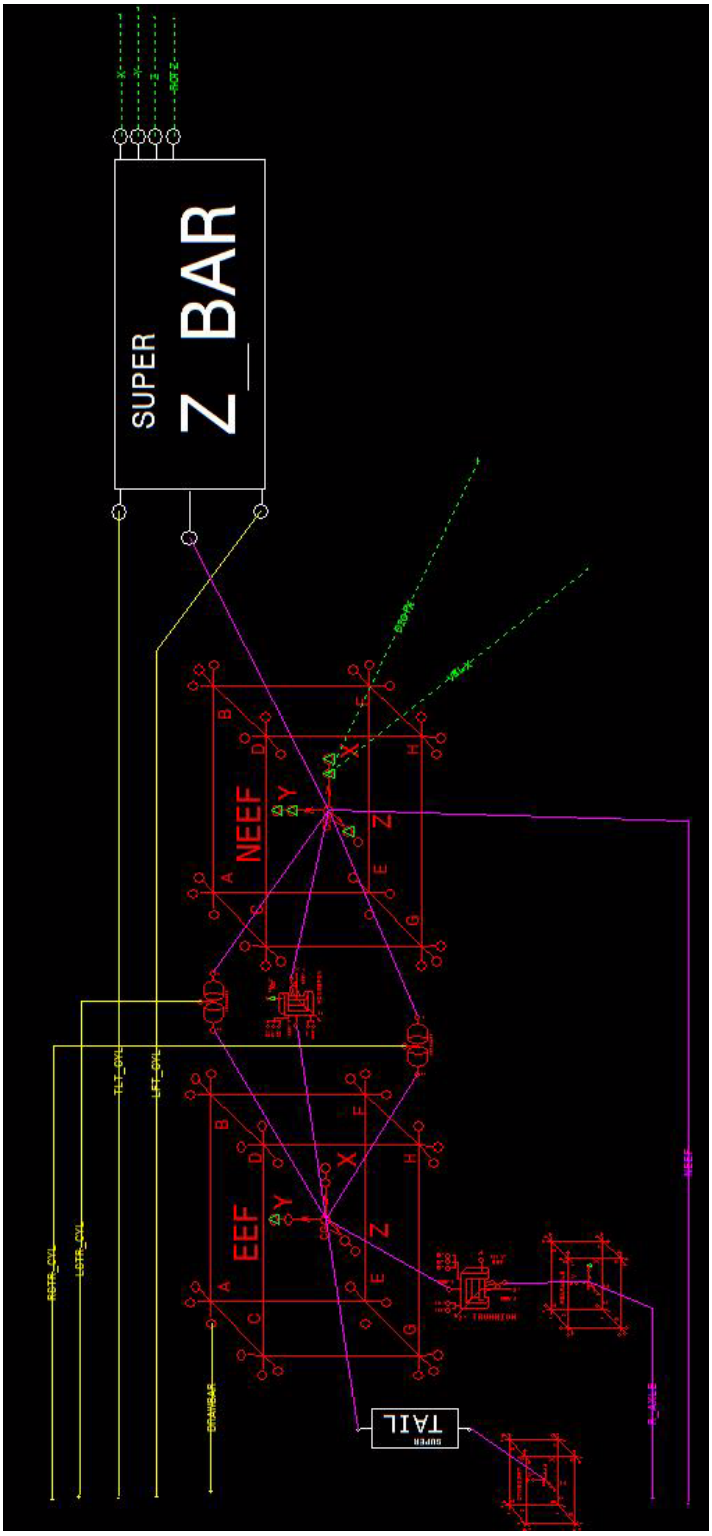


Figure 24. The super linkage block.

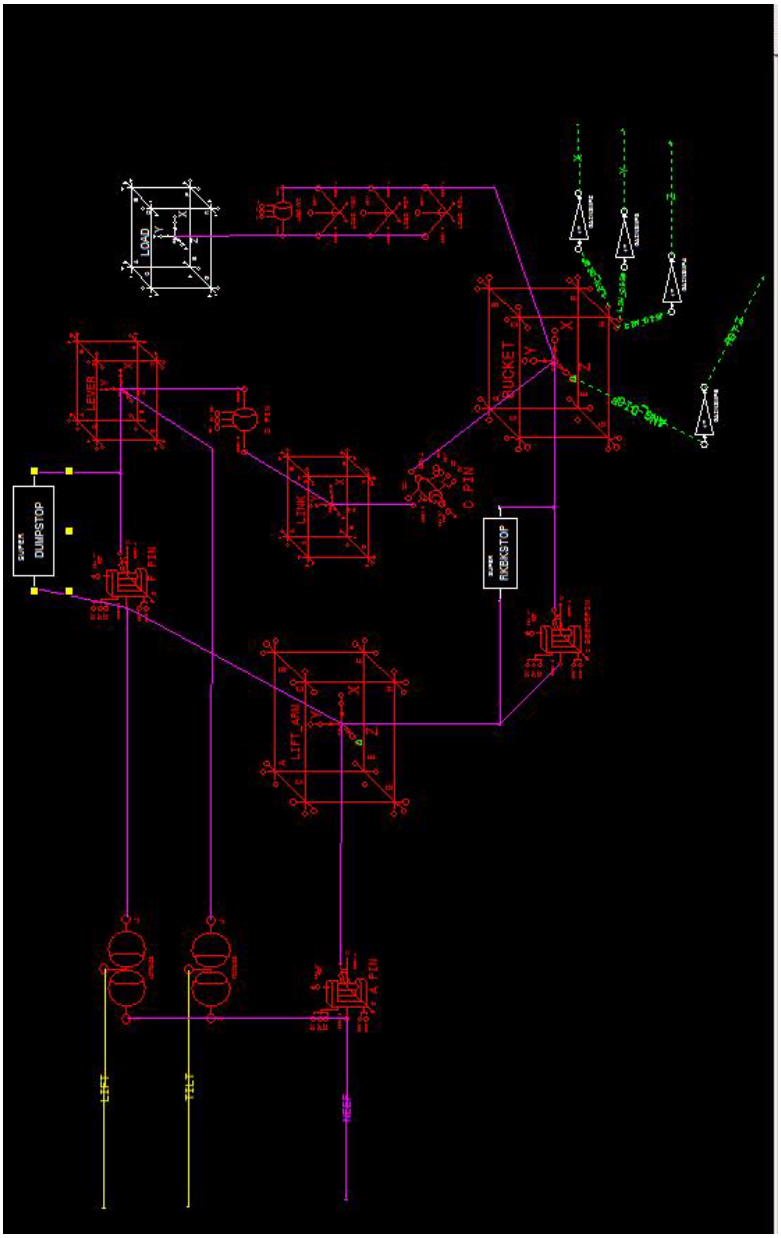


Figure 25. The super Z_bar block.

### 2.4.2 Machine Model Validation

In this section we describe how we validated the machine model. The machine model was validated through two tests

1. Test 1:

   The wheel loader is used to perform the first evaluation test. The full throttle is applied, the neutral gear is selected, the park brake on and the bucket is slightly above the ground. The human operator starts to give commands to lift and tilt lever to reach a certain pre-defined high point. After reaching the pre-defined high point the human operator gives commands to lift and tilt lever to lower the bucket to any height. This procedure is repeated three times. The human commands are recorded while testing through the electronic control module (ECM) channel. The bucket tip position is also recorded during testing. The human operators human commands recorded during testing is fed to the machine model, and compare the bucket tip position of the machine model to the actual machine results. The comparison results are presented in figure 26. The wheel loader bucket tip path is in red. The machine model bucket tip path is in blue. First the machine model was given commands through PID controller to put the bucket in a position and angle exactly as the real machine, then the human commands were fed to the machine model. We can see that the performance of the machine model is very close to the real machine. The maximum error between the two bucket tip path was 30 cm. The error was considered acceptable.

2. Test 2:

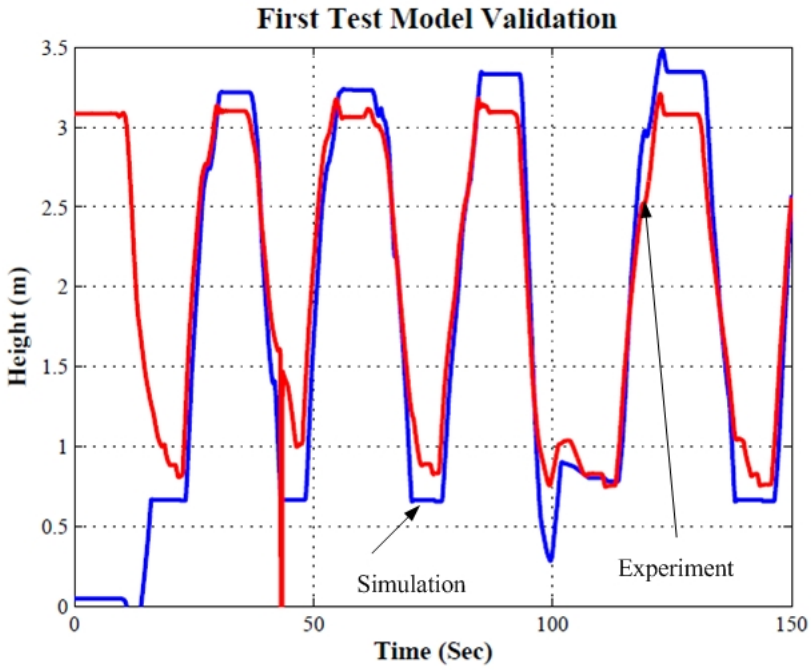


Figure 26. The first test model validation: simulation versus experiment.

The full throttle is applied, the neutral gear is selected, the park brake on and the bucket is slightly above the ground. The human operator starts to give commands to lift lever to reach a certain pre-defined point. After reaching the pre-defined point, the human operator gives commands to raise the bucket to a specific height. This procedure is repeated three times. The human commands are recorded while testing through the ECM channel. The bucket tip position is also recorded during testing. The human operators human commands recorded during testing is fed to the machine model, and compare the bucket tip position of the machine model to the actual machine results. The comparison results is presented in figure 27. First the machine model was given commands through a PID controller to but the bucket in a position and angle exactly as the real machine, then the human commands were fed to the machine model. We can see that the performance of the machine model is very close to the real machine. The maximum error between the two bucket tip path was 15 cm. The error was considered acceptable.

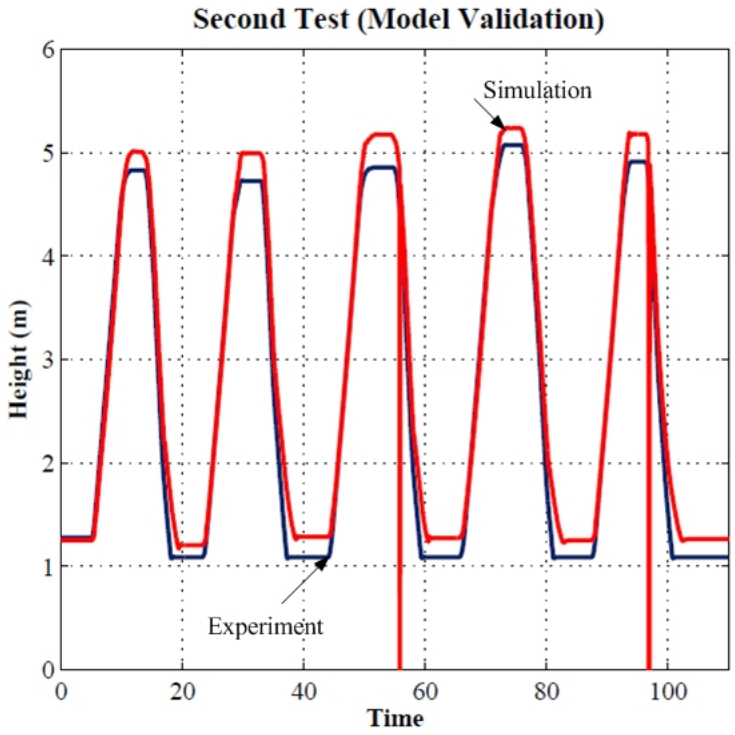


Figure 27. The second test model validation: simulation versus experiment.

# CHAPTER 3

# VIRTUAL OPERATOR MODEL

The operator model schematic as shown in figure 28 consists of two main parts: the strategy model and controllers for sub tasks. The inputs of the operator model can be categorized into 3 categories, which are the mission, site conditions and loader conditions. The output to the machine model is the human like commands based on real time feedback from sensory sources.

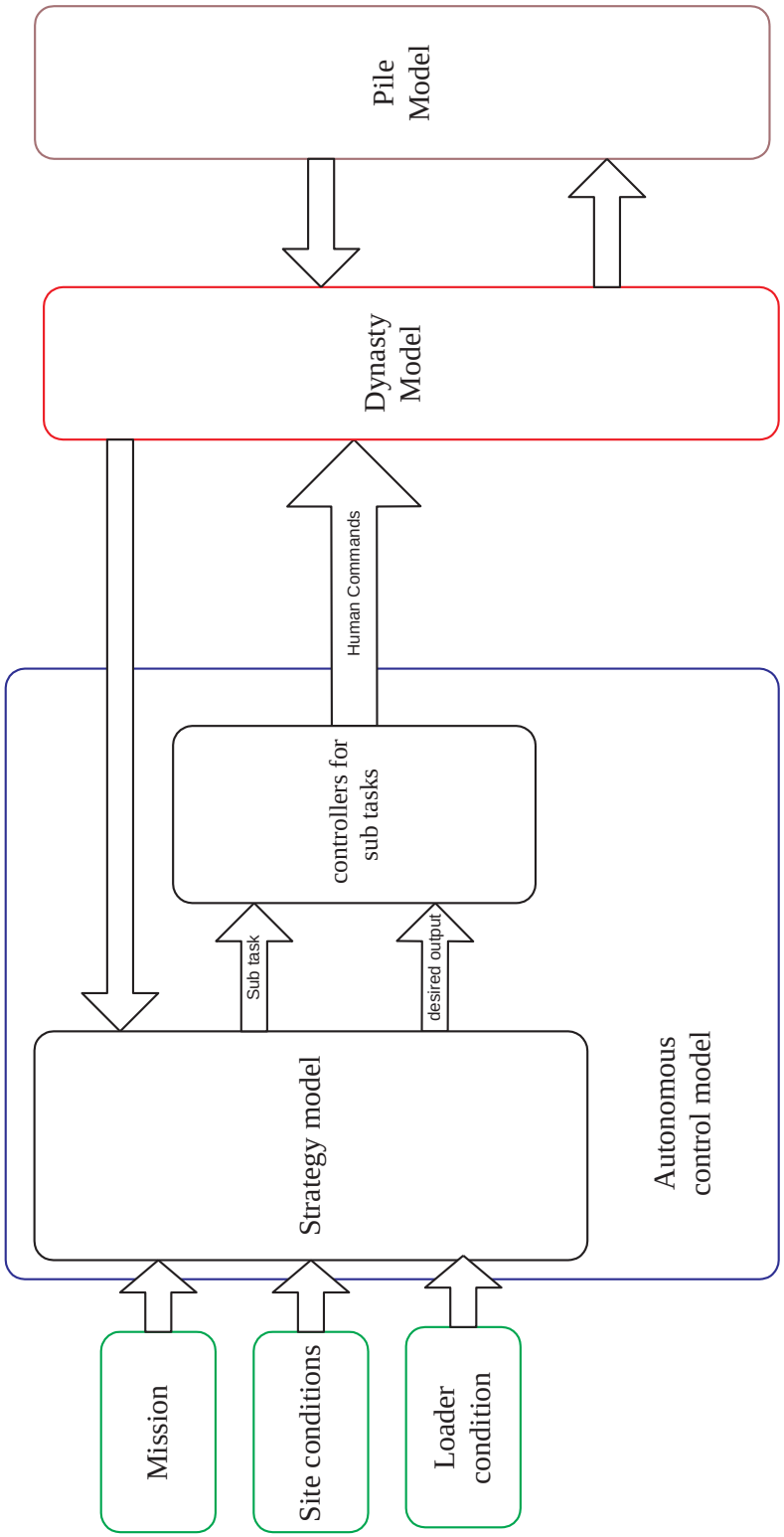


Figure 28. Virtual Operator Model Schematic.

The mission is the first category of inputs. The mission input determine the task that should be accomplished by the wheel loader, i.e. select from a complete truck loading cycle until the truck is full or a certain pre defined volume of load are loaded to truck(s), part of a truck loading cycle, or to do one of the evaluation tasks defined in the background section. The second category is the site conditions, which defines position of the truck, the position of the dig site. The height of the truck and the available space in the site for the wheel loader to travel between the dig site and the truck. This information set can be optained from GPS and construction site communication network. The third category is the loader conditions, which define the position of the wheel loader with respect to the start point of the site at the beginning, the position of the bucket with respect to wheel loader, the volume of load in the bucket, and the steering angle and the direction of the vehicle. This information set can be obtained from vehicle based sensors and GPS reciever information. The outputs of the operator model resembles the outputs of the human operator to control the wheel loader. Simply are the inputs to machine model or the machine itself which are throttle command input percentage from 0 to 100% , steering wheel angle, the gear shift, the brake command input percentage from 0 to 100 %, the lift and tilt of the bucket command input from -100% to 100 % where from -100 % to 0 for lower the bucket in the case of the lift command and tilt in for the tilt command, and from 0 to 100 % for raising the bucket in the case of the lift command and tilt out for the tilt command. The feedback from the machine model or wheel loader to the operator model is the information that can be perceived by the human operator either through gauges reading in the cabin or by his vision which are the position of the two sides of the bucket X, Y and Z, the

velocity of the wheel loader, the engine speed in revolutions per minute, the displacement or the distance moved by the wheel loader, the distance between the wheel loader and the target either was the truck or the dig site, the steering angle, the direction of the wheel loader, the volume of the load in the bucket, the speed of the tires in revolution per minute to determine slipping and the position of the external points of the wheel loader.

## 3.1 The Strategy Model

The strategy model (schematic is shown in figure 29) has the highest level of control in the operator model. It is a finite state machine model implemented in State Flow environment .The strategy model receives the inputs for the virtual operator model which are the mission, site conditions and loader conditions defined in the previous section. It also receives the feedback from the machine model. Depending on this information, it decides on the sequence of the sub tasks needed to accomplish the required mission, and selects the sub tasks to be done either in parallel or series. It can also decide if the vehicle is stable or not and if an emergency situation exists and selects the subtask which can deal with current situation. It also determines which controllers of subtasks will be used, and the desired output of the actuator. It continuously calculates the error between the desired output and the current output and decides to continue use the same controller or switch to another one.

First after selecting the mission, if it is a complete truck loading cycle or part of it, the strategy model selects the main finite state machine model. If it is one of the evaluation tests defined in the background section, the strategy mode selects another finite state machine models embedded in the strategy model, which are more suitable for the evaluation tests. Depending

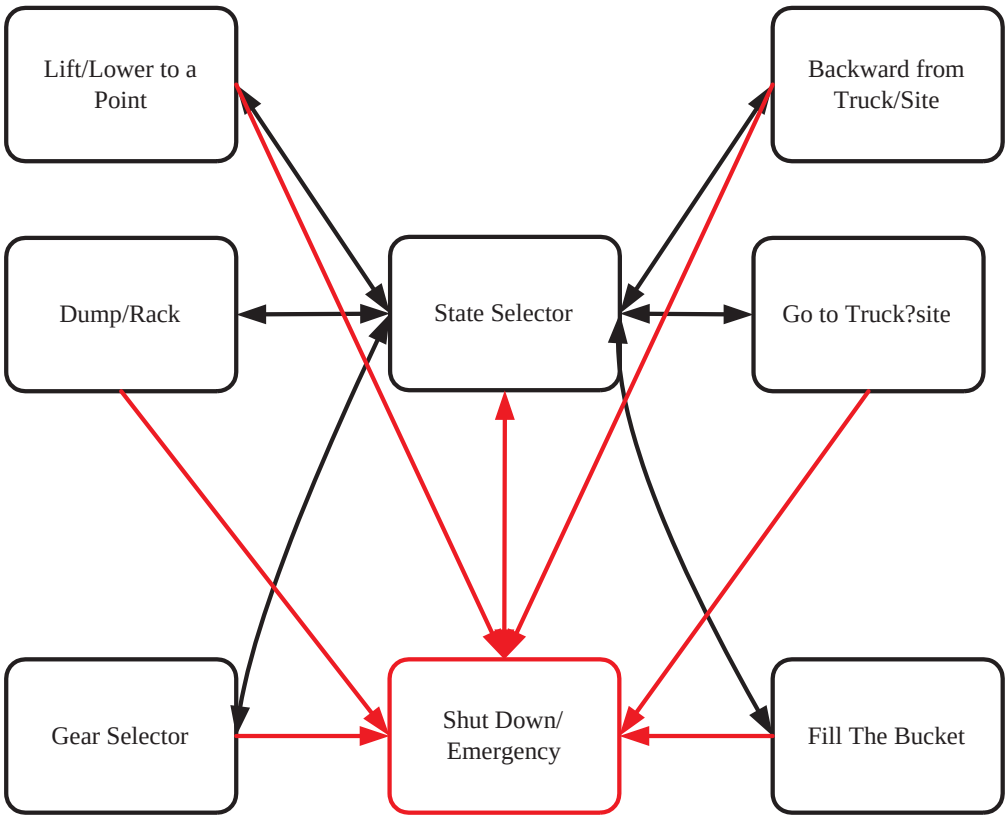


Figure 29. The Strategy Model Schematic.

on the site conditions and the loader conditions the strategy model selects the tasks to put the wheel loader in a start state and position to ease accomplish the mission required. It then selects a task from the following and the sequence needed and the tasks needed to be done in parallel and the ones needed to be done in series.

The tasks are as follows:

1. Shut down / emergency Brake or stop.

2. Back from the truck /site.
3. Go to truck/Site.
4. Lift /lower to a point.
5. Dump load /rack bucket.
6. Gear Selector.
7. Filling the bucket.

### 3.1.1 The Strategy Model Tasks

In the section we will define each tasks the inputs and outputs and their operation.

1. Shut down / Emergency Brake or Stop

   The task controls steer, brake, throttle, gear, lift and tilt. The task is responsible to shut down the operations when the mission is completed and Emergency Brake or Stop if the strategy model detects that the wheel loader is close to hit the truck or any other object in the site or if the instability of the vehicle while travel is detected. The inputs of this task are direction, velocity, acceleration, steer angle, gear, height and the angle of the bucket. This task gets signal either from other tasks directly if an emergent situation is detected by other tasks while executing them or state selector when the mission selected by the user is completed.

2. Back from the truck /dig site

   The task controls: steer, brake, and throttle. This task is responsible to back from the truck after dumping the load or to back from the dig site after filling the bucket. The


Figure 30. Selecting the path criteria.

wheel loader should back with enough distance and facing a direction, which can enable the wheel loader to easily travel to the dig site after dumping the load in the truck or to the truck after filling the bucket in the dig site.

Depending on the position of start point (the truck after dumping the load or the dig site after filling the bucket) and the target point (the dig site or the truck) the task selects a

path to take it while backing the wheel loader. The selection criteria as shown in figure 30. The task divides the field area into three parts starting from the start point where the X-axis direction is in the direction of the wheel loader and the Z-axis is the direction perpendicular to the wheel loader direction. X and Z are the coordinates of the target point with respect to the start point on X-axis and Z-axis. The first region, X is smaller than or equals twice the negative the length of the wheel loader. In this case the wheel loader backs from the truck or the site choosing path C where the steer command equals to zero. The second region, X is greater than twice the negative the length of the wheel loader and Z is greater than zero. In this case the task choose path B for the wheel loader to back from truck/dig site. In the third and last region, X is greater than twice the negative the length of the wheel loader but Z is smaller than zero. The task chooses path A. The selection of path criteria was chosen according to the experimental testing and the operator behavior analysis of the experimental testing results. The velocity of the wheel loader while backing is chosen in a range with respect to operator comfort and to prevent spilling of the load if the bucket is full. The velocity is controlled using the throttle and brake commands. The accelerating and decelerating of the wheel loader has limits to prevent shaking of the vehicle, and spilling the load from the bucket. The acceleration and deceleration limits are chosen according to operator behavior analysis of the experimental testing. This task usually works in parallel with the gear selector that will be defined later. This task is selected by the state selector only in case the user selected a complete truck loading cycle or a part from it as a mission to be done.

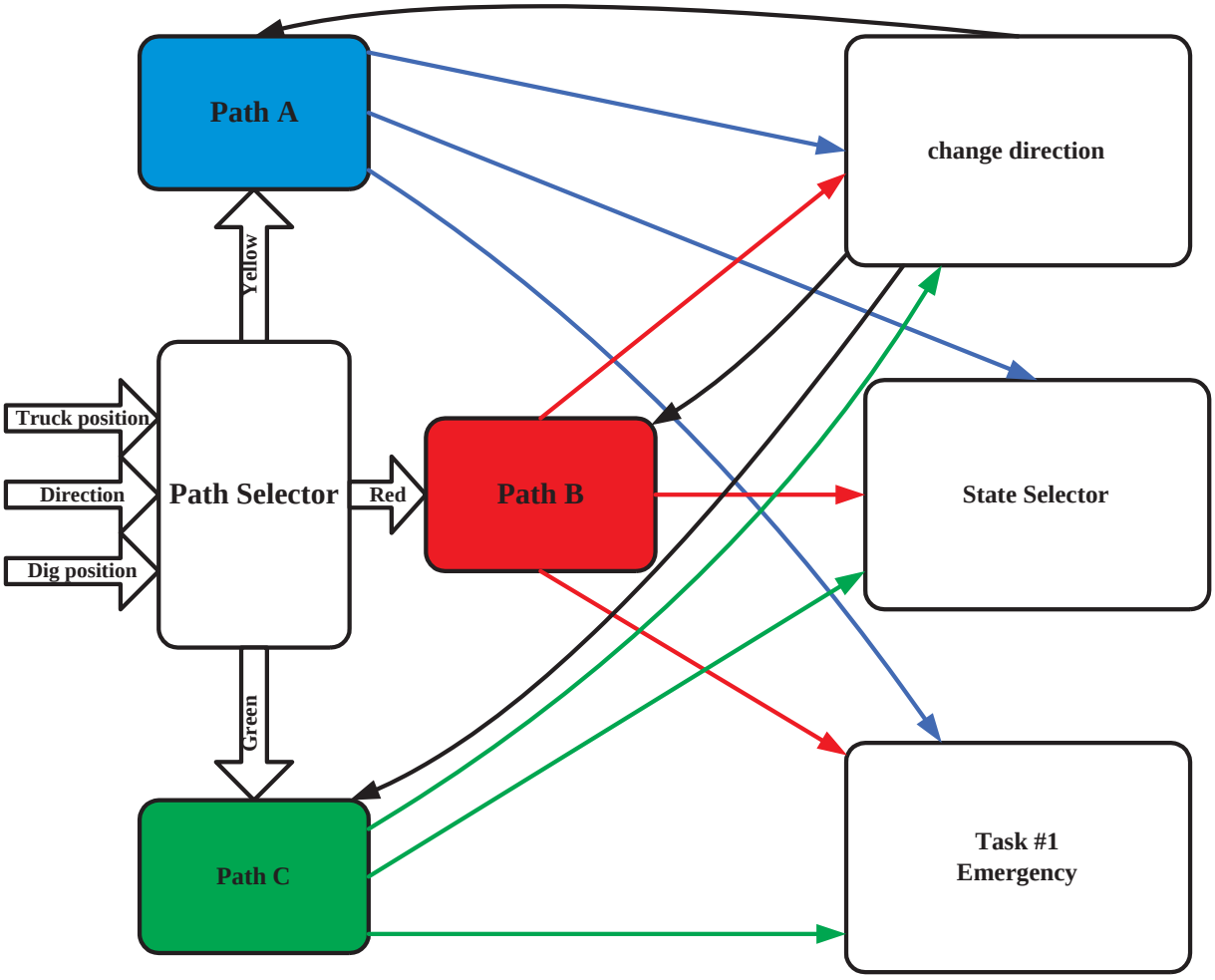


Figure 31. Back from the truck /dig site schematic.

The schematic of the task is shown in figure 31. The inputs to the task are truck / dig site position, direction, velocity and acceleration of the vehicle and outputs the steer command directly, and the desired velocity to throttle and brake controllers to control speed. The path selector chooses a path depending on truck/dig site position and direction of the wheel loader. While the wheel loader following the selected path, if it backed an enough displacement and the task is done the task gives signal to task # 3 to start. If the path is in a way to hit another object, the task change the direction to avoid hitting the object. If the tires are slipping and the controllers cant prevent it due to ground conditions the task change the direction to prevent slipping. If the wheel loader is very close to hit an object or detects an emergency the task gives signal to task #1 to start control.

3. Go to site/truck

   The task controls steer, throttle and brake controllers. The task is responsible to control the wheel loader to reach the target point (the truck to dump the load or the dig site to fill the bucket). The task controls the wheel loader to reach the truck/dig site perpendicular to its direction to ease dumping the load/filling the bucket, and using the shortest distance, with a reasonable speed that allows the fast reach to the target point. The velocity of the wheel loader was chosen to prevent the spilling of the load if the bucket were full, and to prevent the instability of the vehicle. The acceleration and deceleration ranges were chosen to allow a comfortable control of the vehicle with respect to the operator. The velocity and the acceleration ranges were chosen depending on the operator behavior

analysis while experimental testing. This task is selected if the user selected the complete truck loading cycle or a part of it and the evaluation test no 5.

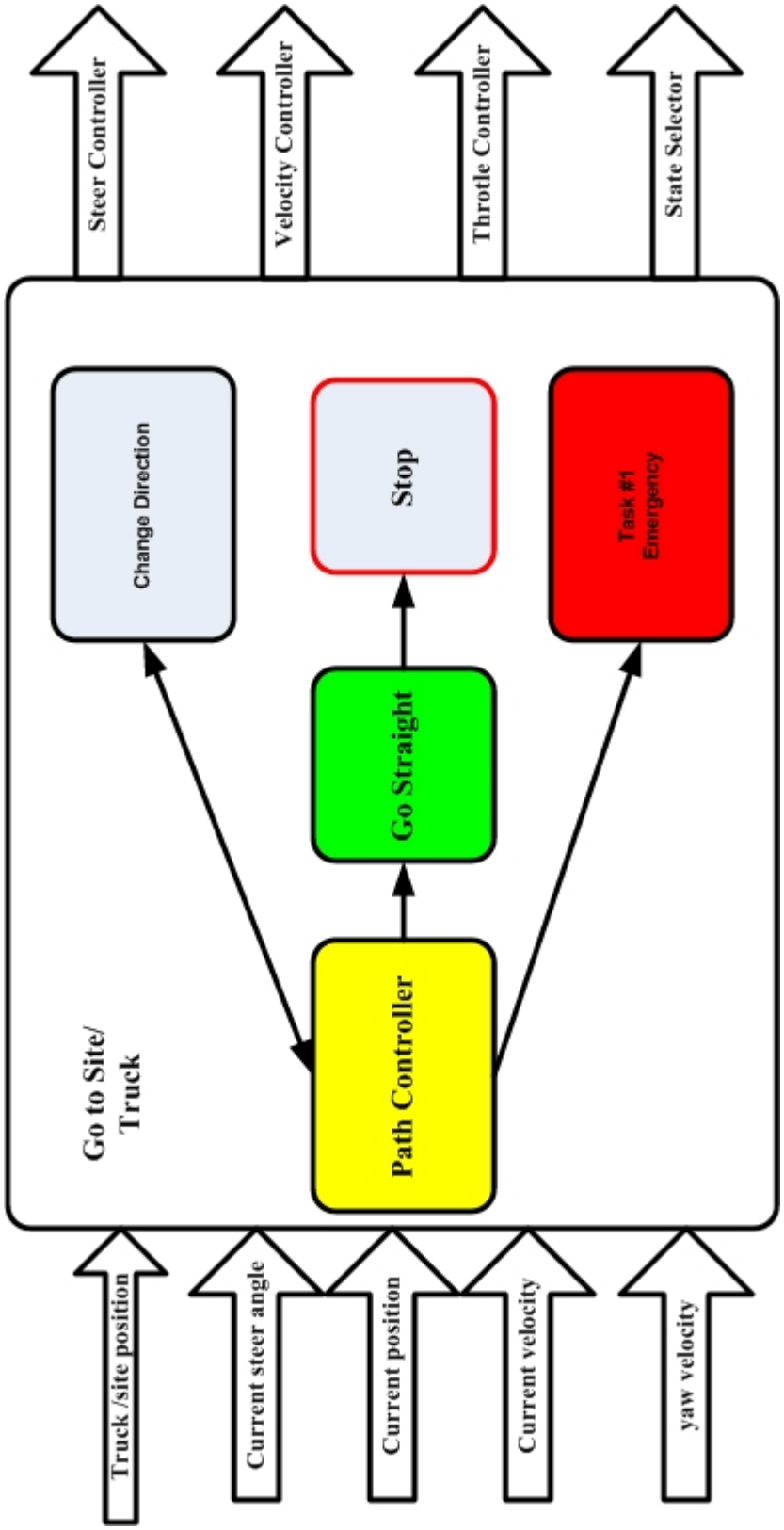


Figure 32. Go to truck /dig site schematic.

The schematic of the task is shown in figure 32. The inputs are the target position, the current position, steer angle and the yaw velocity. This task works in parallel with gear selector task and lift/lower the bucket if needed. Using the input information the path controller selects the steer controller in parallel with the velocity control algorithm to control the wheel loader to reach a point 2 meters before the target point. After reaching this point the wheel loader goes straight until it reaches the target. This way helps the wheel loader to reach the target point in a direction perpendicular on the truck/dig site direction. While the vehicle is moving in straight direction the state selector gives signal to task # 4 (lift /lower the bucket) to start in parallel to ease the start of task # 5 (dump load/ rack the bucket) or task # 6 (filling the bucket). After the target is reached, the state selector gives a signal to start the next task to be done.

The path controller continuously calculates the error between the current position and the target if it exceeds a certain limit which means the steer controller is not controlling the direction properly, the task changes the direction by giving directly a steer command bypassing the steer controller to correct the direction, then gives the control back to the steer controller. If the tires are slipping due to ground conditions the task change direction then goes back to the steer controller. When the task detects instability, very high speed, high acceleration or very close to hit an object the path controller gives signal to task #1 (emergency control) to take control.

4. Lift /lower the bucket

This task controls the lift and tilt controllers, which are the main controllers in the model.

It is responsible for the height and the angle of the bucket. This task is selected by the state selector in all missions that this operator model can do. The accuracy of this task determines the controllability of the wheel loader to a great extent.

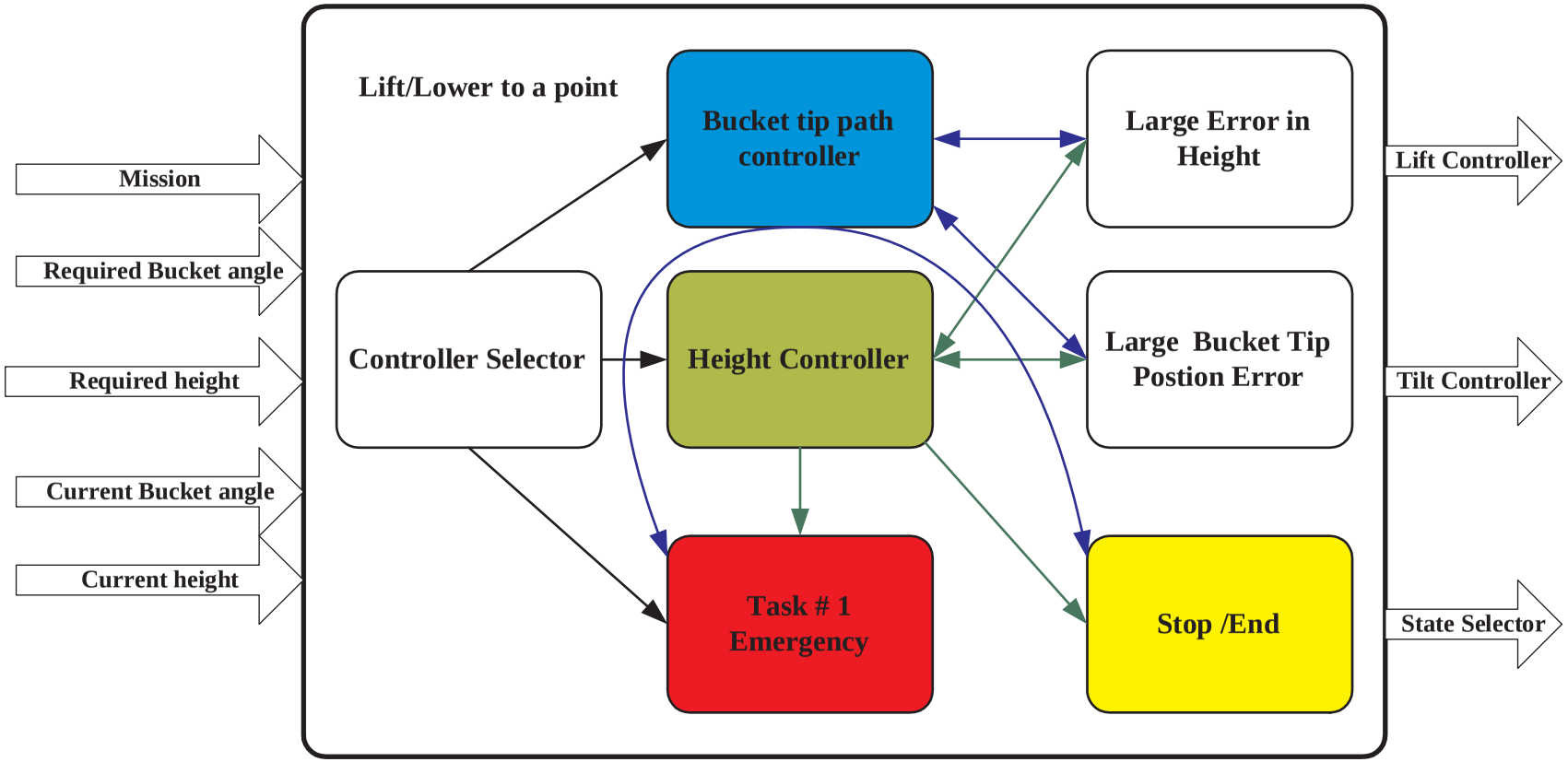


Figure 33. Lift/Lower the bucket schematic.

The inputs are the mission, current bucket angle, current height, and required height and bucket angle in the case of evaluation tests. The controller selector selects either the bucket tip path controller or the height controller depending on the mission. The height controller is selected during the complete truck loading cycle or doing a part of it and the third evaluation test. The bucket tip controller is selected in all evaluation tests. The schematic is shown in figure 33. After selecting the controller, the error between the current and the desired position and angle is continuously calculated. If the error exceeded a certain limit, this means the selected controller is not controlling the bucket properly. The task gives a direct lift /tilt command bypassing the controller to correct the direction then gives the control back to the selected controller. If the bucket tip was close to hit another object while operation, the task gives signal to task#1 to take control. This task is selected to work alone in evaluation tests or parallel with the two previous tasks in the truck complete truck loading cycle.

5. Dump load /Rack bucket

   This task controls the lift and tilt controllers, which are the main controllers in the model. It is responsible to dump the load in the truck and rack the bucket after that or evaluation test number 3.

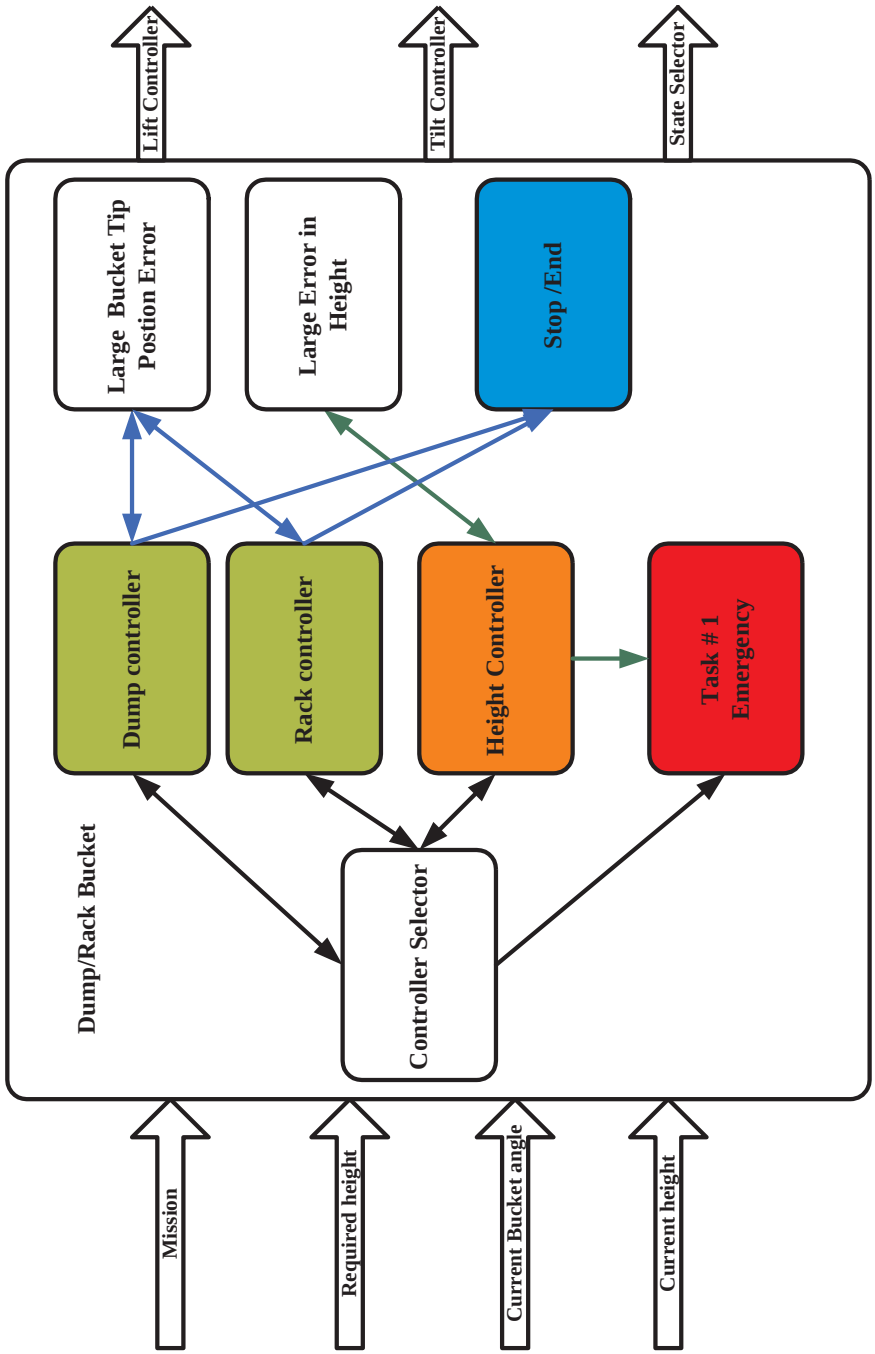


Figure 34. Dump/Rack the load schematic.

The schematic of this task is shown in figure 34. The inputs are mission, required height/truck height, current height and the current angle. The controller selector selects from height controller or dump controller or rack controller depending on the mission and the sequence of the tasks needed. The height controller is selected in parallel with either the dump controller or the rack controller. The dump controller controls the bucket angle through tilt command to fully tilt out the bucket to dump the load completely without hitting the stops or producing unwanted high vibrations in the vehicle. The rack controller controls the bucket angle through tilt command to fully tilt in the bucket. The height controller works in parallel with both controllers to control the height of the bucket tip. After selecting the controller, the error between the current and the desired position and angle is continuously calculated. If the error exceeded a certain limit, this means the selected controller is not controlling the bucket properly. The task gives a direct lift /tilt command bypassing the controller to correct the direction then gives the control back to the selected controller.

6. Gear Selector

   This task controls the gear selection only. It works in parallel with all the tasks. The schematic for the task is shown in figure 35. The inputs are the direction, the current gear the current task, engine speed in revolutions per minute and the load.

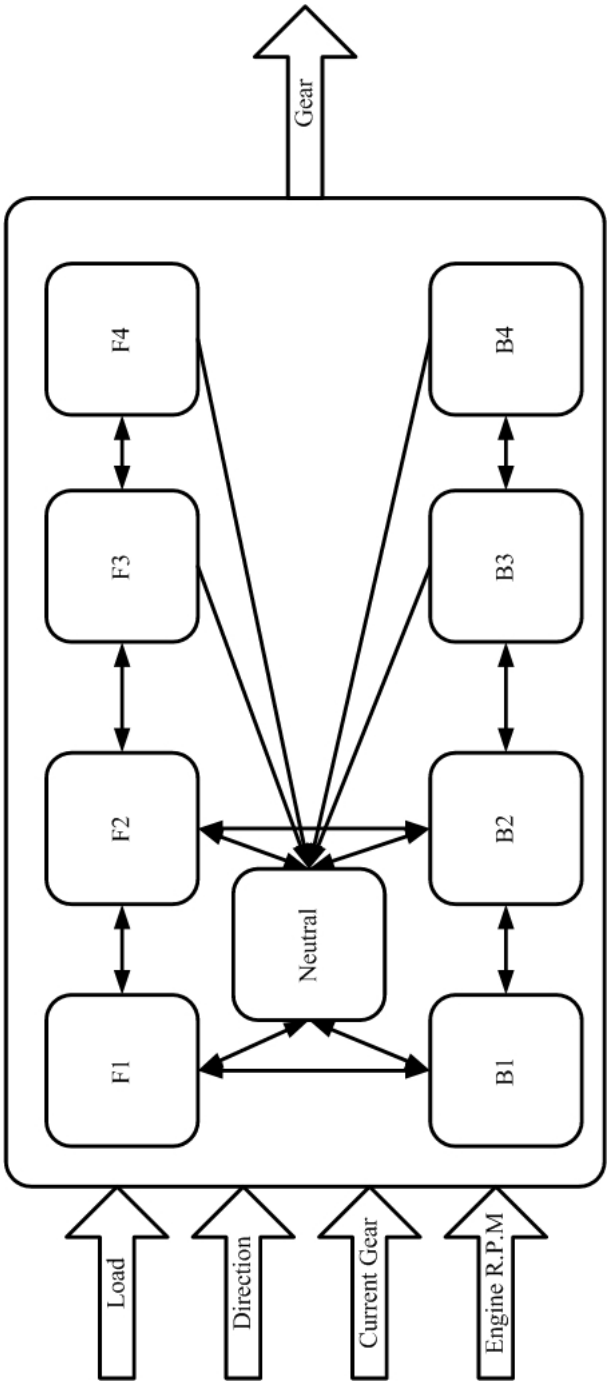


Figure 35. Gear selector schematic.

For tasks number 3 and 4 the gear selector selects the neutral gear if they tasks were not done in parallel with other tasks. If other tasks are done in parallel the gear is selected according to the other task. For task number 1 which is the emergency stop, the neutral gear is selected. The other tasks the gear is selected according to engine speed and load in the bucket.

While moving forward or backward, the gear can start from neutral to first or second depending on the load in the bucket to prevent tire slipping. If the tire slips when high torque is applied a higher gear is selected. The gear selector can change the gear directly from any shift back to neutral.

7. Filling the Bucket

This task controls throttle, gear, steer, lift and tilt controllers. The task is responsible to fill the bucket with its payload. It is the main function of the wheel loader. The schematic of the task is shown in figure 36. The inputs are load, current steer angle, current bucket height and current bucket angle.

First the task checks for the direction of the vehicle. The wheel loader should be perpendicular on the target point to ease digging and filling the bucket. If it was not perpendicular the task steer right or left. Then the steer command is set to zero while filling the bucket.

The controller selector selects between a height controller and bucket angle controller to choose a reasonable penetration angle to optimize filling the bucket. The task selects the first gear and increases the throttle to increase the digging force.

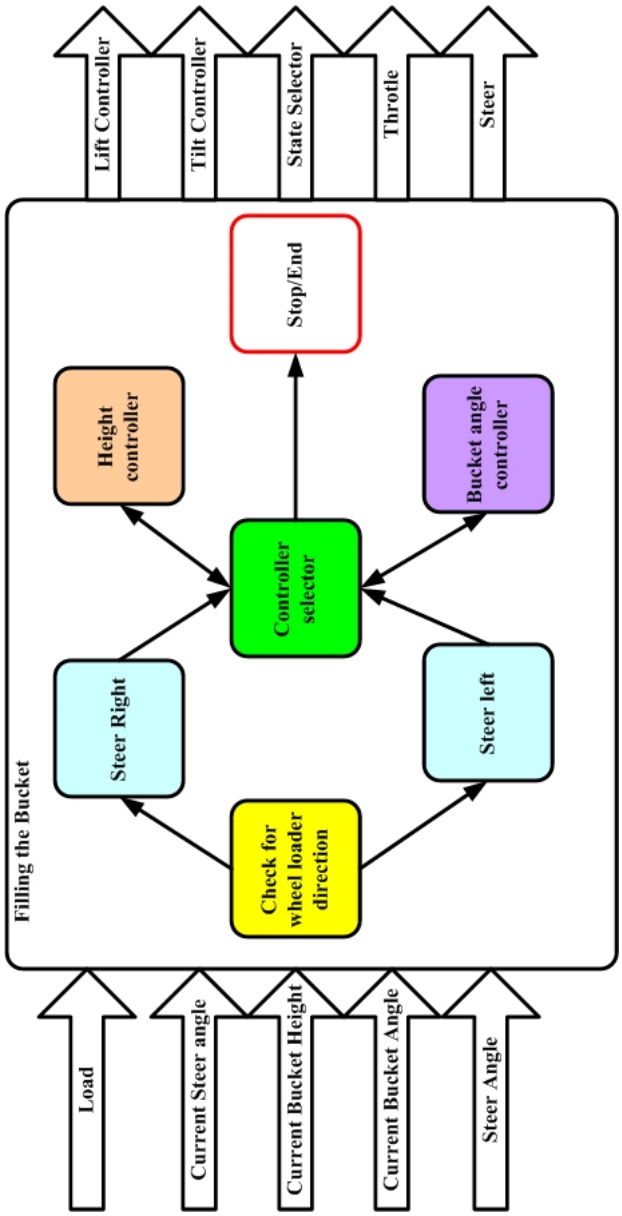


Figure 36. Filling the bucket schematic.

### 3.1.2 The Tracking Servo Controllers for Sub Tasks

In this section we define the servo controllers used to actuate the control valves to make the machine track the operator commands that is to control steer, throttle, brake, lift and tilt to achieve the best performance of the wheel loader and allow the operator model to modify itself to control all models of the wheel loader without further modifying from the user.

The controllers used are based on neural networks and proportinal-integral-dervative controllers (PID) were used in the first version [1], but the problem with PID the tuning as not enough information were known about the systems so they were tuned experimentally. First, the proportional term was increased from zero until the tilt function began to oscillate. It was then slightly reduced. Next an integral term was added to offset the steady state velocity errors that existed. An integral gain term quickly removed steady state errors without introducing excessive phase lag to the system. Finally, a derivative term was added in order to catch high frequency changes in the error signal. It worked with a good performance, but it worked only with one model and for every model retuning was required.

The neural network controllers used are called model reference control; they can be trained offline to tune the controllers to a reasonable performance then online to modify itself to control various models of the wheel loader. Due to that fact that the command in the wheel loader models control the velocity output of the actuator, and the output of the strategy model is usually a desired position output therefore the error between the desired position output and the actual position output is fed to PD controller then the output is fed to the neural network

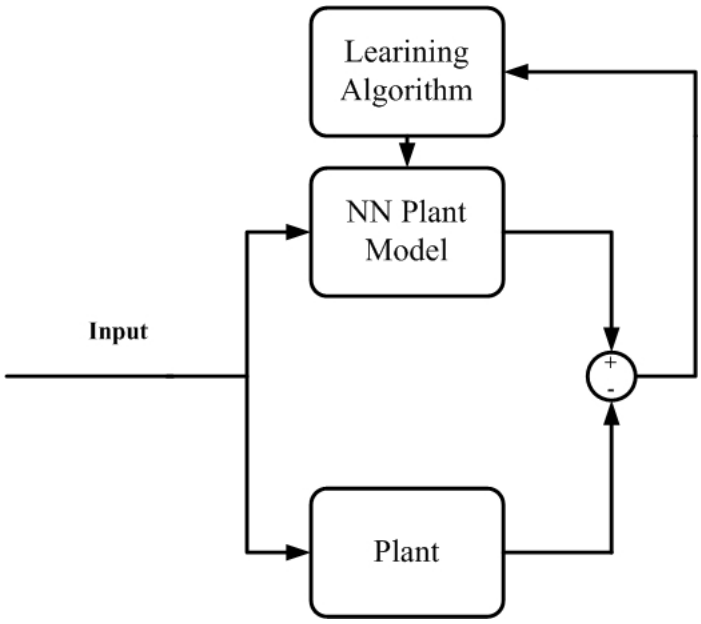


Figure 37. Offline training procedure first step [18].

controller. The neural network controller compares this input to the actual velocity of the actuator. The command is then determined depending on the error between this two values.

Training the neural network controllers takes three steps. The first step shown in figure 37 is done offline. A neural network model for the plant is trained to closely clone the plant performance. This procedure saves a lot of time in training the controller. An input is fed to the plant and the neural network plant model. And the error between the two responses is fed to a learning algorithm, which modifies the weights and the biases of the neural network. In our controllers the neural network plant model was trained against the data recorded from experiments conducted on the wheel loader.

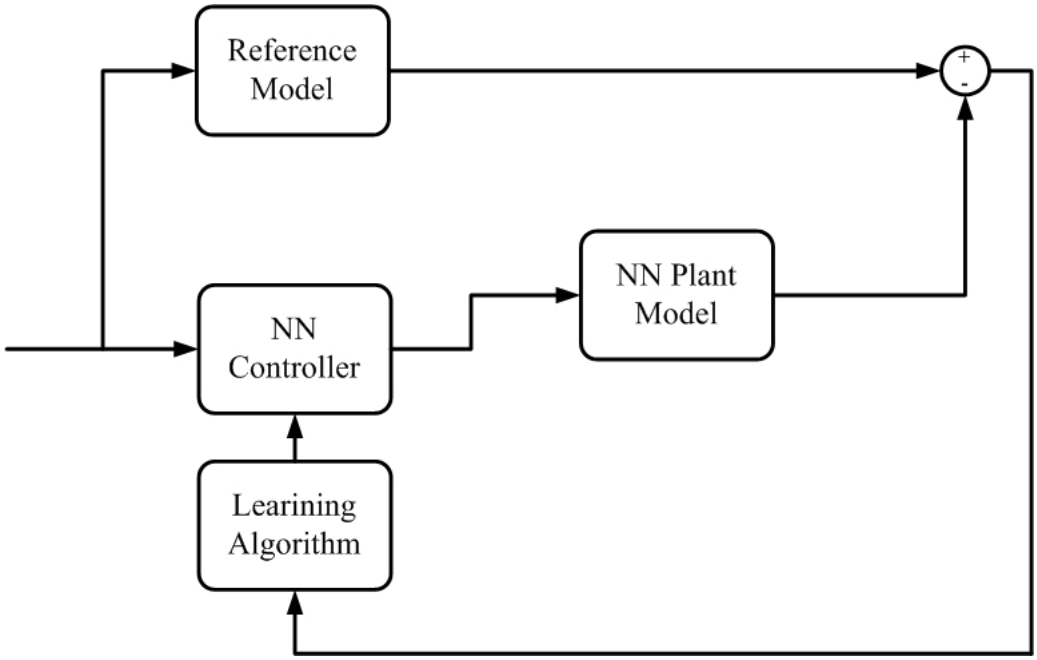


Figure 38. Offline training procedure second step[18].

The second step shown in figure 38 is also done offline. A desired output is fed to the neural network controller and gives the control action to the neural network plant model. The response of the neural network plant model is compared with the response of the reference model. The error between the two responses is fed to a learning algorithm that modifies the weights and biases of the neural network controller till it gives an acceptable performance. The performance of the neural network controller is measured by the error between the plant response and the reference model.

The last step is the online training against the plant (shown in figure 39). While operating the desired input is given to the neural network controller. The controller gives a control

signal to the plant and the neural network plant model. The error between the plant and the neural network plant model responses are fed to a learning algorithm to modify the neural network plant model weights and biases. The neural network plant model after modifications are then saved for further offline training if needed. The error between the plant response and the reference model output is fed to a learning algorithm, which modifies the neural network controller weights and biases if needed. By this way the reference model controller is trained automatically to control new wheel loader models without any user modifications.

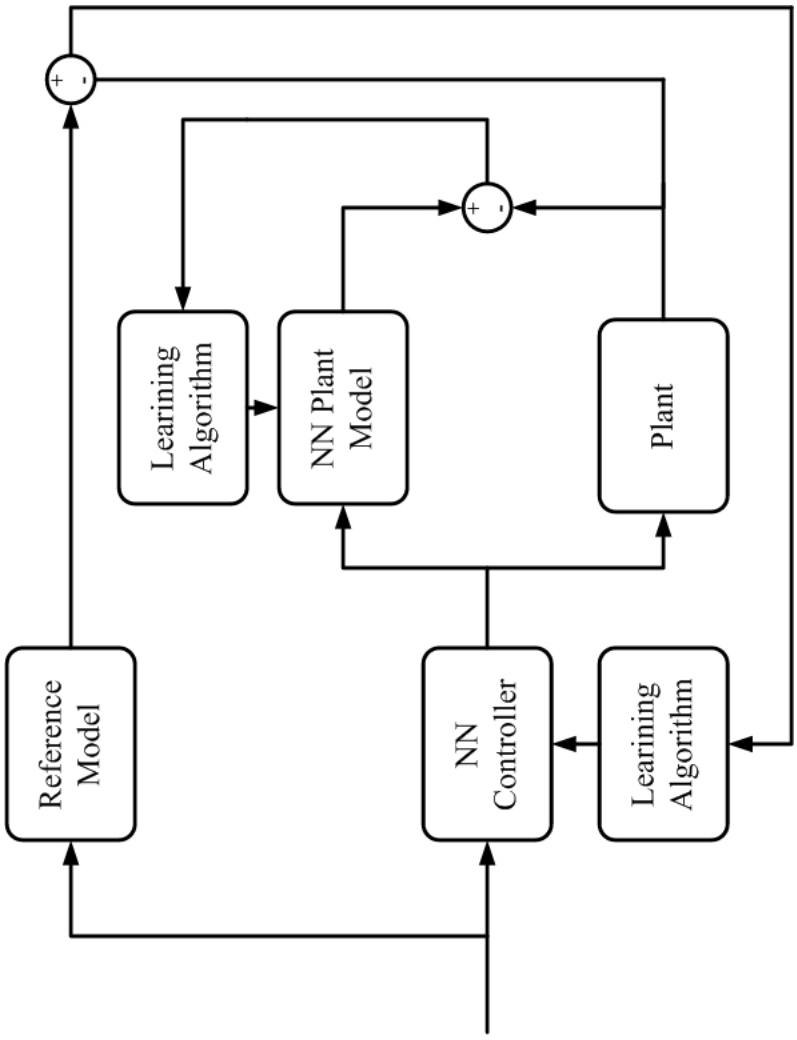


Figure 39. Online training procedure [18].

#### 3.1.2.1 The Training Methods and Algorithms

The neural networks used are feed forward backpropagation type network. The back propagation neural networks were created applying multi-layer network and non-linear differentiable transfer functions to Widrow-Hoff learning method [18]. Inputs and outputs are being used to train the neural network until it can simulate the function needed approximately [18]. Networks with biases, a sigmoid layer, and a linear output are capable of simulating any function approximately.Standard backpropagation is a gradient descent algorithm.We are using The simplest implementation of backpropagation learning. The learining algorithm updates the network weights and biases in the direction in which the performance function decreases most rapidly. Three learning algorithms were used in our model. The algorithms used are based on Quasi-Newton method[18].

$$x_{k+1} = x_k - a_k g_k$$

where $x_k$ is a vector of current weights and biases, $g_k$ is the current gradient, and $a_k$ is the learning rate. Three learning algorithms were used in our model.

1. BFGS Algorithm [18]

   Newton's method is an alternative for fast optimization. The basic step of Newton's method is

$$x_{k+1} = x_k - A_k^{-1} g_k$$

where $A_k$ is the Hessian matrix (second derivatives) of the performance index at the current values of the weights and biases.

The BFGS algorithm is described in [18]. This method was used in training the neural network plant model in the first offline training step.

2. Levenberg-Marquardt [18]

   This method was used in the offline training of the neural network controller in the second step of the training procedure. Like the quasi-Newton methods, the Levenberg-Marquardt algorithm was designed to approach second-order training speed without having to compute the Hessian matrix.The Hessian matrix can be approximated as

$$H = J^T J$$

   and the gradient can be computed as

$$g = J^T e$$

   where $J$ is the jacopian matrix that contains first derivatives of the network errors with respect to the weights and biases, and $e$ is a vector of network errors. that contains first derivatives of the network errors with respect to the weights and biases, and $e$ is a vector of network errors[18]. The Levenberg-Marquardt algorithm uses this approximation to the Hessian matrix in the following Newton-like update:

$$x_{k+1} = x_k - \left[J^T J + \mu I\right]^{-1} J^T e$$

This method has a very efficient MATLAB implementation. This method is described in [18].

3. Reduced Memory Levenberg-Marquardt [18].

   The main problem of the Levenberg-Marquardt algorithm is that it requires the storage of large matrices which slowers the process[18]. So it is difficult to be used in online training. In Reduced Memory Levenberg-Marquardt this matrix does not have to be computed and stored as a whole. The Jacobian into two equal sub-matrices and the approximate Hessian matrix [18] is computed as follows:

$$H = J^T J = \begin{bmatrix} J_1^T & J_2^T \end{bmatrix} \begin{bmatrix} J_1 \\ \\ J_2 \end{bmatrix} = J_1^T J_1 + J_2^T J_2$$

   This method was used in the online training.

# CHAPTER 4

# RESULTS

In this chapter we discuss the results of the virtual operator model in simulation and compare the results to the experimental results.

## 4.1 Truck Loading Cycle Results

First, we will present the results of the complete truck loading cycle using CAT model 972 H. The path chosen by the operator model for the wheel loader to complete a truck loading cycle is shown in figure 40. The wheel loader started in a position after dumped the load in the truck. According to the dig site position the operator model selected path B to back from the truck. After the wheel loader backed enough distance from the truck, the operator model selected the shown path to go to the dig site. While going to the site the operator model changed the bucket position to start digging and filling the bucket. When the bucket was filled with the load, the operator model selected path B to back from the site. Then the operator model took the path shown in the figure to go back to the truck. After assuring that the wheel loader is perpendicular to the truck, the operator model started giving the command to dump the load.

In figure 41 the human commands delivered from the operator model is shown. In the first task (backing from the truck) the figure shows the application of a steer, throttle commands. After enough distance is reached the brake command is applied, also the gear command worked

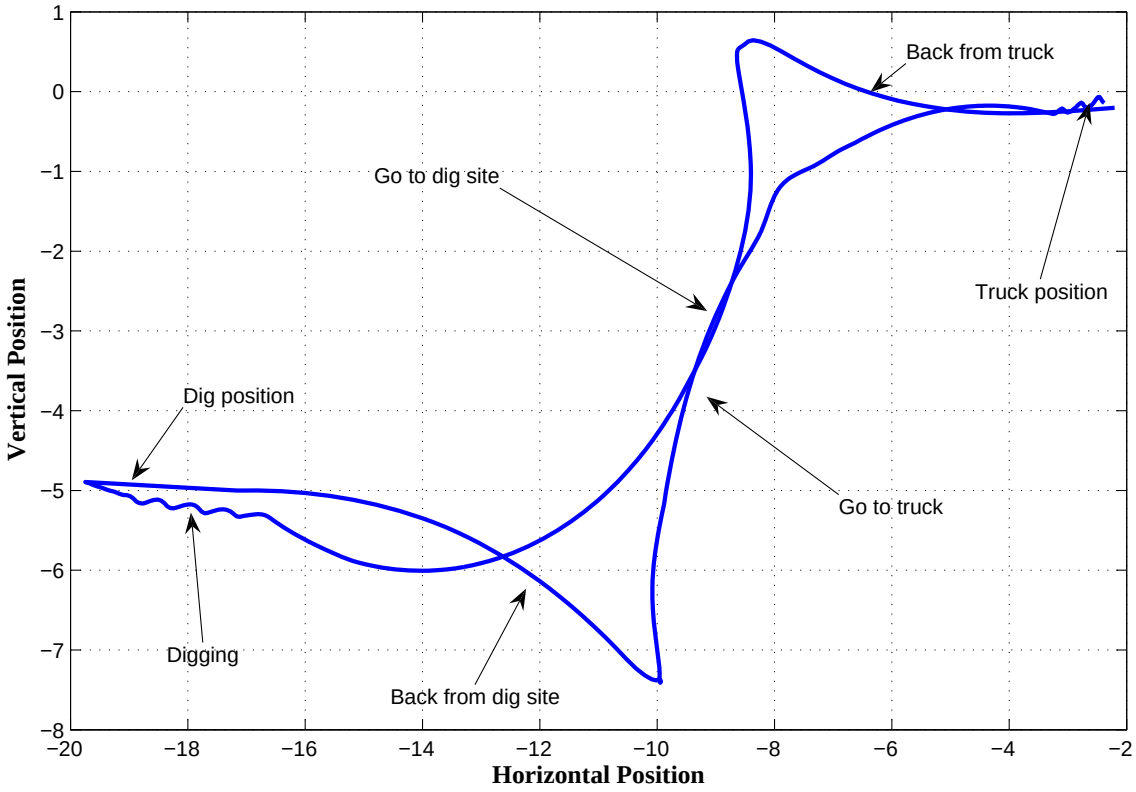


Figure 40. Full truck loading cycle: bucket tip path.

in parallel with the task. The first backward gear is engaged then neutral while braking. The second task selected is go to the site, the gear selector selected the first forward gear, the wheel loader started moving trying to keep a speed of 2 m/sec. The steer command was applied until a point 2 m behind the target point was reached, then the steer command stopped to allow the wheel loader to go straight to reach the target point perpendicular to the dig site. The wheel loader started digging using lift and tilt command. We can see that the throttle was 100 % while digging to use maximum performance. After the bucket was filled, the wheel loader backed from the bucket. The human commands applied were steer, throttle and brakes. After backing enough distance, the wheel loader started going to the truck using steer throttle and brake command. The gear selector was working in parallel as shown in the figure. After reaching the truck, the operator model gave commands to dump the load in the truck.

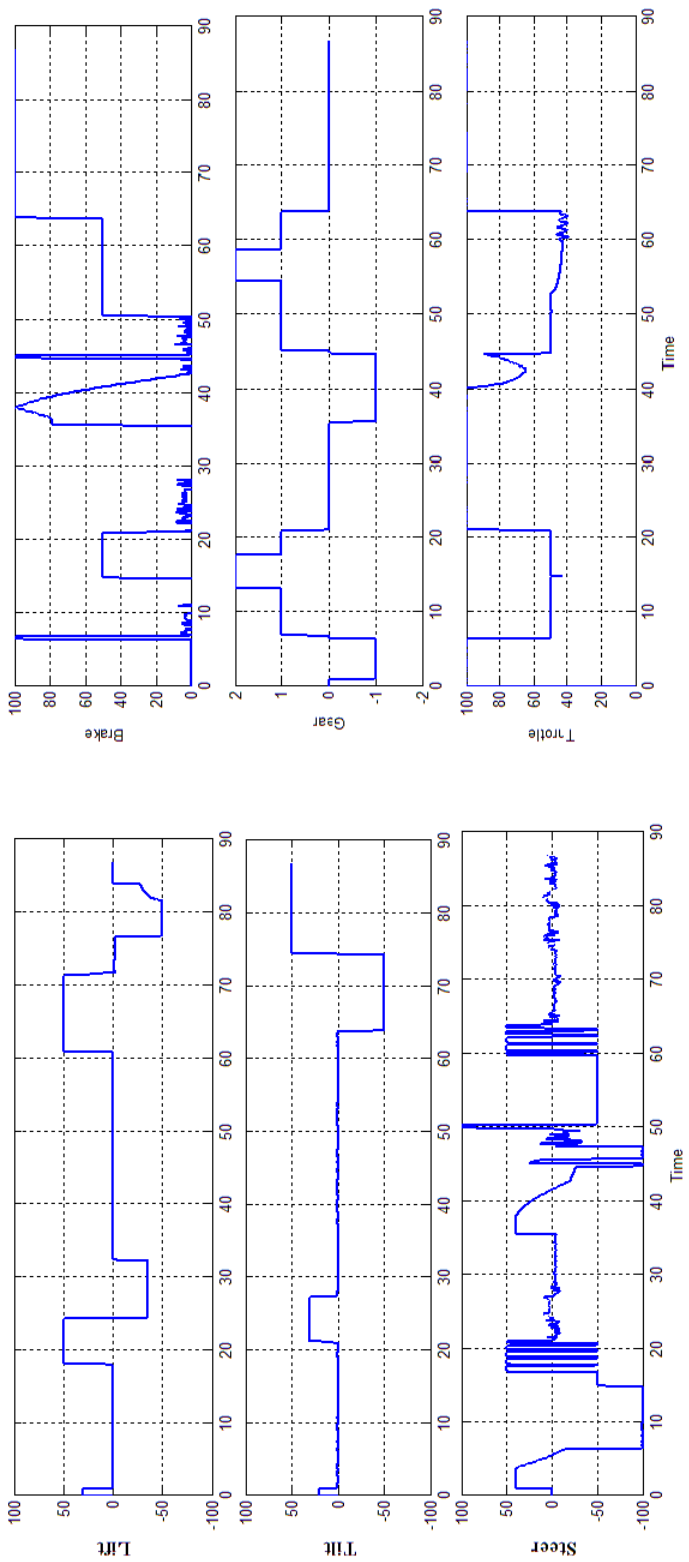


Figure 41. Virtual operator model commands during full truck loading cycle.

## 4.2 First Evaluation Test Results

In figure 42 shows a comparison between the experimental results and the simulation results of the operator model Using 966 H for the first evaluation test. The human operator started the test from up position then he performed three trials of the test. We can see that each trial is little different from one another. The operator model was able to mimic the performance of the human operator with an error close in range of the human error. The target was point at 3 meters high and 0.6 m easting. The human operator was able to reach a point 3.1357 m high and 0.6 m easting. The operator model reached a point of 3.1123m high and 0.6 m easting. The pattern of performing the test three times was achieved. The randomness in human performing was captured by the operator model as shown in the figure. The time consumed by the operator model was the approximately the same time taken by the human operator.

In figure 43 shows a comparison between the commands of the human operator and the operator model using 966 H for the first evaluation test. We are comparing only the raising of the bucket part of the curve as this was the goal of the test. In the lowering part, the operator model was just giving a random command to lower the bucket. It shows a capture of the same pattern of the human operator commands. With the difference due to the fact as the operator model was controlling a virtual machine.

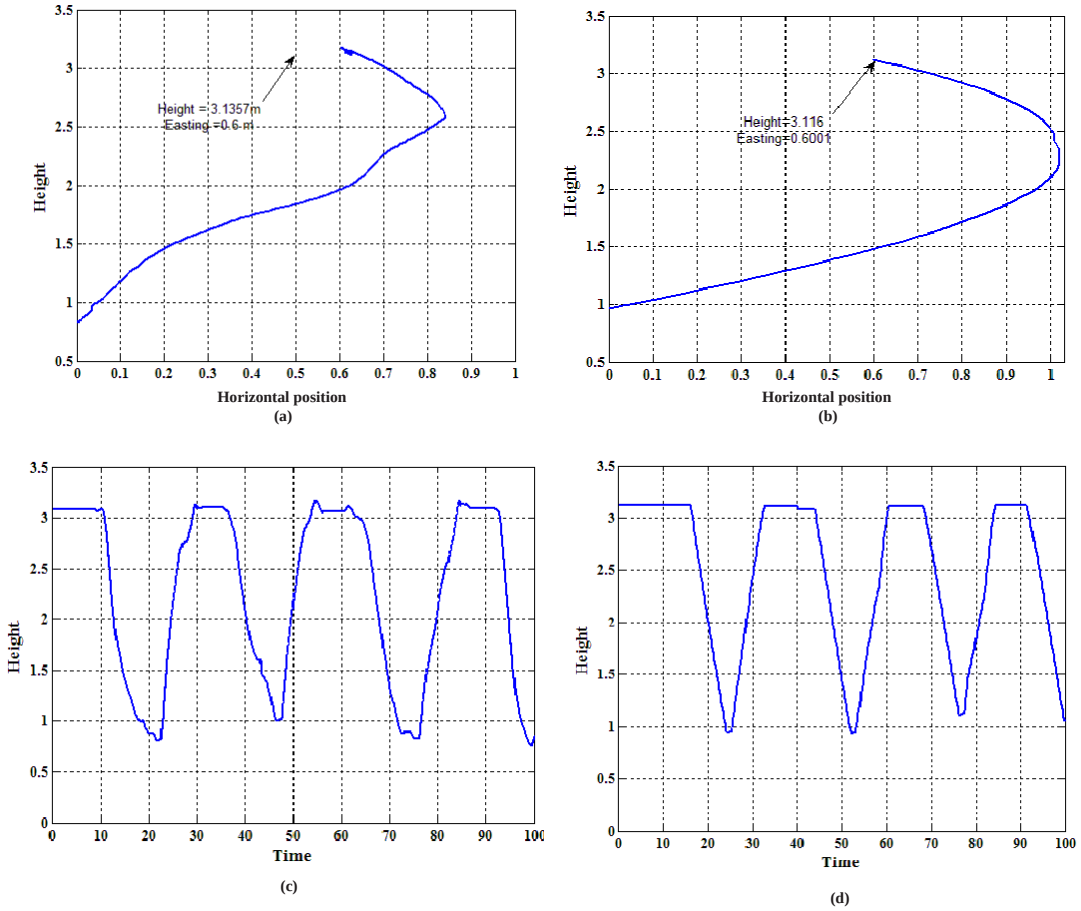


Figure 42. Comparison between experimental and simulation results for test 1 for CAT 966 H a)Experimental results (first trial bucket tip path) b) Simulation results (first trial bucket tip path) c)Expermintal results (bucket tip height vs time) d) Simulation results (bucket tip height vs time).

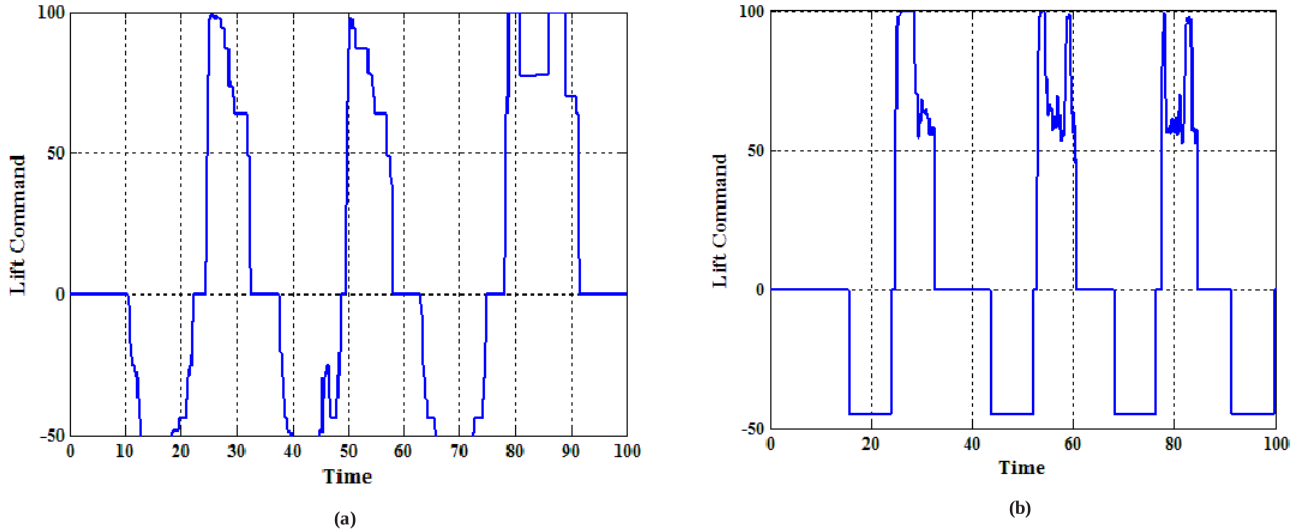


Figure 43. Comparison between the commands of Test 1 for CAT 966 H a) Experimental results (human commands) b) Simulation results (virtual operator model commands).

In figure 44 the results of medium wheel loader CAT model 972 H is presented. The bucket tip path of the first trial of the test is shown in the left and the three trials height vs time is shown in the right. The operator model started the test from up position. Comparing this results with results of the CAT model 966 H in figure 25 we can see that the operator model was able to perform three trial from the test in 101 second for the 972 H comparing to 100 sec for the 966 H, the target was point at 3 meters high and 0.4 m easting the operator model reached 3.016 m high and 0.4215 m easting, the pattern of performing the three trials was close to the run done by the 966 H model. We can find from the results that the 972 H has a bigger error in the easting and lower error in the height which means the controllability of the lift in 972 H model is better (controls the height of the bucket tip position) and the controllability of the tilt is lower than the 966 H model.

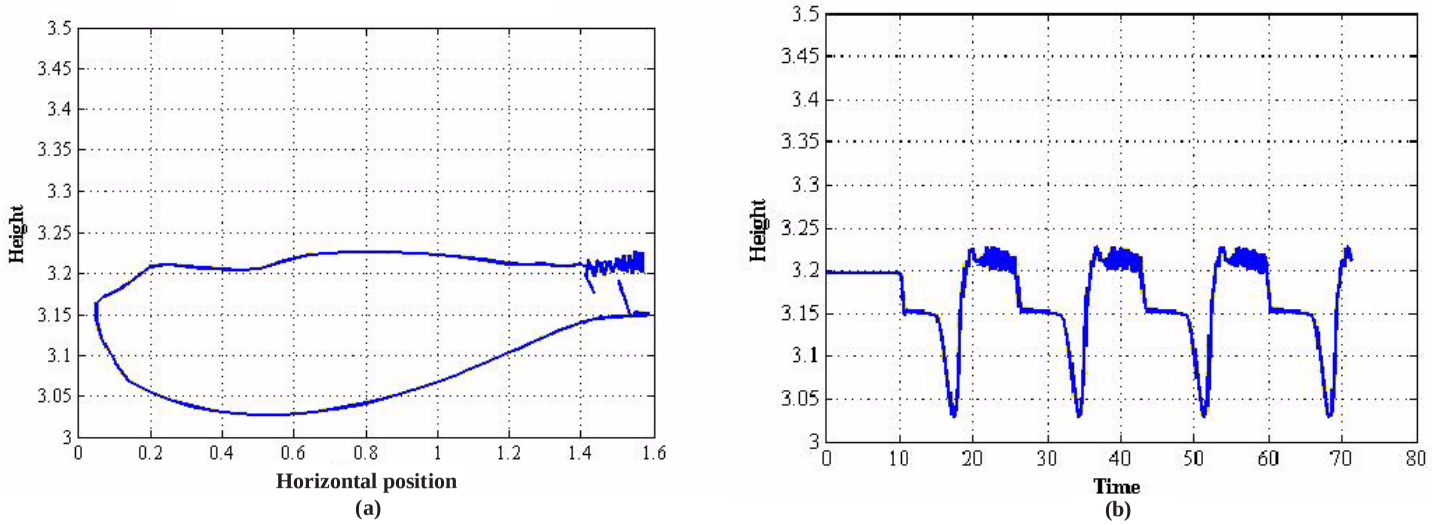


Figure 44. Evaluation test 1 results for CAT 972 H a) Simulation results (first trial bucket tip path) b) Simulation results (bucket tip height vs time).

## 4.3 Second Evaluation Test Results

In figure 45 shows a comparison between the experimental results and the simulation results of the operator model using 966 H for the second evaluation test. The target was to lower the bucket to starting from high random point to a point 1 m high from the ground and 0.3 m far from the wheel loader. The human operator was able to reach a point 0.28758 m far from the wheel loader and 1.1375 m high. We can see that the operator model was able to mimic the performance of the human operator, and was able to reach a point of 1.1254 m high and 0.29877 m far from the wheel loader. The error to reach the point is within 1.1 %. The time trace of the bucket height is also shown in the figure 46 the human operator and the operator model started the test from a low point then started to perform three trials of the test. The time taken to perform the three trials was 60.3 seconds for the human operator and 63.2 seconds for the operator model. In figure 28 shows a comparison between the commands of the human operator and the operator model while performing the second evaluation tests. We are comparing only the part of lowering the bucket in this evaluation test. In raising the bucket, a random command was given to reach a high point and stop when reaches 5 m high. The figure shows also a capture of the same pattern of the human operator commands. Both used full command till the bucket tip reached to the point. The time duration for applying the lift command was average 7.4 sec per trial for the human operator. The time duration for applying the command was 6.1 sec average for the operator model.

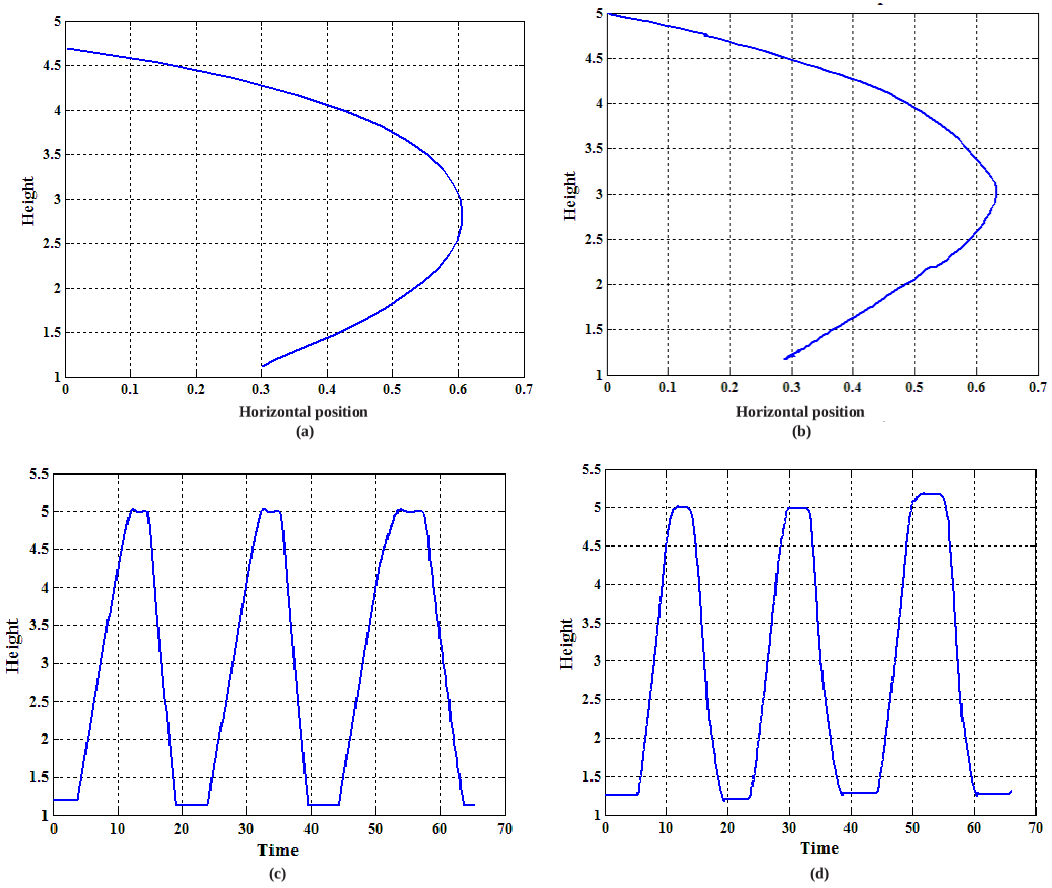


Figure 45. Comparison between the second evaluation test results for CAT 966 H a) Simulation results (first trial bucket tip path) b) Experimental results (first trial bucket tip path) c) Simulation results (bucket tip height vs time) d) Expermintal results (bucket tip height vs time).

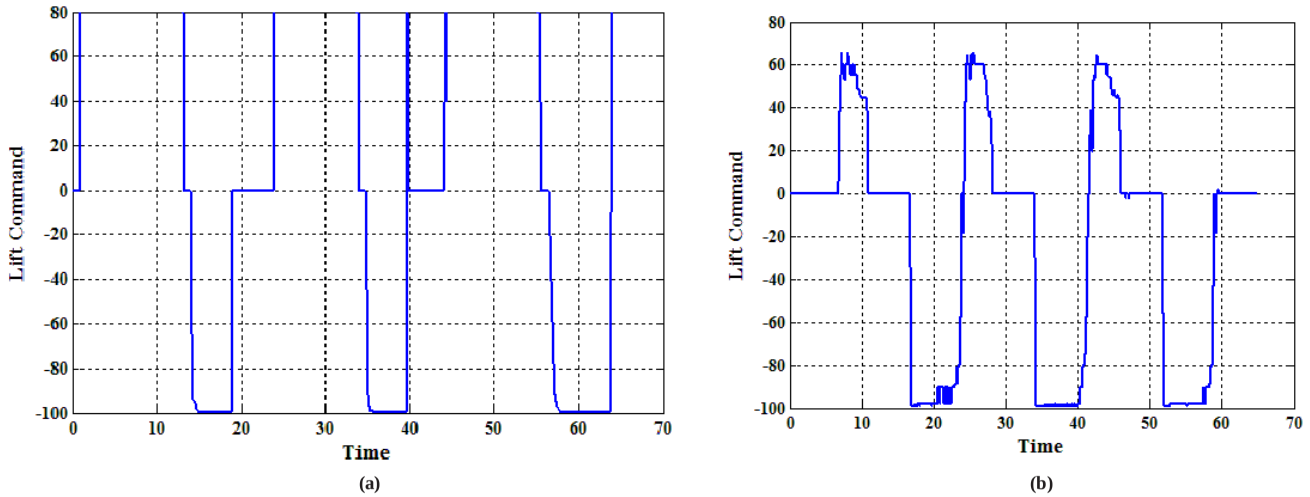


Figure 46. Comparison between the second evaluation test commands for CAT 966 H a) Experimental results (human commands) b) Simulation results (virtual operator model commands).

In Figure 47, the results of medium wheel loader CAT model 972 H is presented. The bucket tip path of the first trial of the test is shown in the left and the three trials height vs. time is shown in the right. The operator model started the test in down position. Comparing this results to the 966 H model results shown in figure 26 we can find that the operator model was able to do three trial of the test in 57.2 seconds comparing to 60.1 seconds for the 966 H. The pattern of the three trials is close to the one done using the 966 H model. The target point was height 1 m and 0.6 m easting the operator model was able to reach a height of 0.9986 m and 0.613 m easting. The error in the height was lower in the 972 H model but the error in easting was bigger. This result confirms the results of test 1 that the controllability of the lift in 972 H model is better while the controllability of the tilt is lower while comparing to the 966 H model.

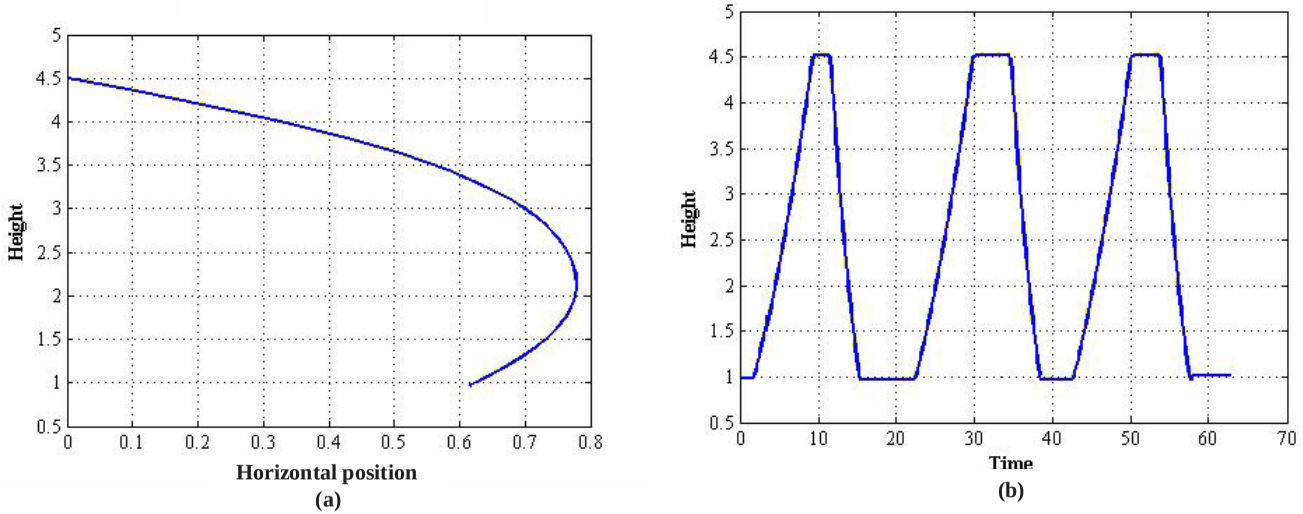


Figure 47. Evalation test 2 results for CAT 972 H a) Simulation results (first trial bucket tip path) b) Simulation results (bucket tip height vs time).

## 4.4 Third Evaluation Test Results

In figure 48 shows a comparison between the experimental results and the simulation results of the operator model using 966 H for the third evaluation test, which is curl the bucket at a fixed height. Due to the variety of different human operator performance, we found that the common thing for this test is the error range. So the operator model was trained to perform the test within human operator human range. We found that the operator model was able to keep the error in height within 20 cm, which was the same range for the human operator. The target was to keep the bucket tip point at height of 3.15 m. The human operator range was between 3.2963 m and 3.0769 m. The operator model range was between 3.262 m and 3.051m. The human operator did three trials in 99.8 seconds. The operator model did the three trials of the test in 99.83 seconds.

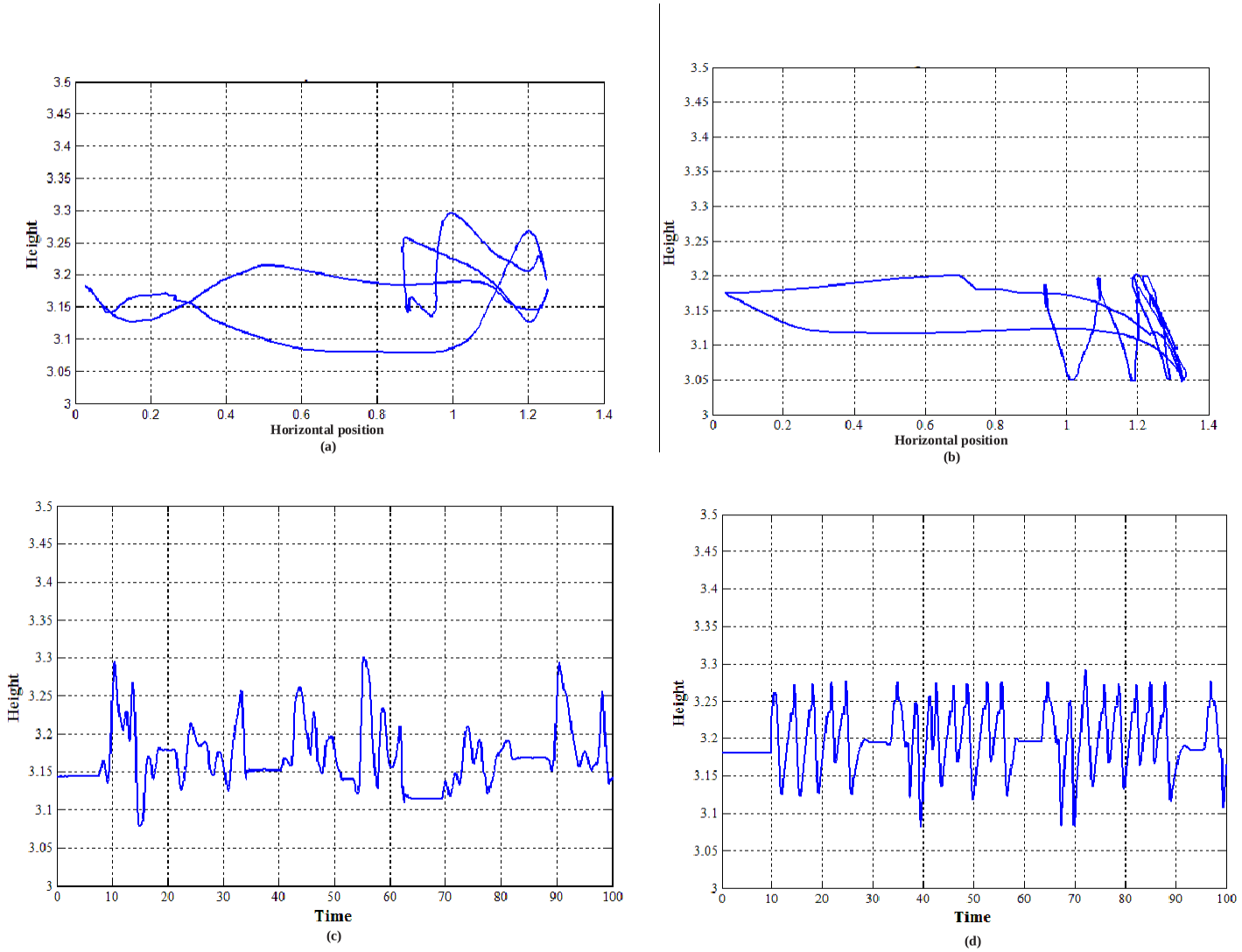


Figure 48. Comparison between the third evaluation test results for CAT 966 H a) Experimental results (first trial bucket tip path) b) Simulation results (first trial bucket tip path) c) Expermintal results (bucket tip height vs time) d) Simulation results (bucket tip height vs time).

## 4.5 Fourth Evaluation Test Results

In figure 49 shows a comparison between the experimental results and the simulation results of the operator model for the fourth evaluation test, which is the vertical line test. Due to the variance of performance of the human operators while performing this test. The operator model was trained to perform the test within the same error range and to take the same time while doing the test. We found that the operator model was able to keep the error in height within 25 cm, which was the same range for the human operator.

In figure 50 shows the results of medium wheel loader CAT model 972 H. the error vs. time is shown in up left, the height vs. time is shown up right. The bucket tip path while doing the first trial is shown down. Comparing the results with the 966 H model results shown in figure 50. The target was to keep the bucket tip path as close as possible to the zero line while going up and down between 1 m to 4 m height .we can see that the error is within the acceptable range 30 cm but was 5 cm more than 966 H model. This means that the controllability of the tilt of 972 H model is lower than the 966 H model. The three trials of the test were done in 70 seconds i.e. 30 seconds less as the operator model in this case didnt stop for 5 seconds between changing directions up and down.

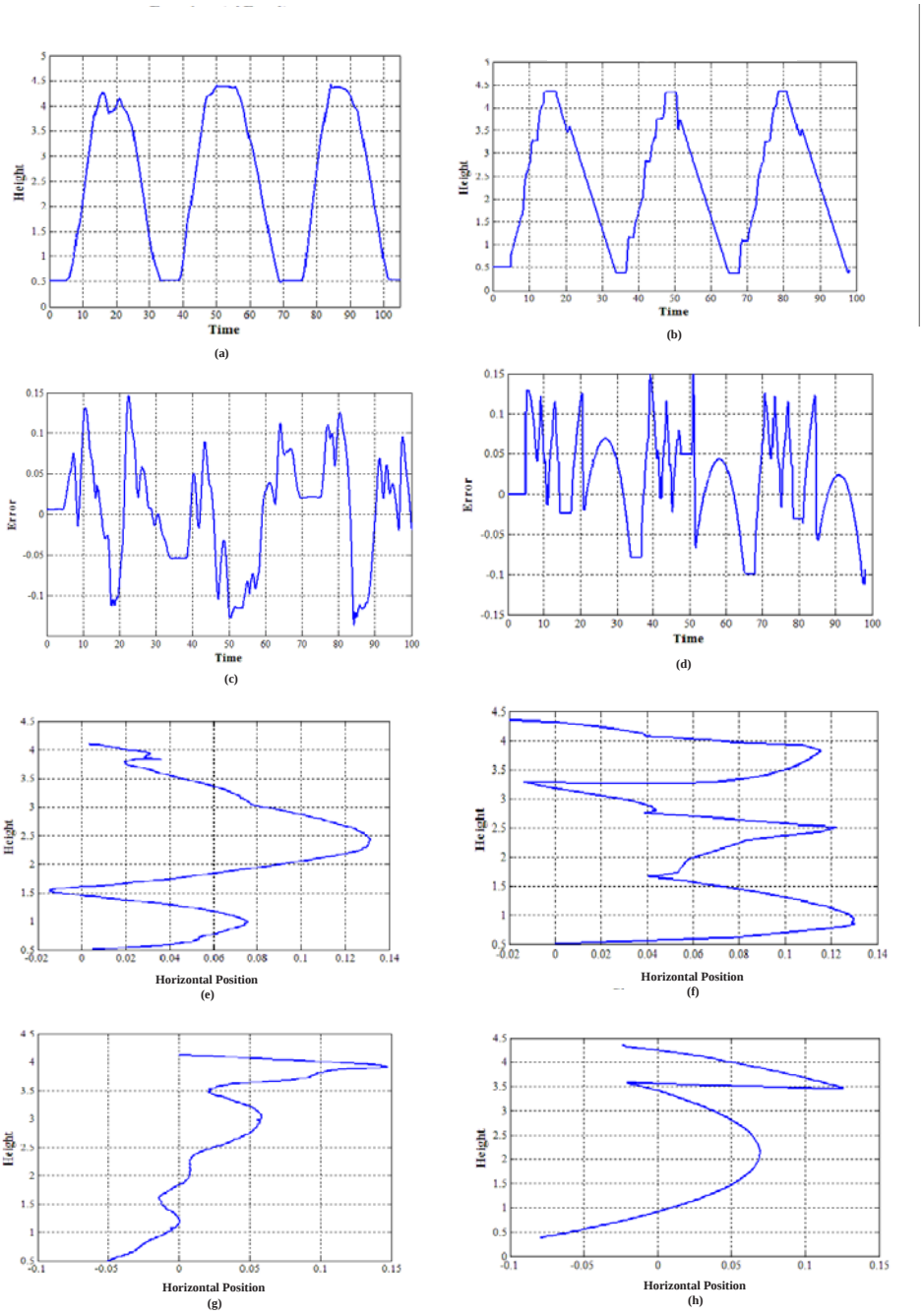


Figure 49. Comparison between the fourth evaluation test results for CAT 966 H a) Experimental results (bucket tip height vs time) b) Simulation results (bucket tip height vs time) c) Expermintal results (error vs time) d) Simulation results (error vs time) e) Expermintal results (first trial bucket tip path up direction) f) Simulation results (first trial bucket tip path up direction)g)Expermintal results (first trial bucket tip path down direction) h) Simulation results (first trial bucket tip path downdirection).

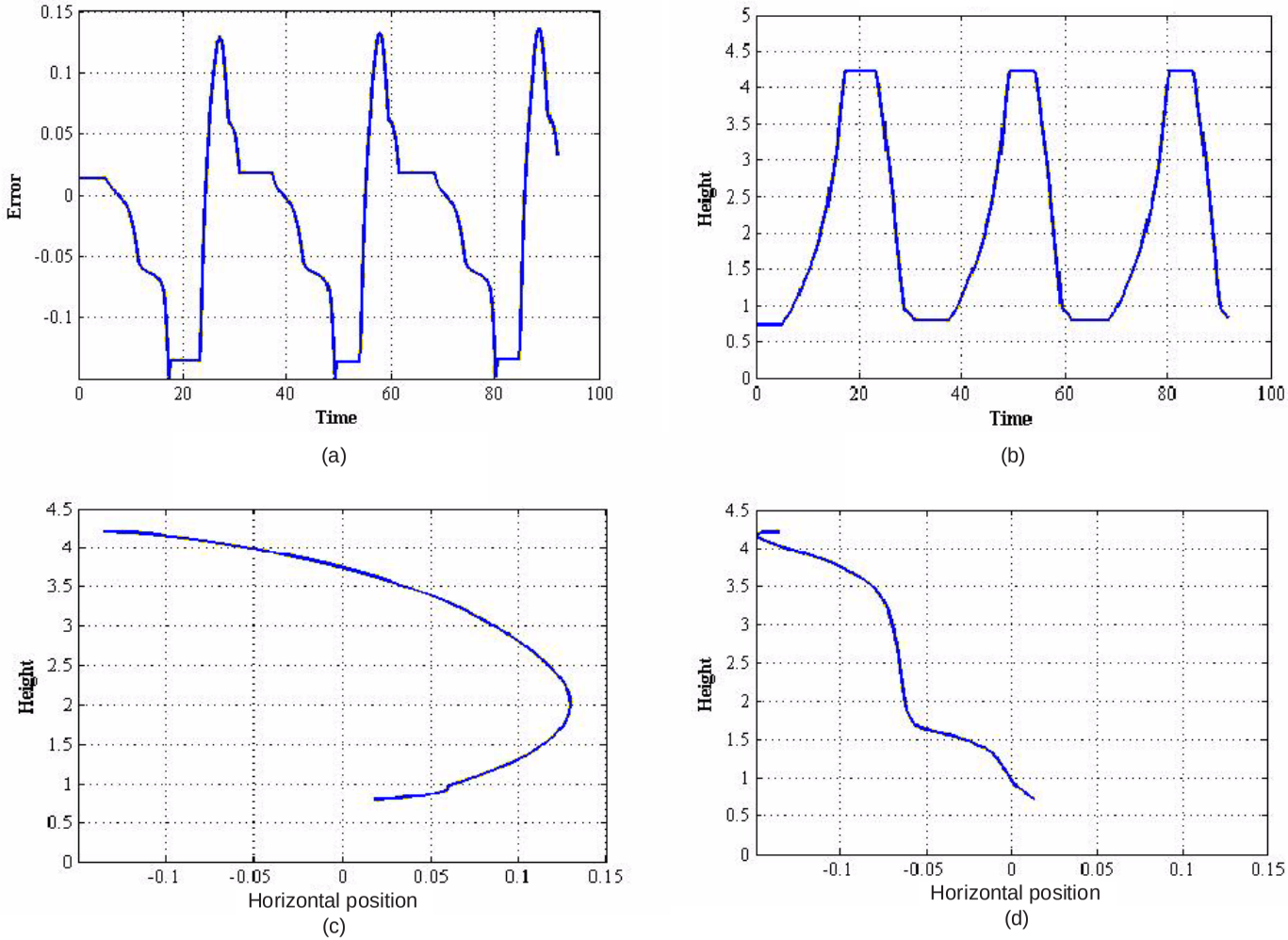


Figure 50. The fourth evaluation test results for CAT 972 H a) Simulation results(error vs time) b) Simulation results (bucket tip height vs time) c) Simulation results (first trial bucket tip path down direction) d) Simulation results (first trial bucket tip path down direction).

## 4.6 Fifth Evaluation Test Results

In figure 51 shows a comparison between the experimental results and the simulation results of the operator model for the fifth evaluation test, which is follow a horizontal string line test. We can find from the results shown that the human operator driving the wheel loader when he passed the bump while maintaining 1.5 m, the bucket tip reached a height of 1.71m then went to 1.201m, while the operator model when passing the bump the bucket tip height reached 1.73 m then went to height 1.19 m. The performance of the human operator and the operator bump was close in overcoming the bump. After passing the pump we found that the vibration in the real machine was higher due to inaccuracy in modeling the tires.

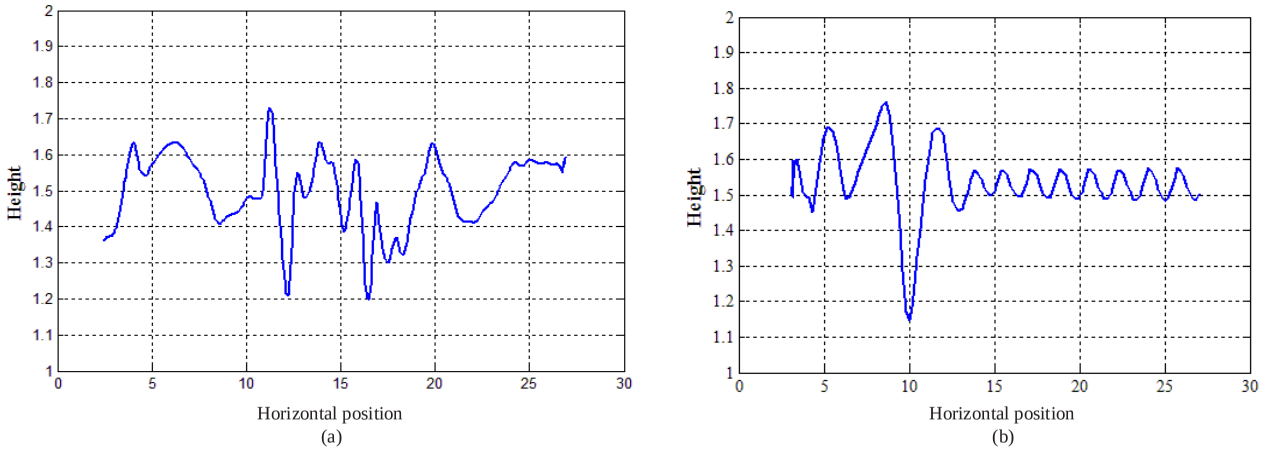


Figure 51. Comparison between the fifth evaluation test resultsfor CAT 966 H a) Experimental results (bucket tip path) b) Simulation results (bucket tip path).

Figure 52 shows the results of meduim wheel loader CAT model 972 H, comparing this to the results of the 966 H model results shown in figure 30. The target was to try to keep the bucket tip at 1.5 m while moving and overcoming an obstcale. We can see that the pattern of the test is close. The steady state error of the height in the 972 H is lower than the 966 H. The controlability of the lift in the 972 H is better than the controlability of the lift in 966H machine. The same tire model was used in the 972H and the 966 H model.

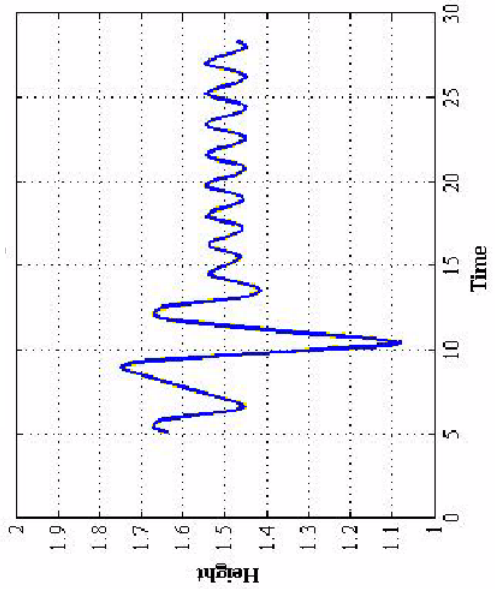


Figure 52. The fifth evaluation test results for CAT 972 H bucket tip path

## 4.7 Online Training Capibility

In figure 53 shows the online training capability of the operator model when it was used to control a different model to perform the evaluation test number three. The operator model in performing the test three times was able to achieve the acceptable error range. The first trial the bucket tip maximum error was at height 3.013 m equals to 0.137 m. The second trial the bucket tip maximum error was at height 3.0264 m equals to 0.1236 m. The third trial was at height 3.051 m equals to 0.099 m, which is within the acceptable range. Also while experimental testing the human operator was allowed to do the test three trials before measuring for training.

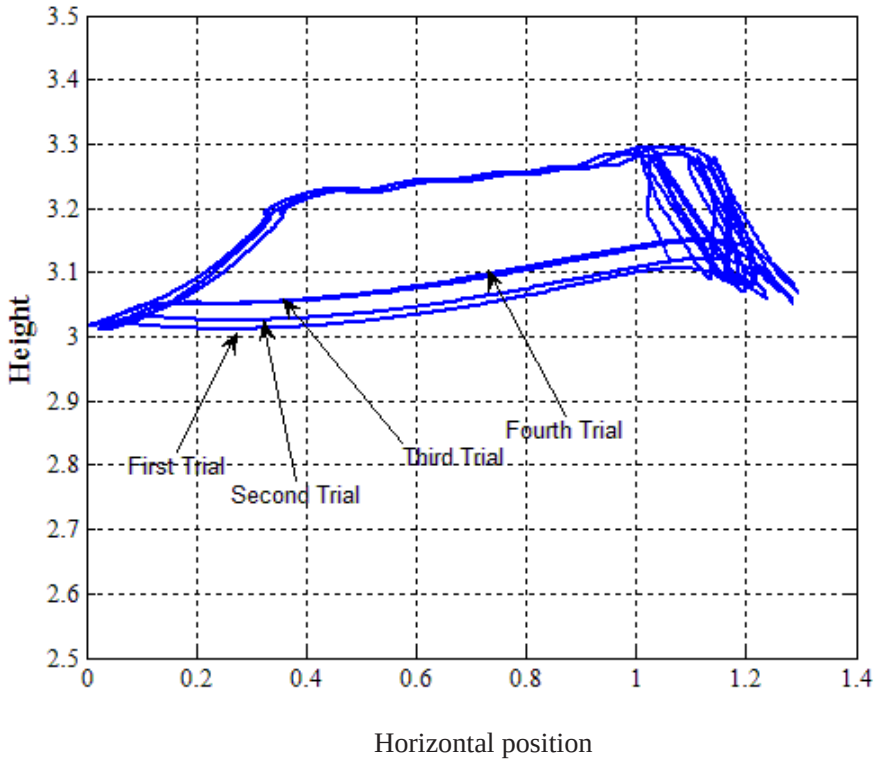


Figure 53. Online training capability.

# CHAPTER 5

# CONCLUSION AND FUTURE WORK

## 5.1 Conclusion

A virtual operator model with a human like performance was developed. The error range is less than 3 % with respect to the human performance in the truck loading cycle when compared the time of the cycle and efficiency. The error range in the evaluation tests was within 1%. The virtual operator model was able to modify itself through online training to control various models and sizes of the wheel loader. The online training time is within 1% error compared with online training for human operator. The operator model is currently used to test digital mockups of machines.

The new contribution of the thesis is the development of a virtual operator model for construction machines in order to test digital mockups of the machines before building the prototypes of the machines thus help decrease the design cost and time significantly. A novel operator model based on neural networks that can modify itself to test different sizes and models of the machine without required modification from the user were developed. The operator model is considered a further step towards a complete autonomous operation.

For future work, the following further development is recommended:

1. Expanding the capabilities of virtual autonomous operator for other machine applications such as excavators, motor graders and trucks.
2. Autonomous operation in multi vehicles construction and mining site, incorporating safety sensors and site-networking capabilities.

# APPENDICES

# Appendix A

## MACHINES USED IN TESTING

## CAT 966H WHEEL LOADER

## Appendix A (Continued)


Figure 54. CAT 966 H

# Appendix A (Continued)

## Engine

| Engine Model | Cat® C11 ACERT™ | |
|---|---|---|
| Gross Power – SAE J1995 | 213 kW | 286 hp |
| Net Power – ISO 9249 | 195 kW | 262 hp |
| Net Power – SAE J1349 | 193 kW | 259 hp |
| Net Power – 80/1269/EEC | 195 kW | 262 hp |
| Peak Torque (Net) @ 1,400 rpm | 1215 N•m | 896 ft-lb |
| Bore | 130 mm | 5.12 in |
| Stroke | 140 mm | 5.51 in |
| Displacement | 11.1 L | 677 $in^3$ |

- Caterpillar engine with ACERT™ Technology – EPA Tier III, EU Stage III Compliant
- These ratings apply at 1,800 rpm when tested under the specified standard conditions.
- Rating for net power advertised based on power available when the engine is equipped with alternator, air cleaner, muffler and on-demand hydraulic fan drive at maximum fan speed.

## Weights

| Operating Weight | 23 698 kg | 52,254 lb |
|---|---|---|

- For 4.25 $m^3$ (5.5 $yd^3$) general purpose bucket with BOCE

## Buckets

| Bucket Capacities | 3.4-4.2 $m^3$ | 4.5-5.5 $yd^3$ |
|---|---|---|
| Max Bucket Capacity | 4.2 $m^3$ | 5.5 $yd^3$ |

## Operating Specifications

| Static Tipping Load, Full Turn | 15 474 kg | 34,120 lb |
|---|---|---|
| Breakout Force | 188 kN | 42,300 lb |

- For 4.25 $m^3$ (5.5 $yd^3$) general purpose bucket with BOCE

## Transmission

| Forward 1 | 6.7 km/h | 4.2 mph |
|---|---|---|
| Forward 2 | 12.6 km/h | 7.8 mph |
| Forward 3 | 22.1 km/h | 13.7 mph |
| Forward 4 | 37.4 km/h | 23.2 mph |
| Reverse 1 | 7.4 km/h | 4.6 mph |
| Reverse 2 | 13.9 km/h | 8.6 mph |
| Reverse 3 | 24.3 km/h | 15.1 mph |
| Reverse 4 | 37.4 km/h | 23.2 mph |

- Maximum travel speeds (26.5-25 tires).

## Hydraulic System

| Bucket/Work Tool System – Pump Output | 305 L/min | 80.6 gal/min |
|---|---|---|
| Steering System Pump Type | Piston | |
| Hydraulic Cycle Time – Raise | 5.9 Seconds | |
| Hydraulic Cycle Time – Dump | 1.6 Seconds | |
| Hydraulic Cycle Time – Lower, Empty, Float Down | 2.4 Seconds | |
| Hydraulic Cycle Time – Total | 9.9 Seconds | |

- Implement System (Standard), Piston Pump – Rated at 2,100 rpm and 1,000 psi (6900 kPa).
- Cycle time with rated payload

## Brakes

| Brakes | Meets required standards. |
|---|---|

- Meet OSHA, SAE J1473 OCT90 and ISO 3450-1985 standards.

## Axles

| Front | Fixed front | |
|---|---|---|
| Rear | Oscillating ± 13° | |
| Maximum Single-Wheel Rise and Fall | 502 mm | 19.8 in |

## Tires

| Tires | Choose from a variety of tires to match your application. |
|---|---|

- Choice of:
  26.5R25, L-2
  26.5R25, L-3 (XHA)
  26.5R25, L-5 (VSDL)
  26.5-25, L-3 (SRG, SHRL)
  750/65R25, L-3
- NOTE: In certain applications (such as load and carry) the loader's productive capabilities might exceed the tires' tonnes-km/h (ton-mph) capabilities. Caterpillar recommends that you consult a tire supplier to evaluate all conditions before selecting a tire model. The 26.5-25 size range and other special tires are available on request.

Figure 55. CAT 966 H Specifications

# Appendix A (Continued)

## Dimensions

All dimensions are approximate.

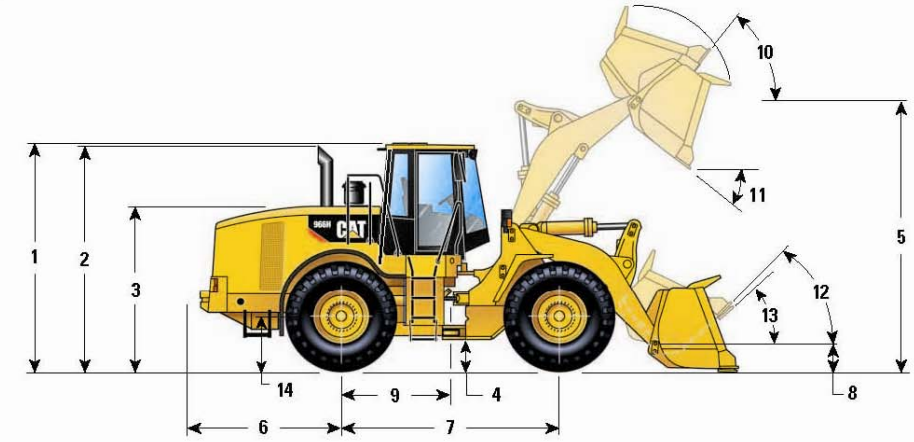


| | | |
|---|---|---|
| 1 | Height to top of ROPS | 3600 mm (11'10") |
| 2 | Height to top of exhaust pipe | 3552 mm (11'8") |
| 3 | Height to top of hood | 2678 mm (8'9") |
| 4 | Ground clearance with 26.5R25 L-4 Firestone (see tire chart for other tires) | 496 mm (1'8") |
| 5 | B-Pin height | 4224 mm (13'10") |
| 6 | Center line of rear axle to edge of counterweight | 2461 mm (8'1") |
| 7 | Wheelbase | 3450 mm (11'4") |
| 8 | B-Pin height @ carry | 507 mm (1'8") |
| 9 | Center line of rear axle to hitch | 1725 mm (5'8") |
| 10 | Rack back @ maximum lift | 60.8 |
| 11 | Dump angle @ maximum lift | 45 |
| 12 | Rack back @ carry | 47.4 |
| 13 | Rack back @ ground | 41.8 |
| 14 | Height to center line of axle | 815 mm (2'8") |

## Tire Dimensions/Specifications

| | Width over tires | | Change in vertical dimensions | | Change in operating weight | | Change in static tipping load | |
|---|---|---|---|---|---|---|---|---|
| | mm | inches | mm | inches | kg | lb | kg | lb |
| 26.5R25 GP2B GY L2 Radial | 3012 | 119 | -20 | -0.8 | -82 | -181 | -67 | -148 |
| 26.5R25 VMT BS L3 Radial | 3015 | 119 | -30 | -1.2 | 48 | 106 | -45 | -99 |
| 26.5R25 RT3B GY L3 Radial | 3017 | 119 | -20 | -0.8 | -24 | -53 | -24 | -53 |
| 26.5R25 XHA MX L3 Radial | 3017 | 119 | -20 | -0.8 | -34 | -75 | -31 | -68 |
| 26.5R25 VSDL BS L5 Radial | 2956 | 116 | 0 | 0.0 | 1214 | 2,677 | 906 | 1,998 |
| 750/65R25 MX L3 Radial Low Profile | 3076 | 121 | -20 | -0.8 | -262 | -578 | -52 | -115 |
| 26.5-25 20 PR SRG FS L3 Bias | 2992 | 118 | -44 | -1.7 | -358 | -789 | -492 | -1,085 |
| 26.5-25 20 PR SHRL GY L3 Bias | 2974 | 117 | -20 | -0.8 | 7 | 15 | -158 | -348 |
| 26.5-25 SRG DT FS LDL4 Bias | 3002 | 118 | 0 | 0.0 | 0 | 0 | 0 | 0 |

NOTE: Tread width for 26.5-25 is 2230 mm (7'4")

Figure 56. CAT 966 H Specifications

# Appendix B

## MACHINES USED IN TESTING

## CAT 972H WHEEL LOADER

## Appendix B (Continued)


Figure 57. CAT 972 H

# Appendix B (Continued)

## Engine

| Engine Model | Cat® C13 ACERT™ | |
|---|---|---|
| Gross Power – SAE J1995 | 232 kW | 311 hp |
| Net Power – ISO 9249 | 214 kW | 287 hp |
| Net Power – SAE J1349 | 212 kW | 284 hp |
| Net Power – 80/1269/EEC | 214 kW | 287 hp |
| Peak Torque (Net) @ 1,400 rpm | 1332 N•m | 983 ft-lb |
| Bore | 130 mm | 5.12 in |
| Stroke | 157 mm | 6.18 in |
| Displacement | 12.5 L | 762.8 $in^3$ |

- Caterpillar engine with ACERT™ Technology – EPA Tier III, EU Stage III Compliant
- These ratings apply at 1,800 rpm when tested under the specified standard conditions.
- Rating for net power advertised based on power available when the engine is equipped with alternator, air cleaner, muffler and on-demand hydraulic fan drive at maximum fan speed.

## Weights

| Operating Weight | 25 148 kg | 55,451 lb |
|---|---|---|

- For 4.6 $m^3$ (6.0 $yd^3$) general purpose bucket with BOCE

## Buckets

| Bucket Capacities | 3.8-4.6 $m^3$ | 5.0-6.0 $yd^3$ |
|---|---|---|
| Max Bucket Capacity | 4.6 $m^3$ | 6 $yd^3$ |

## Operating Specifications

| Static Tipping Load, Full Turn | 16 903 kg | 37,271 lb |
|---|---|---|
| Breakout Force | 230 kN | 51,750 lb |

- For 4.6 $m^3$ (6.0 $yd^3$) general purpose bucket with BOCE

## Transmission

| Forward 1 | 7.2 km/h | 4.5 mph |
|---|---|---|
| Forward 2 | 12.6 km/h | 7.8 mph |
| Forward 3 | 21.4 km/h | 13.3 mph |
| Forward 4 | 36.9 km/h | 22.9 mph |
| Reverse 1 | 8.2 km/h | 5.1 mph |
| Reverse 2 | 14.2 km/h | 8.8 mph |
| Reverse 3 | 24.3 km/h | 15.1 mph |
| Reverse 4 | 38.8 km/h | 24 mph |

- Maximum travel speeds (26.5-25 tires).

## Hydraulic System

| Bucket/Work Tool System – Pump Output | 305 L/min | 80.6 gal/min |
|---|---|---|
| Steering System Pump Type | Piston | |
| Hydraulic Cycle Time – Raise | 5.9 Seconds | |
| Hydraulic Cycle Time – Dump | 2.1 Seconds | |
| Hydraulic Cycle Time – Lower, Empty, Float Down | 2.4 Seconds | |
| Hydraulic Cycle Time – Total | 10.4 Seconds | |

- Implement System (Standard), Piston Pump – Rated at 2,100 rpm and 1,000 psi (6900 kPa).
- Cycle time with rated payload

## Brakes

| Brakes | Meets required standards. |
|---|---|

- Meet OSHA, SAE J1473 OCT90 and ISO 3450-1985 standards.

## Axles

| Front | Fixed front | |
|---|---|---|
| Rear | Oscillating ± 13° | |
| Maximum Single-Wheel Rise and Fall | 502 mm | 19.8 in |

## Tires

| Tires | Choose from a variety of tires to match your application. |
|---|---|

- Choice of:
  26.5R25, L-2
  26.5R25, L-3 (XHA)
  26.5R25, L-5 (VSDL)
  26.5-25, L-3 (SRG, SHRL)
  750/65R25, L-3
- NOTE: In certain applications (such as load and carry) the loader's productive capabilities might exceed the tires' tonnes-km/h (ton-mph) capabilities. Caterpillar recommends that you consult a tire supplier to evaluate all conditions before selecting a tire model. The 26.5-25 size range and other special tires are available on request.

Figure 58. CAT 972 H Specifications

# Appendix B (Continued)

## Dimensions

All dimensions are approximate.

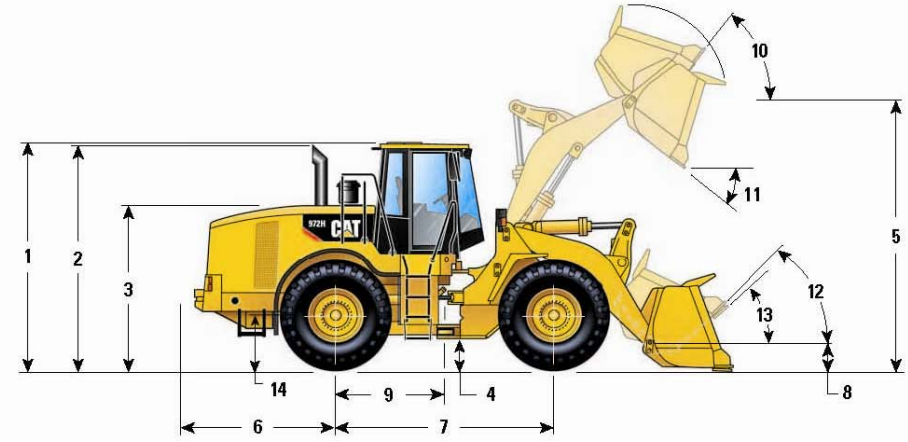


| | | |
|---|---|---|
| **1** | Height to top of ROPS | 3606 mm (11'10") |
| **2** | Height to top of exhaust pipe | 3557 mm (11'8") |
| **3** | Height to top of hood | 2683 mm (8'10") |
| **4** | Ground clearance with 26.5R25 L-4 Firestone (see Tire Options chart for other tires) | 496 mm (1'8") |
| **5** | B-Pin height | 4466 mm (14'8") |
| **6** | Center line of rear axle to edge of counterweight | 2461 mm (8'1") |
| **7** | Wheelbase | 3450 mm (11'4") |
| **8** | B-Pin height @ carry | 507 mm (1'8") |
| **9** | Center line of rear axle to hitch | 1725 mm (5'8") |
| **10** | Rack back @ maximum lift | 55° |
| **11** | Dump angle @ maximum lift | 51.6° |
| **12** | Rack back @ carry | 46.5° |
| **13** | Rack back @ ground | 41.1° |
| **14** | Height to center line of axle | 815 mm (2'8") |

## Tire Dimensions/Specifications

| | Width over tires | | Change in vertical dimensions | | Change in operating weight | | Change in static tipping load | |
|---|---|---|---|---|---|---|---|---|
| | mm | inches | mm | inches | kg | lb | kg | lb |
| 26.5R25 GP2B GY L2 Radial | 3012 | 119 | -20 | -0.8 | -82 | -181 | -57 | -126 |
| 26.5R25 VMT BS L3 Radial | 3015 | 119 | -30 | -1.2 | 48 | 106 | -41 | -90 |
| 26.5R25 RT3B GY L3 Radial | 3017 | 119 | -20 | -0.8 | -24 | -53 | -16 | -35 |
| 26.5R25 XHA MX L3 Radial | 3017 | 119 | -20 | -0.8 | -34 | -75 | -24 | -53 |
| 26.5R25 VSDL BS L5 Radial | 2956 | 116 | 0 | 0.0 | 1214 | 2,677 | 847 | 1,868 |
| 750/65R25 MX L3 Radial Low Profile | 3076 | 121 | -20 | -0.8 | -262 | -578 | -64 | -141 |
| 26.5-25 20 PR SRG FS L3 Bias | 2992 | 118 | -44 | -1.7 | -358 | -789 | -478 | -1,054 |
| 26.5-25 20 PR SHRL GY L3 Bias | 2974 | 117 | -20 | -0.8 | 7 | 15 | -131 | -289 |
| 26.5-25 SRG DT FS LDL4 Bias | 3002 | 118 | 0 | 0.0 | 0 | 0 | 0 | 0 |

**NOTE:** Tread width for 26.5-25 is 2230 mm (7'4")

Figure 59. CAT 972 H Specifications

# Appendix C

## ENGINES USED IN TESTING

## CAT C11 & CAT C13

# Appendix C (Continued)

CATERPILLAR®

**On-Highway Diesel Engine with ACERT® Technology**

**C11**

305-370 hp @ 2100 rpm

1050-1450 lb-ft @ 1200 rpm Peak Torque

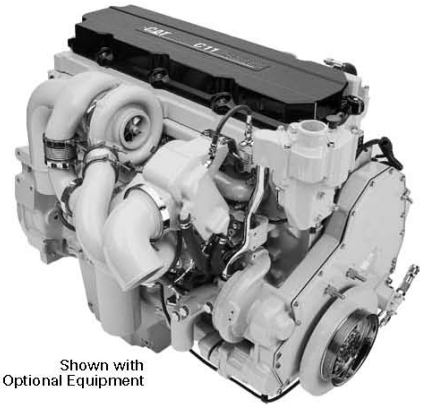

Shown with Optional Equipment

## CATERPILLAR® ENGINE SPECIFICATIONS

In-line 6-Cylinder, 4-Stroke-Cycle Diesel
Bore — in (mm) ..... 5.12 (130)
Stroke — in (mm) ..... 5.51 (140)
Displacement — cu in (L) ..... 677 (11.1)
Aspiration ..... Series Turbocharged
Compression Ratio ..... 17:1
Rotation (from flywheel end) .. Counterclockwise
Cooling System[1] — gal (L) ..... 3.04 (11.5)
Lube Oil System (refill) — gal (L) ..... 10.5 (40)
Weight, Net Dry (approx) — lb (kg)
with standard equipment ..... 2270 (1030)

[1] Engine only. Capacity will vary with radiator size and use of cab heater.

## STANDARD EQUIPMENT

Cooling: gear-driven water pump, oil cooler
Crankcase breather
Diesel Oxidation Catalyst (required)
Electronic Control Module (ECM)
Electronic Data Link, SAE/ATA, SAE/J1939
Electronically Controlled Unit Injection Fuel System
Fuel: spin-on secondary filter, transfer pump
Gear-driven water pump
Governor: full-range, electronically controlled
Hydraulic steering pump drive, SAE A
Lifting eyes
Lubrication: gear-driven pump, front or rear sump pan, full flow spin-on filter, oil filler, oil level gauge (dipstick)
Pad mount air conditioner compressor
Pad mount alternator
SAE No. 1 Flywheel Housing
Series-turbochargers
Vibration damper

## ACCESSORY EQUIPMENT

Air compressor: gear driven, 15.7 or 31.4 cfm
Air inlet elbow
Air inlet shut off
Alternator (12 Volt-115 Amp)
Automatic Transmission adapter
Cat® Compression Brake, 12V or 24V
Dry charge coolant conditioner
Exhaust couplings
Fan drive mounting bracket
Flywheel
Front engine support
Front PTO adapter
Fuel priming pump
Lubricating oil filter, bypass spin on
Optional secondary auxiliary oil filter
Optional turbocharger mounting locations
Rear PTO (RPTO)
Starting motor: 12V or 24V
Turbocharger compressor outlet elbow

## DIMENSIONS

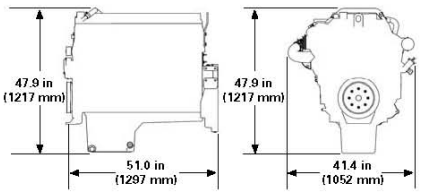


Figure 60. Engine C11 Series Specifications

## Appendix C (Continued)

CATERPILLAR®

**C11 ON-HIGHWAY DIESEL ENGINE — 305 to 370 hp**

### PERFORMANCE CURVES

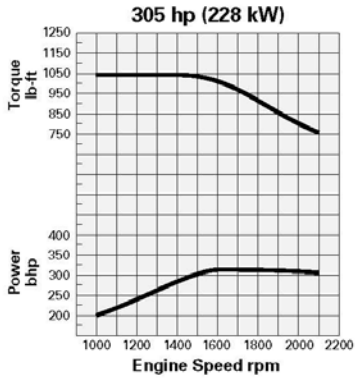


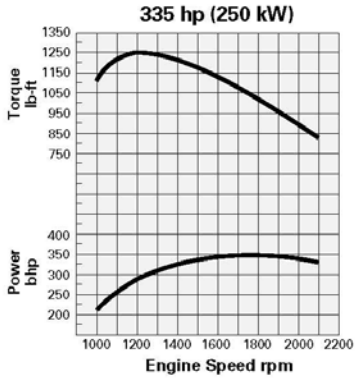


### PERFORMANCE DATA

| | |
|---|---|
| Operating Range (rpm) | 1200–2100 |
| **Governed Speed — rpm** | **2100** |
| Advertised hp (kW) | 305 (228) |
| Max hp (kW) | 315 (235) |
| **Peak Torque — lb-ft (N•m)** | **1050 (1424)** |
| Peak Torque — rpm | 1200 |
| Torque rise (%) | 38 |
| Altitude Capability — ft (m) | 10,000 (3048) |

| | |
|---|---|
| Operating Range (rpm) | 1200–2100 |
| **Governed Speed — rpm** | **2100** |
| Advertised hp (kW) | 335 (250) |
| Max hp (kW) | 350 (261) |
| **Peak Torque — lb-ft (N•m)** | **1250 (1695)** |
| Peak Torque — rpm | 1200 |
| Torque rise (%) | 49 |
| Altitude Capability — ft (m) | 10,000 (3048) |

### PERFORMANCE CURVES

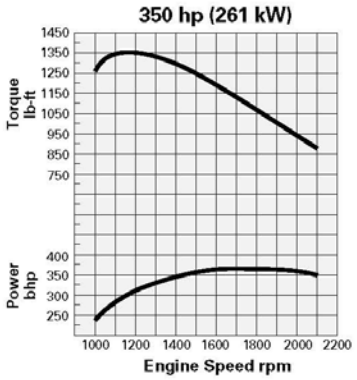


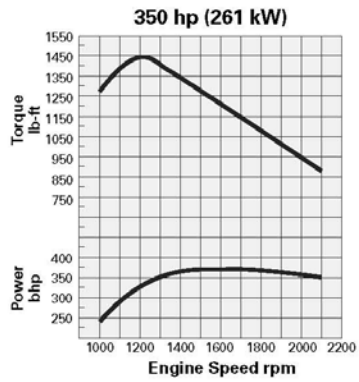


### PERFORMANCE DATA

| | |
|---|---|
| Operating Range (rpm) | 1200–2100 |
| **Governed Speed — rpm** | **2100** |
| Advertised hp (kW) | 350 (261) |
| Max hp (kW) | 365 (271) |
| **Peak Torque — lb-ft (N•m)** | **1350 (1830)** |
| Peak Torque — rpm | 1200 |
| Torque rise (%) | 54 |
| Altitude Capability — ft (m) | 10,000 (3048) |

| | |
|---|---|
| Operating Range (rpm) | 1200–2100 |
| **Governed Speed — rpm** | **2100** |
| Advertised hp (kW) | 350 (261) |
| Max hp @ (kW) | 369 (275) |
| **Peak Torque — lb-ft (N•m)** | **1450 (1966)** |
| Peak Torque — rpm | 1200 |
| Torque rise (%) | 66 |
| Altitude Capability — ft (m) | 10,000 (3048) |

LEHT4572-01

Page 2 of 3

Figure 61. Engine C11 Series Specifications

## Appendix C (Continued)

CATERPILLAR®

**On-Highway Diesel Engine with ACERT® Technology**

**C13**
**EPA 07 Certified**
305-470 hp @ 2100 rpm
1150-1750 lb-ft @ 1200 rpm Peak Torque

Shown with Optional Equipment

### CATERPILLAR® ENGINE SPECIFICATIONS

In-line 6-Cylinder, 4-Stroke-Cycle Diesel
Bore — in (mm) ..... 5.12 (130)
Stroke — in (mm) ..... 6.18 (157)
Displacement — cu in (L) ..... 763 (12.5)
Combustion/Aspiration... Series Turbocharged
Compression Ratio ..... 17.1:1
Rotation (from flywheel end) .. Counterclockwise
Cooling System[1] — gal (L)..... 5.76 (21.8)
Lube Oil System (refill) — gal (L) ..... 10 (38)
Weight, Net Dry (approx) — lb (kg)
with standard equipment..... 2610 (1184)

[1] Engine only. Capacity will vary with radiator size and use of cab heater.

### STANDARD EQUIPMENT

Caterpillar® Regeneration System
Cooling: gear-driven water pump, oil cooler
Diesel particulate filter
Electronic Control Module (ECM)
Electronic Data Link, SAE/ATA, SAE/J1939
Electronically Controlled Unit Injection Fuel System
Fuel: spin-on secondary filter, transfer pump
Gear-driven water pump
Governor: full-range, electronically controlled
Hydraulic steering pump drive, SAE A
Lifting eyes
Lubrication: gear-driven pump, front or rear sump pan, full flow spin-on filter, oil filler, oil level gauge (dipstick)
Open crankcase ventilation
Pad mount air conditioner compressor
Pad mount alternator
SAE No. 1 Flywheel Housing
Series-turbochargers
Vibration damper

### ACCESSORY EQUIPMENT

Air compressor: 16.1 cfm (0.46 $m^3$/min) or 31.6 cfm (0.9 $m^3$/min)
Air inlet elbow
Air inlet shut off
Alternator (12 Volt-115 Amp)
ATAAC inlet elbow
Automatic transmission adapter
Cat compression brake
Exhaust couplings
Fan drive mounting bracket
Flywheel
Front engine support
Front PTO adapter
Fuel priming pump
Lubricating oil filter, bypass spin on
Optional secondary auxiliary oil filter
Optional turbocharger mounting locations
Primary fuel filter (10 micron)
Rear PTO (RPTO)
Starting motor: 12V or 24V

### DIMENSIONS

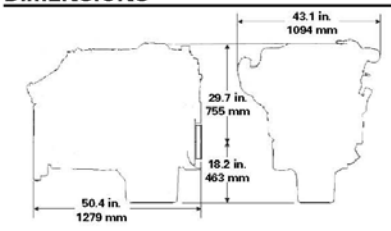


Figure 62. Engine C13 Series Specifications

## Appendix C (Continued)

CATERPILLAR®

**C13 ON-HIGHWAY DIESEL ENGINE — 305 to 350 hp**

### PERFORMANCE CURVES

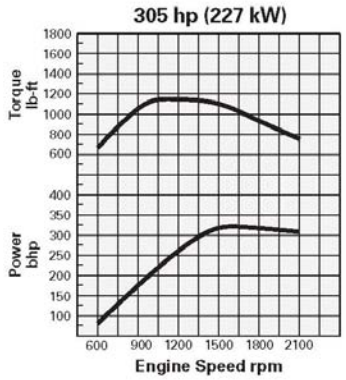


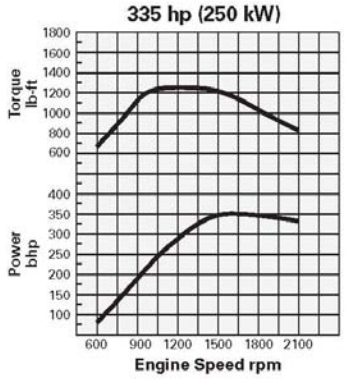


### PERFORMANCE DATA

| | |
|---|---|
| Operating Range (rpm) | 1200–2100 |
| **Governed Speed — rpm** | **2100** |
| Advertised hp (kW) | 305 (227) |
| Max hp (kW) | 320 (239) |
| **Peak Torque — lb-ft (N•m)** | **1150 (1559)** |
| Peak Torque — rpm | 1200 |
| Torque rise (%) | 51 |
| Altitude Capability — ft (m) | 10,000 (3048) |

| | |
|---|---|
| Operating Range (rpm) | 1200–2100 |
| **Governed Speed — rpm** | **2100** |
| Advertised hp (kW) | 335 (250) |
| Max hp (kW) | 350 (261) |
| **Peak Torque — lb-ft (N•m)** | **1250 (1695)** |
| Peak Torque — rpm | 1200 |
| Torque rise (%) | 49 |
| Altitude Capability — ft (m) | 10,000 (3048) |

### PERFORMANCE CURVES

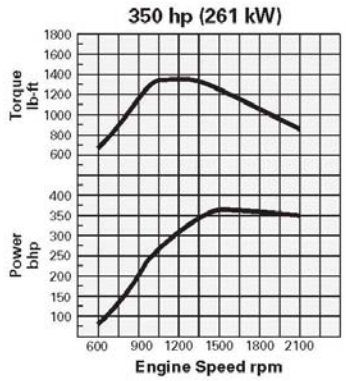


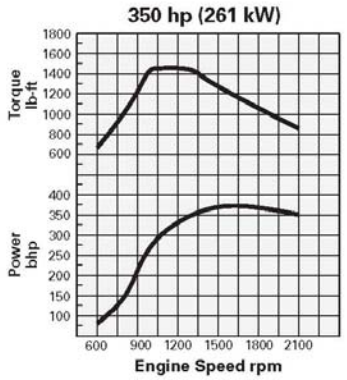


### PERFORMANCE DATA

| | |
|---|---|
| Operating Range (rpm) | 1200–2100 |
| **Governed Speed — rpm** | **2100** |
| Advertised hp (kW) | 350 (261) |
| Max hp (kW) | 365 (272) |
| **Peak Torque — lb-ft (N•m)** | **1350 (1830)** |
| Peak Torque — rpm | 1200 |
| Torque rise (%) | 54 |
| Altitude Capability — ft (m) | 10,000 (3048) |

| | |
|---|---|
| Operating Range (rpm) | 1200–2100 |
| **Governed Speed — rpm** | **2100** |
| Advertised hp (kW) | 350 (261) |
| Max hp (kW) | 365 (272) |
| **Peak Torque — lb-ft (N•m)** | **1450 (1966)** |
| Peak Torque — rpm | 1200 |
| Torque rise (%) | 66 |
| Altitude Capability — ft (m) | 10,000 (3048) |

Figure 63. Engine C13 Series Specifications

# CITED LITERATURE

[1] Elezaby, A., Abdelaziz, M., and Cetinkunt, S., Operator Model for Construction Equipment, 2008 IEEE/ASME International Conference on Mechatronics and Embedded Systems and Applications October 12-15, 2008, Beijing, China.

[2] Filla, R., Ericsson, A., and Palmberg J., Dynamic Simulation of Construction Machinery: Towards an Operator Model, IFPE2005 Technical Conference, Las Vegas (NV), USA, pp 429-438, March 16-18, 2005.

[3] Filla, R., An Event-driven Operator Model for Dynamic Simulation of Construction Machinery, The Ninth Scandinavian International Conference on Fluid Power, Linkping, Sweden, June 1-3, 2005.

[4] Filla, R. and Palmberg, J., Using Dynamic Simulation in the Development of Construction Machinery, The Eighth Scandinavian International Conference on Fluid Power, Tampere, Finland, Vol. 1, pp 651-667, May 7-9, 2003.

[5] Cetinkunt, S. Mechatronics. John Wiley & Sons, Inc. 2006.

[6] Wu, L., A Study on Automatic Control of Wheel Loaders in Rock/Soil Loading, Dissertation, University of Arizona, Tucson, AZ, USA, 2003.

[7] Singh, S., State of the Art in Automation of Earthmoving, 2002, Proceedings of the Workshop on Advanced Geomechatronics, Sendai University, Japan, 2002.

[8] Marshall, J. A., Towards Autonomous Excavation of Fragmented Rock: Experiments, Modelling, Identification and Control, Master Thesis, Queen's University, Kingston, Ontario, Canada, 2001.

[9] Hemami, A., Motion trajectory study in the scooping operation of an LHD-loader, Proceedings of the Workshop on Advanced Geomechatronics, Sendai University, Japan, 2002.

[10] Shi, X. et al., Experimental results of robotic excavation using fuzzy behavior control, Control Engineering Practice, Vol. 4, No. 2, Feb. 1996, pp 145-152.

[11] Ericsson, A. and Slttengren J, A model for predicting digging forces when working in gravel or other granulated material, 15th European ADAMS Users' Conference, Rome, Italy, Nov 15-17, 2000.

[12] Vogel, K., Modeling Driver Behavior: a control theory based approach, Dissertation, Linkping University, Linkping, Sweden, 2002.

[13] Lee, H. K. et al., Mechanical restriction versus human overreaction triggering congested traffic states, International Conference on Fluid Power, Linkping, Sweden, June 1-3, 2005

[14] Bengtsson, J., Adaptive Cruise Control and Driver Modeling, Licentiate Thesis, Lund Institute of Technology, Lund, Sweden, 2001.

[15] Macadam, C. C., Understanding and Modeling the Human Driver, Vehicle System Dynamics, Vol. 40, Nos. 1-3, Jan. 2003, pp 101-134.

[16] Grant, P. et al., Preparation of a Virtual Proving Ground for Construction Equipment Simulation, IEEE Transactions on Industry Applications, Vol. 30, No. 5, Sept./Oct. 1994, pp 1333-1338.

[17] Coulter, R. C. (1992). Implementation of the pure pursuit path tracking algorithm, Technical Report CMU-RI-TR-92-01, Robotics Institute, Carnegie Mellon University, Pittsburgh, PA.

[18] Matlab Help, Mathworks.com.

[19] Gomm, R. and Cetinkunt, S. , Real-Time Motion Planning for Mobile Construction Equipment Vehicle Linkage Mechanism, International Forum on Systems and Mechatronics, Tainan, Taiwan, December 2006.

[20] Singh, S., Synthesis of Tactical Plans for Robotic Excavations, Dissertation, Carnegie Mellon University, Pittsburgh, PA, USA, 1995.

[22] Cobo, M.,Ingram, R., Cetinkunt, S., " Modeling, identification , and real-time control of bucket hydraulic system for a wheel type loader earth moving equipment ",Mechatronics,1998, vol. 8, no8, pp. 863-885.

[23] Bradley, D.,Seward, D., Mann, J. ,"Artificial intelligence in the control and operation of construction plant: the autonomous robot excavator ", Journal of Automation in construction, 1993, vol. 2, no3, pp. 217-228.

[24] MacArthur, D. and Crane, C., "Unmanned Ground Vehicle State Estimation using an Unmanned Air Vehicle," Proceedings of the 7th IEEE International Symposium on Computational Intelligence in Robotics and Automation, Jacksonville, June 2007

[25] Crane, C., Armstrong, D., Arroyo, A., Baker, A., Dankel, D., Garcia, G., Johnson, N., Lee,J., Ridgeway,S., Schwartz,E., Thorn,E., Velat,S.,Yoon,J.and Washburn,J., "Team Gator Nation's Autonomous Vehicle Development for the 2007 DARPA Urban Challenge", Journal of Aerospace Computing, Information, and Communication, Vol. 4, Dec. 2007,pp. 1059-1085.

[26] Bradley, D.,Seward, "The Development, Control and Operation of an Autonomous Robotic Excavator", Journal of Intelligent and Robotic Systems,Volume 21, Jan. 1998,pp. 73-97.

[27] Stentz,A., "Robotic Technologies for Outdoor Industrial Vehicles", In Proceedings of SPIE AeroSense 2001,Orlando,FL, USA.

[28] Baiden, G., Multiple LHD Teleoperation and Guidance at INCO Limited, Proc. of the International Mining Conference, 1993.

[29] Billingsley, J., Schoenfisch, M., Vision Guidance of Agricultural Vehicles, Autonomous Robots, Vol 2, 1995.

[30] Bullock, D.M., Apte, S., Oppenheim, I.J., Force and Geometry Constraints in Robot Excavation, Proc. of Space 90:Engineering, Construction and Operations in Space, 1990.

[31] Erbach, D.C., Choi, C.H., Noh, K., Automated Guidance for Agricultural Tractors, Automated Agriculture for the 21st Century, ASAE, 1991.

[32] Gerrish, J.B., Fehr, B.W., Van Ee, G.R., Welch, D.P., Self-Steering Tractor Guided by Computer Vision, Applied Engineering in Agriculture, Vol. 13, No. 5, 1997.

[33] Huang, X.D., Bernold, L. E., Control Model for Robotic Backhoe Excavation and Obstacle Handling, Proc. of Robotics for Challenging Environments, 1994.

[34] Hurteau, R., St-Amant, M., Laperriere, Y., Chevrette, G., Optical Guidance System for Underground Mine Vehicles, Proc. of the International Conference on Robotics and Automation, 1992.

[35] Lever, P.,Wang, F., Chen, D., Intelligent Excavator Control for a Lunar Mining System, Proc. of ASCE Conference on Robotics for Challenging Environments, 1994.

[36] Lever, P. J., Ntaimo, L., ”Autonomous Digging Control for a Wheel Loader: Implementation and Results,” Proc. of SPIE AeroSense, April 2000.

[37] Makela, H., Lehtinen, H., Rintanen, K., Koskinen, K., Navigation System for LHD Machines, Intelligent Autonomous Vehicles, 1995.

[38] Oconner, M., Bell, T., Elkaim, G., Parkinson, B., Automatic Steering of Farm Vehicles Using GPS, Proc. of the 3rd International Cnference on Precision Agriculture, 1996.

[39] Pilarski, T., Happold, M., Pangels, H., Ollis, M., Fitzpatrick, K., Stentz, A., The DEMETER System for Autonomous Harvesting, Proc. of the8thInternationalTopicalMeeting on Robotics and Remote Systems, April 1999.

[40] Rowe, P., Adaptive Motion Planning for Autonomous Mass Excavation, Carnegie Mellon Robotics Institute doctoral dissertation, Technical Report CMU-RI-TR-99-09, January 1999.

[41] Elezaby, A. A., Cetinkunt, S., Virtual Operator Model for Construction Equipment Design, Fault Tolerant Drive by Systems on Vehicle Safety and Reliability, Bentham Science, pp. 72- 92, 2011.

# VITA

Personal Information

Full name: Ahmed Adel Elezaby

E-mail address: ahmedelezaby@gmail.com

Academic Background

Doctor of Philosophy: University of Illinois at Chicago, 2011

Master Degree : Ain Shams University, Cairo, Egypt, 2006.

Bachelor Degree : Ain Shams University, Cairo, Egypt, 2001.

Languages

English , Arabic